TOWARDS THE CONTINUUM: LOSS-OF-FUNCTION IN PARALLEL WITH GAIN-OF-FUNCTION IN C9ORF72-MEDIATED ALS AND FTD

by

CHEN LIANG

(Under the Direction of Jianfu Chen)

Amyotrophic lateral sclerosis (ALS) and frontotemporal dementia (FTD) are devastating and fatal degenerative diseases. ALS is the most common motor neuron disease and FTD represents an estimated 10%-20% of all dementia cases. The discovery in 2011 that the C9orf72 gene mutation is the major genetic cause of both ALS and FTD provided a molecular link for these two diseases. Both loss of function and gain of function hypotheses have been proposed for the disease mechanisms. Loss of function mechanisms focus on loss of the C9orf72 protein, whose function was largely unknown back then. Gain of function mechanisms focus on toxicity from C9orf72 repeat RNA or from dipeptide repeat proteins produced by repeat-associated on-ATG translation.

This thesis work has examined the normal molecular and cellular functions of C9orf72 as well as its associated protein Smcr8, and how partial depletion of C9orf72 affects the cellular and behavioral functions under the gain of toxicity background. I have examined the roles of the C9orf72/Smcr8 complex in autophagy and axonal transport. C9orf72/Smcr8 complex associates with the ULK1/ATG13/FIP200 complex. Loss of C9orf72 or Smcr8 disrupts autophagy induction and autophagy flux. Smcr8

deficient mice exhibit motor behavioral deficits, axonal swellings and autophagosome-lysosomal accumulations. Combining the Smcr8 deficient mouse model with a C9orf72 deficient mouse model, I discovered that C9orf72 deficiency exacerbates the lysosomal and axonal deficits of Smcr8 deficient mice. Time-lapse imaging revealed roles of C9orf72 and Smcr8 in axonal transport of autophagosomes. These studies have uncovered potential functions of C9orf72 in maintaining motor neurons, which may be masked by its interactor Smcr8.

To understand how loss of function of C9orf72 affects neurodegeneration in the disease conditions, I crossed the C9orf72 deficient mouse model with a C9ALS/FTD gain of function mouse model. C9orf72 haploinsufficiency exacerbated the motor, social and cognitive deficits of the gain of function mouse model. Mechanistic studies revealed more severe axonal swellings at the neuromuscular junctions and increased dipeptide repeat accumulations due to partial loss of C9orf72 function in the gain of function background. These experiments have filled the gap between the loss- and gain-of-function and provided the field with a broader picture of the disease mechanisms and potential therapeutic targets.

INDEX WORDS: Neurodegeneration, autophagy, axonal transport, C9orf72, Smcr8, motor deficits, mice, C9ALS/FTD, axonal swellings, toxic effects, ULK1, spinal cord.

TOWARDS THE CONTINUUM: LOSS-OF-FUNCTION IN PARALLEL WITH GAIN-OF-FUNCTION IN C9ORF72-MEDIATED ALS AND FTD

by

CHEN LIANG

B.S., China Agricultural University, China, 2012

A Dissertation Submitted to the Graduate Faculty of The University of Georgia in Partial Fulfillment of the Requirements for the Degree

DOCTOR OF PHILOSOPHY

ATHENS, GEORGIA

2020

TOWARDS THE CONTINUUM: LOSS-OF-FUNCTION IN PARALLEL WITH GAIN-OF-FUNCTION IN C9ORF72-MEDIATED ALS AND FTD

by

CHEN LIANG

Major Professor:	Jianfu Chen
Committee:	James Lauderdale
	Jonathan Eggenschwiler
	Jesse Schank

Electronic Version Approved:

Ron Walcott
Interim Dean of the Graduate School
The University of Georgia
August 2020

DEDICATION

To the doctors and nurses around the world on the frontlines of COVID-19.

ACKNOWLEDGEMENTS

I would like to express the deepest appreciation to my thesis advisor Dr. Jianfu Chen, who guided me through my graduate education. He accepted me into the warm family of the Chen lab. Without his support and constant feedback, this PhD would not have been achievable. His hard-working attitude set a good example and kept me towards a high standard. Many thanks also to Dr. James Lauderdale and Dr. Jonathan Eggenschwiler, who have provided strong support for my academic career. I must also thank Dr. Jesse Schank, who kindly agreed to be on my dissertation committee during the middle of my PhD, and Dr. Scott Dougan for his constant support.

I greatly appreciate the expert assistance from Dr. Nikolay Filipov for his help with motor behavioral experiments and Ms. Mary Ard, who sacrificed her weekend time to prepare samples for electronic microscopy imaging. Special thanks go out to my excellent colleagues, especially Dr. Mei Yang, Dr. Wei Zhang and Qing Chang, whose work has made an invaluable contribution towards this thesis. I also thank my fellow graduate students, especially Drs. Munisha Mumingjiang, Stephanie Herrlinger and Sadie Nennig for their friendship. I would like to say a big thank you to my family. I am grateful to my former committee member, Dr. Richard Steet, and to members of the Damocles meeting and CCMB for the stimulating discussions and positive research environment.

This work was supported by National Institute of Health, University of Georgia and University of Southern California.

TABLE OF CONTENTS

Page

LIST OF TABLES

Page

LIST OF FIGURES

Page

CHAPTER 1

INTRODUCTION AND LITERATURE REVIEW

"I regard the brain as a computer which will stop working when its components fail."

– Stephen Hawking.

1.1. Overview

As we age, the brain, which serves as an integrator of life experiences, are exposed to occasional acute insults including trauma, infections, or toxins. Aging neurons accumulate various neuropathological proteins, such as amyloid-β and TDP-43(De Jager et al., 2018). Because neurons cannot divide and they survive a long time, inadequate protein quality-control and degradation pathways leads to accumulation of defective organelles, misfolded and aggregated proteins, which leads to cellular dysfunction, loss of synaptic connections, and brain damage. Neurodegenerative diseases cause progressive loss of memory and cognitive impairments or affect a person's ability to move, speak and breathe. They affect millions of people worldwide and pose major challenges for societies with rapid aging populations. Frontotemporal dementia (FTD) is a progressive neurologic syndrome with psychiatric prodrome, neuropsychiatric symptoms and language difficulties. It is the second most common form of dementia in those younger than 65 years, with a prevalence of 15 to 22/100,000 (Bott et al., 2014; Young et al., 2017). Amyotrophic lateral sclerosis (ALS) is the most

common motor neuron disease in adults and is characterized by degeneration of motor neurons in the brain and spinal cord and eventual loss of voluntary muscular function (Yedavalli et al., 2018). The average age of onset of ALS is currently 58-60 years and the average survival from onset to death is 3-4 years (Talbott et al., 2016). In 2011, a hexanucleotide GGGGCC repeat expansion in the *C9orf72* gene was discovered to be the most frequent genetic cause of both diseases in Europe and North America (DeJesus-Hernandez et al., 2011; Renton et al., 2011). Although the *C9ORF72* locus has been well researched on the gain of toxicity of RNA foci and poly-dipeptide resulting from the expanded repeats (Wen et al., 2014; May et al., 2014; Mizielinska et al., 2014), little is known about the normal function of C9orf72, and how the loss of function mechanisms interact with the gain of toxicity pathways.

To advance the field in understanding the C9orf72 ALS/FTD disease at the molecular, cellular and system level, and to provide insights about potential therapeutic targets for clinical treatment of the disease, I have been focusing my efforts on the following aspects: (1) The role of C9orf72/Smcr8 complex in autophagy; (2) Smcr8 deficiency disrupts axonal transport-dependent lysosomal function and promotes axonal swellings; (3) C9orf72 haploinsufficiency promotes neurodegeneration and behavioral deficits of a C9ALS/FTD mouse model.

1.2. Autophagy, axonal transport and neurodegenerative diseases

1.2.1 Autophagy

Autophagy is the major intracellular degradation system by which cytoplasmic materials are delivered to and degraded in the lysosome (Mizushima &

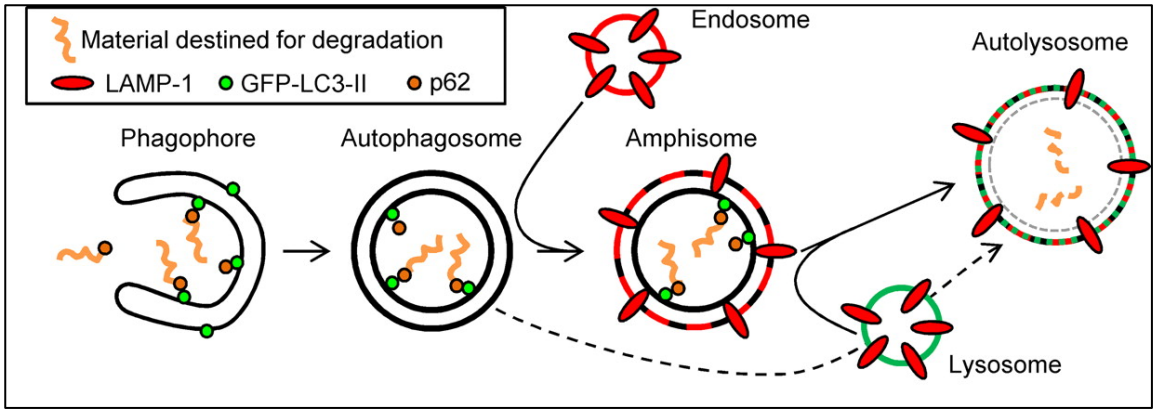

Figure 1.1. The autophagy pathway. From Kemball et al., 2010.

Komatsu, 2011) (Figure 1.1). Autophagy-inducing signals (for example, amino acid starvation and pathogen infection) initiate formation of the isolation membrane (or 'phagophore') (Shibutani et al., 2015). Under normal growth conditions, mTORC1 associates with the Ulk1/2-Atg13-FIP200 complex, via direct interaction between raptor and Ulk1/2 (Hosokawa et al., 2009). The active mTOR phosphorylates Atg13 and Ulk1/2 (Ganley et al., 2009; Hosokawa et al., 2009; Jung et al., 2009), thereby suppressing Ulk1/2 kinase activity. Under starvation conditions or when mTORC1 activity is pharmacologically inhibited, these sites are rapidly dephosphorylated (Sebastian et al., 2011). The activated Ulk1/2 autophosphorylates and phosphorylates both FIP200 and Atg13, which in turn leads to translocation of the entire complex to the pre-autophagosomal membrane (phagophore) (Chan et al., 2007; Chang & Neufeld, 2009; Hara et al, 2008; Ganley et al., 2009; Hosokawa et al., 2009; Jung et al., 2009). Then bulk cytoplasmic material is sequestered into the phagophore, which expands around the cargo and finally forms a sealed, double-membrane vesicle known as the autophagosome (Hollenstein & Kraft, 2020). Autophagosomes either fuse with late endosomes to form amphisomes, which then fuse with lysosomes, or they fuse directly with lysosomes to form autolysosomes (Nakamura & Yoshimori, 2017), leading to the

degradation of the intra-autophagosomal contents by lysosomal proteases (Tanida et al., 2005).

1.2.2 Methods to monitor and measure autophagy

To accurately estimate autophagic activity, it is essential to determine autophagic flux, which is defined as the amount of autophagic degradation (Yoshii, S.R. & Mizushima, N., 2017). The mammalian autophagy protein, LC3, is a marker of autophagosomes. Soon after synthesis, nascent LC3 is processed at its C terminus by Atg4 and becomes LC3-I, which has a glycine residue at the C-terminal end (Mizushima et al., 2010). Upon induction of autophagy, the exposed glycine of LC3-I is conjugated by Atg7 (an E1-like activity), Atg3 (an E2-like conjugating activity) and by Atg12-Atg5-Atg16L multimers (E3-like ligase activity) to the highly lipophilic phosphatidylethanolamine (PE) moiety to generate LC3-II (Mizushima, 2007; Nakatogawa et al., 2009; Barth et al., 2010). This allows the association of LC3-II with the autophagosome (Kabeya et al., 2000).

The polyubiquitin-binding protein p62/SQSTM1 is a classical receptor of autophagy (Liu, W.J. et al., 2016). It binds directly to Atg8/LC3 to facilitate degradation of ubiquitinated protein aggregates by autophagy (Pankiv et al., 2007). Autophagosomes either fuse with late endosomes to form amphisomes, which then fuse with lysosomes, or they fuse directly with lysosomes to become autolysosomes (Shuhei N. & Tamotsu Y., 2017; Berg et al., 1998; Fader et al., 2008). Endo-lysosomal organelles, including late endosomes, lysosomes, amphisomes, and autolysosomes are labeled by Lamp-1 (Cheng et al., 2018; Cheng et al., 2018). After fusion of the

autophagosomes with the lysosomes, p62 and LC3-II are degraded together with the contents of the autophagosomes (Yoshii, S.R. & Mizushima, N., 2017).

LC3 and p62 turnover is a reliable indicator of autophagic flux. In the early phase of autophagy, autophagy induction will lead to increase in LC3-II level, and suppression of autophagy initiation will lead to decrease in LC3-II. In the late stage, block of autophagosome-lysosome fusion and/or block of degradation in autolysosomes will lead to increase of LC3-II. The level of SQSTM1 is strictly regulated by continuous degradation by basal autophagy. Impairment of autophagy causes massive accumulation of SQSTM1 (Sahani et al., 2014). mCherry-GFP-LC3 is a marker to monitor the late phase of autophagy flow. When fused to the autophagic marker LC3, GFP fluorescence is quenched upon fusion between autophagosome and lysosome due to the low lysosomal pH, while mCherry remains fluorescent until degradation by lysosomal proteases (Hundeshagen et al., 2011). Owing to this pH-dependent quenching of the GFP-LC3 fluorescence, only mCherry-LC3 can be detected in autolysosomes (i.e. these appear red only), whereas autophagosomes can be visualized by both fluorophores (i.e. these appear yellow) (Lopez et al., 2018). Suppression of the late phase of autophagy will lead to an increase of yellow/red ratio.

Small-molecule modulators of autophagy that target different steps of the autophagic machinery can be used to monitor autophagy flow. Rapamycin stimulates autophagy through inhibition of MTOR (mammalian target of rapamycin) (Tekirdag et al., 2013). Bafilomycin A1 disrupts autophagic flux by inhibiting both acidification-dependent lysosomal degradation and autophagosome-lysosome fusion (Mauvezin et

al., 2015). Leupeptin and pepstatin A are autophagy inhibitors that function by suppressing lysosomal proteases (Yang et al., 2013).

1.2.3 Autophagy and neurodegenerative diseases

Neurons have unusually large extensions of dendritic and axonal cytoplasm. They face particular challenges in preventing dysfunctional organelles and cellular waste from accumulating over a lifetime without the aid of cell division, which mitotic cells can rely on to dilute these waste burdens (Nixon et al., 2013). Well-regulated protein quality control is necessary for the aging neurons. Failures in different steps of autophagy flow, including substrate sequestration and recognition, autophagosome formation, autophagosome-lysosome fusion and lysosome digestion, can lead to neurodegenerative diseases.

In late-onset diseases, the accumulation of misfolded proteins is a common pathological hallmark (Nobuhiro et al., 2018). Numerous autophagic vacuoles have been observed in dystrophic neurites of Alzheimer's disease (AD) brains (Nixon et al., 2005). AD-related PS1 mutations disrupt lysosomal function and promote neuronal loss (Lee et al., 2010). Beclin 1, a major player in autophagy induction, was reported to be downregulated in AD brains (Pickford et al., 2008). In amyotrophic lateral sclerosis (ALS) and Frontotemporal dementia (FTD) patients, insoluble protein aggregates have been found to accumulate in the brainstem, spinal cord, cerebellum, hippocampus, and frontal and temporal lobes, caused by mutations in superoxide dismutase 1 (SOD1), RNA-binding protein FUS, and TAR DNA-binding protein 43 (TDP43) (Andersen and Al-Chalabi, 2011). In Huntington's disease, the ability of autophagosome vacuoles to recognize and trap cytosolic cargos is impaired due to the interaction between mutant

HTT and p62 (Martinez-Vicente et al., 2010). Efforts have been made to treat a diverse range of neurodegenerative diseases targeting autophagy. Compounds that stimulate autophagy induction or enhance lysosomal stability have been proven to be effective in attenuating disease progression for Alzheimer's disease and Parkinson's disease (Nixon et al., 2013).

1.2.4 Axonal transport and autophagy

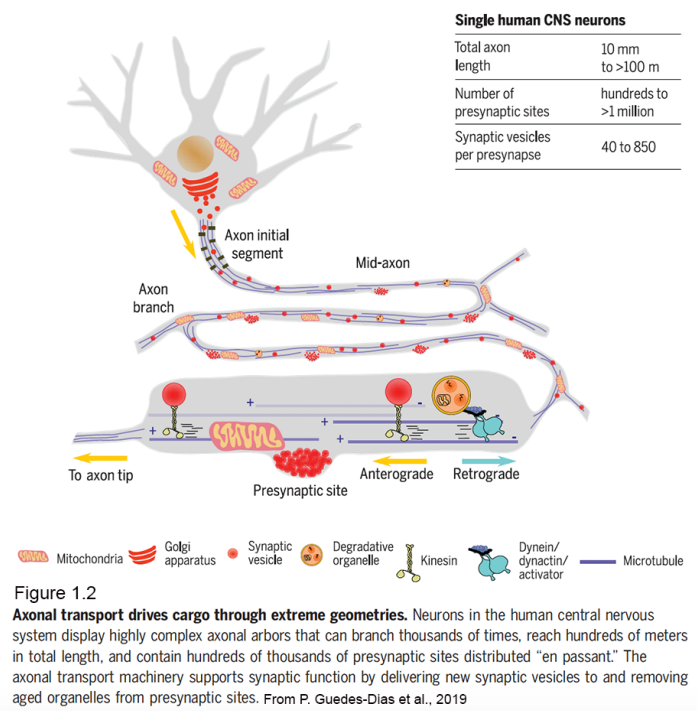

Figure 1.2
Axonal transport drives cargo through extreme geometries. Neurons in the human central nervous system display highly complex axonal arbors that can branch thousands of times, reach hundreds of meters in total length, and contain hundreds of thousands of presynaptic sites distributed "en passant." The axonal transport machinery supports synaptic function by delivering new synaptic vesicles to and removing aged organelles from presynaptic sites. From P. Guedes-Dias et al., 2019

Neurons are highly polarized cells that form the basis of directed information flow within the nervous system (Jones et al., 2016). Each neuron consists of the cell body (soma), multiple dendrites and a long axon toward the next neuron or a target tissue. In humans, motor neuron soma can be as large as 100 μm in diameter with axons projecting over 1 m to distal targets (Fabricius et al., 1994). Anterograde transport supplies distal axons with newly synthesized proteins and lipids, including synaptic components required to maintain presynaptic activity. Retrograde transport is required to maintain homeostasis by removing aging proteins and organelles from the distal axon for degradation and recycling of components (Maday et al., 2014). Axonal lysosome biogenesis arises from the fusion of lysosome precursors, including endosomes and autophagosomes, in distal regions of axons and their further maturation requires

retrograde transport to cell body proximal regions where luminal proteases can be most effectively delivered from the trans-Golgi network (Grutzendler et al., 2015) (Figure 1.2).

Microtubules provide the guiding tracks for motor movement along the axon. Kinesin superfamily motors traffic cargos along the axon in the anterograde direction, moving outward from the soma. The retrograde transport of cargos toward the soma is driven by a single motor, cytoplasmic dynein (Guedes-dias et al., 2019). Axonal transport can be divided into two categories: fast axonal transport, which is responsible for moving membrane-bound organelles (vesicles and mitochondria), and slow axonal transport, which drives the movement of cytoplasmic proteins (including various enzymes) and cytoskeletal proteins (microtubules and neurofilaments) (Lasek et al., 1984).

1.2.5 Axonal transport and neurodegenerative diseases

Mutations in different components of the axonal transport machinery, either from motor proteins, motor adaptors or regulators, can cause a range of neurodevelopmental and neurodegenerative diseases.

Alzheimer's disease can be caused by various axonal transport deficits resulting from pathological forms of APP, tau, PS1 and amyloid- β (Millecamps et al., 2013). Transgenic mouse models of AD overexpressing mutant APP show impairment in retrograde transport of nerve growth factor and lysosomes (Salehi et al., 2006; Grutzendler et al., 2015).

Huntington's disease (HD) is also associated with axonal transport deficits. The polyglutamine (polyQ) expansions in the huntingtin (Ht) protein impair axonal transport

through inhibition of microtubule acetylation, activation of motor protein phosphorylation or loss of normal HTT function (Millecamps et al., 2013).

Amyotrophic lateral sclerosis – the most common motor neuron disease – is characterized by degeneration of spinal motor neurons, many of which show axonal swellings containing vesicles, lysosomes, mitochondria and intermediate filaments (Millecamps et al., 2013). The *SOD1* genetic mutations reduce axonal transport of neurofilament and mitochondria through hyperactivation of p38, which phosphorylates kinesin light chains (Bosco et al., 2010; De Vos et al., 2007; Vande Velde et al., 2011).

1.2.6 Cellular functions of DENN-domain containing proteins

The DENN (differentially expressed in normal and neoplastic cells) domain, comprised of a N-terminal longin domain, followed by DENN, and d-DENN domains, is a protein module conserved throughout evolution (Marat et al., 2011). In higher eukaryotes, proteins containing DENN-domains comprise a major GDP-GTP exchange factor (GEF) family for Rab GTPases, which are key regulators of membrane traffic pathways within eukaryotic cells (Wu et al., 2011).

In 2011 two groups reported that a (G4C2) repeat expansions in the first intron of the gene named *C9orf72* were a common cause of both familial frontotemporal dementia (FTD) and amyotrophic lateral sclerosis (ALS) (Renton et al., 2011; DeJesus-Hernandez et al., 2011). The encoded protein C9ORF72 was later found to be a potential DENN-type GEF, suggesting that C9ORF72 might be related to a specific Rab-dependent vesicular trafficking process (Zhang et al., 2012; Levine et al., 2013). Although C9ORF72 has been observed to be co-localized with Rab GTPases and was implicated in autophagy and proteasome-dependent processes (Farg et al, 2014), the

normal molecular and cellular function of C9ORF72 remains largely unknown. In **Chapter 2**, I focus on the roles of C9ORF72 and its associated protein SMCR8 in autophagy using knockout and knockdown cell lines.

1.3 C9orf72-ALS/FTD pathological mechanisms and animal models

1.3.1 Pathological mechanisms of C9orf72-ALS/FTD

ALS is the most common motor neuron disease. It is a progressive disease that affects motor neurons in the brain and spinal cord (Hardiman et al., 2017). Frontotemporal dementia is a group of brain disorders that affect the frontal and temporal lobes of the brain. Symptoms include changes in social behavior, personality, and loss of language skills. The discovery of C9orf72 as the most common genetic mutations for familial ALS and FTD provided a molecular link for these two diseases. While the number of G4C2 repeat units in the DNA of healthy individuals is up to 25, the number of repeats in the DNA of ALS and FTD patients is usually 400 to several thousands (Leko et al., 2019, Rohrer et al., 2015).

The leading hypothesis in the field for the disease mechanism was gain of toxicity from the expanded repeats. The corresponding repeat-containing sense and antisense transcripts cause a gain of toxicity through the accumulation of the repeat-containing transcripts that fold into stable structures, forming RNA foci enriched with RNA-binding proteins in the nucleus (DeJesus-Hernandez et al., 2011; Zu et al., 2013; Martier et al., 2019). These RNA foci sequester essential RBPs, impairing their ability to regulate their RNA targets and resulting in a range of RNA misprocessing events. Sense and antisense C9orf72 RNA repeats are translated by an unconventional form of translation,

repeat-associated non-AUG initiated translation (RAN translation), resulting in the synthesis of five dipeptide repeat protein (DPR) species; poly-GA, poly-GP, poly-GR, from the sense transcript and poly-GP, poly-PR and poly-PA, from the antisense transcript (Barker et al., 2017). These DPR disrupt pre-mRNA splicing (Yin et al., 2017), induce nucleocytoplasmic transport defects (Zhang et al., 2015), and increase oxidative stress and DNA damage (Lopez-Gonzalez et al., 2016).

It has also been shown that the expression levels of C9orf72 is reduced in the cerebellum, motor cortex, spinal cord and iPSNs of the C9ALS/FTD patients (Donnelly et al., 2013; Gijselinck et al., 2016), possibly due to histone trimethylation (Belzil et al, 2013) and hypermethylation of C9orf72 promoter (Jackson et al., 2020; Gijselinck et al., 2016). Therefore, it is important to know the normal function of C9orf72 and how the "loss of function" mechanisms interact with "gain of function" mechanisms in the disease condition.

1.3.2 C9orf72 knockout mouse models and their phenotypes

To test the "loss of function" hypothesis, several C9orf72 deficient mouse lines were generated independently by different labs. These C9orf72 knockout mouse models develop severe immune dysregulation. They show visibly enlarged cervical lymph nodes and spleens (O'Rourke et al., 2016; Burberry et al., 2016; Atanasio et al., 2016; Jiang et al., 2016; Shao et al., 2019), and develop a robust immune phenotype characterized by increased expression of inflammatory cytokines (Burberry et al., 2016), myeloid expansion, T cell activation, and increased plasma cells (Atanasio et al., 2016). Moreover, they also show lysosomal accumulation and altered immune responses in macrophages and microglia, with age-related neuroinflammation (Shao et al., 2019;

O'Rourke et al., 2016). However, C9orf72 ablation causes no motor neuron degeneration and no to very mild motor deficit (Koppers et al., 2015; Jiang et al., 2016; Anatasio et al, 2016).

Because C9ORF72 forms a cognate protein complex with SMCR8 (Yang et al., 2016; Ugolino et al., 2016; Amick et al. 2016; Sellier et al. 2016; Sullivan et al. 2016), we generated Smcr8 deficient mouse line. We saw similar immune dysregulation in *Smcr8-/-* mice as *C9orf72-/-* mice, including enlarged spleens and lymph nodes (Shao et al., 2019). Therefore, we hypothesized that C9orf72 and Smcr8 might have similar functions. In **Chapter 3**, I will focus on the role of Smcr8 in the motor system and how loss of C9orf72 in the background of loss of Smcr8 exacerbates the phenotypes of *Smcr8-/-* mice.

1.3.3 C9orf72 gain of function animal models and their phenotypes

Efforts have been made to generate C9orf72 gain of function mouse models using C9orf72 bacterial artificial chromosome (BAC) from C9-ALS/FTD patient DNA. All these mouse models showed RNA foci and poly-dipeptide accumulations (Peters et al., 2015; O'Rourke et al., 2015; Jiang et al., 2016; Liu et al., 2016), but they displayed little to mild neurodegeneration or motor behavioral deficits.

Peter et al. (2015) generated a C9orf72 BAC transgenic mouse line carrying a bacterial artificial chromosome containing exons 1 to 6 of the human C9ORF72 gene with approximately 500 repeats of the GGGGCC motif in the SJL/B6 background. The mice showed no overt behavioral phenotype, including normal survival, motor and cognitive functions, and no signs of neuromuscular junction degeneration, TDP-43 accumulation or gliosis.

O'Rourke et al. (2015) generated transgenic mice carrying a bacterial artificial chromosome (BAC) containing the full human C9orf72 gene with either a normal allele (15 repeats) or disease-associated expansion (~100–1,000 repeats; C9-BACexp) in the C57BL/6J background. Despite early and widespread production of RNA foci and RAN dipeptides in C9-BACexp mice, behavioral abnormalities and neurodegeneration were not observed even at advanced ages, including no abnormalities seen in body weight, neuromuscular junction, grip strength, rotarod, open field testing, memory and novelty-seeking behavior.

Jiang et al. (2016) generated a transgenic mouse line expressing a partial human C9orf72 gene with 450 repeats of (G4C2) in the C57BL6/C3H background. These mice showed age-dependent learning defects and increased anxiety levels. However, they showed no defects in social interaction, novel object recognition or fear conditioning. Importantly, multiple assays revealed no motor deficits or loss of motor neurons.

Liu et al. (2016) generated a BAC mouse model by expressing the full length of the human *C9orf72* gene and a (G4C2)500 repeat in the background of FVB/NJ. Despite a subset (~30%–35%) of the female transgenic mice developing an acute, rapidly progressive disease with hindlimb weakness and denervation of neuromuscular junctions, many of the mice were asymptomatic. This line was on FVB/NJ background, which suggests that the different genetic background could be one underlying cause for the observed phenotypes (Wen et al., 2017).

To unravel the contribution of the "loss of function" mechanisms and the "gain of toxicity" mechanisms in C9-ALS/FTD, we crossed *C9orf72-/-* mice with *C9-BAC* mice. We found that C9orf72 haploinsufficiency exacerbates the motor behavioral deficits

(**Chapter 4**), social behavioral deficits and cognitive deficits (**Chapter 5**) in the *C9-BAC* mice, suggesting that loss of function and gain of toxicity mechanisms are not mutually exclusive and may both contribute to the disease.

1.4 References

Bott, N. T. (2014). Frontotemporal dementia: diagnosis, deficits and management. Neurodegenerative Disease Management. 4:6, 439-454

Young, J. J. (2017). Frontotemporal dementia: latest evidence and clinical implications. Therapeutic Advances in Psychopharmacology. 8:1, 33-48

Talbott, E. O. (2016) The epidemiology of amyotrophic lateral sclerosis. Handbook of Clinical Neurology. 138:225-38

Yedavalli, V. S. (2018) Amyotrophic Lateral Sclerosis and its Mimics/Variants: A Comprehensive Review. Journal of Clinical Imaging Science. 8: 53

DeJesus-Hernandez, M. et al. (2011) Expanded GGGGCC hexanucleotide repeat in noncoding region of C9ORF72 causes chromosome 9p-linked FTD and ALS. Neuron 72, 245–256.

Renton, A. E. et al. (2011) A hexanucleotide repeat expansion in C9ORF72 is the cause of chromosome 9p21-linked ALS–FTD. Neuron 72, 257–268.

Wen, X. et al. (2014) Antisense Proline-Arginine RAN Dipeptides Linked to *C9ORF72*-ALS/FTD Form Toxic Nuclear Aggregates that Initiate In Vitro and In Vivo Neuronal Death. Neuron 84: 6, 1213-1225

May, S. et al. (2014) C9orf72 FTLD/ALS-associated Gly-Ala dipeptide repeat proteins cause neuronal toxicity and Unc119 sequestration. Acta Neuropathol 128, 485–503.

Mizielinska, S. et al. (2014) C9orf72 repeat expansions cause neurodegeneration in Drosophila through arginine-rich proteins. Science. Sep 5;345(6201):1192-1194

Mizushima, N. & Komatsu, M. (2011) Autophagy: Renovation of Cells and Tissues. Cell. Nov 11, 147(4):728-741

Shibutani, S. et al. (2015) Autophagy and autophagy-related proteins in the immune system. Nat Immunol 16, 1014–1024. https://doi.org/10.1038/ni.3273

Hollenstein, D. & Kraft, C. (2020) Autophagosomes are formed at a distinct cellular structure. Current Opinion in Cell Biology. Volume 65, August 2020, Pages 50-57

Nakamura, S. & Yoshimori, T. (2017) New insights into autophagosome-lysosome fusion. Journal of Cell Science. 130: 1209-1216; doi: 10.1242/jcs.196352

Tanida, I. et al. (2005) Lysosomal Turnover, but Not a Cellular Level, of Endogenous LC3 is a Marker for Autophagy, Autophagy, 1:2, 84-91, DOI: 10.4161/auto.1.2.1697

Hosokawa, N. et al. (2009) Nutrient-dependent mTORC1 association with the ULK1-Atg13-FIP200 complex required for autophagy. Mol Biol Cell. Apr; 20(7):1981-91.

Ganley, I.G. et al. (2009) ULK1.ATG13.FIP200 complex mediates mTOR signaling and is essential for autophagy. J Biol Chem. May 1; 284(18):12297-305.

Jung, C.H. et al. (2009) ULK-Atg13-FIP200 complexes mediate mTOR signaling to the autophagy machinery. Mol Biol Cell. Apr; 20(7):1992-2003.

Chan, E.Y. et al. (2007) siRNA screening of the kinome identifies ULK1 as a multidomain modulator of autophagy. J Biol Chem. Aug 31; 282(35):25464-74.

Chang Y.Y. & Neufeld T.P. (2009) An Atg1/Atg13 complex with multiple roles in TOR-mediated autophagy regulation. Mol Biol Cell. Apr; 20(7):2004-14.

Hara T. (2008) FIP200, a ULK-interacting protein, is required for autophagosome formation in mammalian cells. J Cell Biol. May 5; 181(3):497-510.

Sebastian A., et al. (2011) Role of AMPK-mTOR-Ulk1/2 in the Regulation of Autophagy: Cross Talk, Shortcuts, and Feedbacks. Molecular and Cellular Biology Dec 2011, 32 (1) 2-11; DOI: 10.1128/MCB.06159-11

Yoshii, S.R. & Mizushima, N. (2017) Monitoring and Measuring Autophagy. Int. J. Mol. Sci. 18, 1865.

Mizushima, N., et al. (2010) Methods in Mammalian Autophagy Research. Cell. 140:3, 313-326

Mizushima, N. (2007) Autophagy: process and function. Genes Dev. Nov 15; 21(22):2861-73.

Nakatogawa H., et al. (2009) Dynamics and diversity in autophagy mechanisms: lessons from yeast. Nat Rev Mol Cell Biol. Jul; 10(7):458-67.

Barth, S., et al. (2010), Autophagy: assays and artifacts. J. Pathol., 221: 117-124. doi:10.1002/path.2694

Kabeya, Y., et al. (2000) LC3, a mammalian homologue of yeast Apg8p, is localized in autophagosome membranes after processing. EMBO J. Nov 1; 19(21):5720-8.

Liu, W.J., et al. (2016) p62 links the autophagy pathway and the ubiqutin–proteasome system upon ubiquitinated protein degradation. Cell Mol Biol Lett 21, 29.

Pankiv, S., et al. (2007) p62/SQSTM1 Binds Directly to Atg8/LC3 to Facilitate Degradation of Ubiquitinated Protein Aggregates by Autophagy. The Journal of Biological Chemistry 282, 24131-24145

Shuhei N. & Tamotsu Y. (2017) New insights into autophagosome–lysosome fusion.

Journal of Cell Science 130: 1209-1216; doi: 10.1242/jcs.196352

Berg, T. O., et al. (1998) Isolation and characterization of rat liver amphisomes. Evidence for fusion of autophagosomes with both early and late endosomes. J. Biol. Chem. 273, 21883-21892.

Fader, C. M., et al. (2008) Induction of autophagy promotes fusion of multivesicular bodies with autophagic vacuoles in k562 cells. Traffic 9, 230-250. doi:10.1111/j.1600-0854.2007.00677.x

Xiu-Tang Cheng, Yu-Xiang Xie, Bing Zhou, Ning Huang, Tamar Farfel-Becker & Zu-Hang Sheng (2018) Revisiting LAMP1 as a marker for degradative autophagy-lysosomal organelles in the nervous system, Autophagy, 14:8, 1472-1474, DOI: 10.1080/15548627.2018.1482147

Xiu-Tang Cheng, Yu-Xiang Xie, Bing Zhou, Ning Huang, Tamar Farfel-Becker, Zu-Hang Sheng; Characterization of LAMP1-labeled nondegradative lysosomal and endocytic compartments in neurons. J Cell Biol 3 September 2018; 217 (9): 3127–3139. doi: https://doi.org/10.1083/jcb.201711083

Christopher C. Kemball, Mehrdad Alirezaei, Claudia T. Flynn, Malcolm R. Wood, Stephanie Harkins, William B. Kiosses, J. Lindsay Whitton (2010) Coxsackievirus Infection Induces Autophagy-Like Vesicles and Megaphagosomes in Pancreatic Acinar Cells In Vivo. Journal of Virology Nov 2010, 84 (23) 12110-12124; DOI: 10.1128/JVI.01417-10

Mayurbhai Himatbhai Sahani, Eisuke Itakura & Noboru Mizushima (2014) Expression of the autophagy substrate SQSTM1/p62 is restored during prolonged starvation

depending on transcriptional upregulation and autophagy-derived amino acids, Autophagy, 10:3, 431-441, DOI: 10.4161/auto.27344

Hundeshagen, P., Hamacher-Brady, A., Eils, R. et al. Concurrent detection of autolysosome formation and lysosomal degradation by flow cytometry in a high-content screen for inducers of autophagy. BMC Biol 9, 38 (2011). https://doi.org/10.1186/1741-7007-9-38

Ana Lopez, Angeleen Fleming and David C. Rubinsztein 2018 Seeing is believing: methods to monitor vertebrate autophagy in vivo. Open Biol.8180106. http://doi.org/10.1098/rsob.180106

Kumsal Ayse Tekirdag, Gozde Korkmaz, Deniz Gulfem Ozturk, Reuven Agami & Devrim Gozuacik (2013) MIR181A regulates starvation- and rapamycin-induced autophagy through targeting of ATG5, Autophagy, 9:3, 374-385, DOI: 10.4161/auto.23117

Caroline Mauvezin & Thomas P Neufeld (2015) Bafilomycin A1 disrupts autophagic flux by inhibiting both V-ATPase-dependent acidification and Ca-P60A/SERCA-dependent autophagosome-lysosome fusion, Autophagy, 11:8, 1437-1438, DOI: 10.1080/15548627.2015.1066957

Yang, Y., Hu, L., Zheng, H. et al. Application and interpretation of current autophagy inhibitors and activators. Acta Pharmacol Sin 34, 625–635 (2013). https://doi.org/10.1038/aps.2013.5

Steven L. Jones and Tatyana M. Svitkina. Axon Initial Segment Cytoskeleton: Architecture, Development, and Role in Neuron Polarity. Neural Plasticity. Volume 2016 |Article ID 6808293 | 19 pages | https://doi.org/10.1155/2016/6808293

Fabricius, C., Berthold, C. H. & Rydmark, M. Dimensions of individual alpha and gamma motor fibres in the ventral funiculus of the cat spinal cord. J Anat 184 (Pt 2), 319–333 (1994).

Maday S. et al. (2014) Axonal Transport: Cargo-Specific Mechanisms of Motility and Regulation. Volume 84, Issue 2, Pages 292-309

Pedro Guedes-dias, Erika L. F. Holzbaur (2019) Axonal transport: Driving synaptic function. Vol. 366, Issue 6462, eaaw9997. DOI: 10.1126/science.aaw9997

Swetha Gowrishankar, Peng Yuan, Yumei Wu, Matthew Schrag, Summer Paradise, Jaime Grutzendler, Pietro De Camilli, Shawn M. Ferguson (2015) Massive accumulation of luminal protease-deficient axonal lysosomes at Alzheimer's disease amyloid plaques. Proceedings of the National Academy of Sciences 112 (28) E3699-E3708; DOI: 10.1073/pnas.1510329112

Lasek, R. J., Garner, J. A. & Brady, S. T. Axonal transport of the cytoplasmic matrix. J. Cell Biol. 99, 212s–221s (1984).

Millecamps, S., Julien, J. Axonal transport deficits and neurodegenerative diseases. Nat Rev Neurosci 14, 161–176 (2013). https://doi.org/10.1038/nrn3380

Salehi A. et al. (2006) Increased App Expression in a Mouse Model of Down's Syndrome Disrupts NGF Transport and Causes Cholinergic Neuron Degeneration. VOLUME 51, ISSUE 1, P29-42

Bosco, D. A. et al. Wild-type and mutant SOD1 share an aberrant conformation and a common pathogenic pathway in ALS. Nature Neurosci. 13, 1396–1403 (2010).

De Vos, K. J. et al. Familial amyotrophic lateral sclerosis-linked SOD1 mutants perturb fast axonal transport to reduce axonal mitochondria content. Hum. Mol. Genet. 16, 2720–2728 (2007).

Vande Velde, C. et al. Misfolded SOD1 associated with motor neuron mitochondria alters mitochondrial shape and distribution prior to clinical onset. PLoS ONE 6, e22031 (2011).

Nixon, R. The role of autophagy in neurodegenerative disease. Nat Med 19, 983–997 (2013). https://doi.org/10.1038/nm.3232

Nobuhiro, F. et al. (2018) Association Between Autophagy and Neurodegenerative Diseases. Frontiers in Neuroscience. 12, 255. 10.3389/fnins.2018.00255

Nixon, R.A., Wegiel, J., Kumar, A., Yu, W.H., Peterhoff, C., Cataldo, A., and Cuervo, A.M. (2005). Extensive involvement of autophagy in Alzheimer disease: an immuno-electron microscopy study. J. Neuropathol. Exp. Neurol. 64, 113-122.

Lee, J.H., Yu, W.H., Kumar, A., Lee, S., Mohan, P.S., Peterhoff, C.M., Wolfe, D.M., Martinez-Vicente, M., Massey, A.C., Sovak, G., et al. (2010). Lysosomal proteolysis and autophagy require presenilin 1 and are disrupted by Alzheimer-related PS1 mutations. Cell 141, 1146-1158.

Pickford, F., Masliah, E., Britschgi, M., Lucin, K., Narasimhan, R., Jaeger, P. A., et al. (2008). The autophagy-related protein beclin 1 shows reduced expression in early Alzheimer disease and regulates amyloid beta accumulation in mice. J. Clin. Invest. 118, 2190–2199. doi: 10.1172/jci33585

Andersen, P.M., and Al-Chalabi, A. (2011). Clinical genetics of amyotrophic lateral sclerosis: what do we really know? Nat. Rev. Neurol. 7, 603-615.

Martinez-Vicente, M., Talloczy, Z., Wong, E., Tang, G., Koga, H., Kaushik, S., de Vries, R., Arias, E., Harris, S., Sulzer, D., et al. (2010). Cargo recognition failure is responsible for inefficient autophagy in Huntington's disease. Nat. Neurosci. 13, 567-576.

Marat, A. et al. (2011) DENN Domain Proteins: Regulators of Rab GTPases. The Journal of Biological Chemistry. 286, 13791-13800. doi: 10.1074/jbc.R110.217067

Xudong Wu, Michael J. Bradley, Yiying Cai, Daniel Kümmel, Enrique M. De La Cruz, Francis A. Barr, Karin M. Reinisch. Insights regarding guanine nucleotide exchange from the structure of a DENN-domain protein complexed with its Rab GTPase substrate Proceedings of the National Academy of Sciences Nov 2011, 108 (46) 18672-18677; DOI: 10.1073/pnas.1110415108

Alan E. Renton et al. (2011) A Hexanucleotide Repeat Expansion in C9ORF72 Is the Cause of Chromosome 9p21-Linked ALS-FTD. Neuron. 72 (2) 257-268; doi.org/10.1016/j.neuron.2011.09.010.

DeJesus-Hernandez, M. et al. (2011) Expanded GGGGCC Hexanucleotide Repeat in Noncoding Region of C9ORF72 Causes Chromosome 9p-Linked FTD and ALS. Neuron. VOLUME 72, ISSUE 2, P245-256.

Zhang Dapeng, Iyer Lakshminarayan, He Fang, Aravind L. (2012) Discovery of Novel DENN Proteins: Implications for the Evolution of Eukaryotic Intracellular Membrane Structures and Human Disease. Frontiers in Genetics. 3, 283. DOI=10.3389/fgene.2012.00283

Timothy P. Levine, Rachel D. Daniels, Alberto T. Gatta, Louise H. Wong, Matthew J. Hayes. The product of C9orf72, a gene strongly implicated in neurodegeneration, is

structurally related to DENN Rab-GEFs, Bioinformatics, Volume 29, Issue 4, 15 February 2013, Pages 499–503, https://doi.org/10.1093/bioinformatics/bts725

Manal A. Farg, Vinod Sundaramoorthy, Jessica M. Sultana, Shu Yang, Rachel A.K. Atkinson, Vita Levina, Mark A. Halloran, Paul A. Gleeson, Ian P. Blair, Kai Y. Soo, Anna E. King, Julie D. Atkin, C9ORF72, implicated in amytrophic lateral sclerosis and frontotemporal dementia, regulates endosomal trafficking, Human Molecular Genetics, Volume 23, Issue 13, 1 July 2014, Pages 3579–3595, https://doi.org/10.1093/hmg/ddu068

Mirjana Babić Leko et al. (2019) Molecular Mechanisms of Neurodegeneration Related to C9orf72 Hexanucleotide Repeat Expansion. Behavioural Neurology. Volume 2019 |Article ID 2909168 | 18 pages.

Rohrer et al. (2015) C9orf72 expansions in frontotemporal dementia and amyotrophic lateral sclerosis. Lancet Neurol 2015; 14: 291–301.

Zu T. et al. (2013) RAN proteins and RNA foci from antisense transcripts in C9ORF72 ALS and frontotemporal dementia. Proc. Natl. Acad. Sci. USA. 2013; 110: E4968-E4977

Martier R. et al. (2019) Targeting RNA-Mediated Toxicity in C9orf72 ALS and/or FTD by RNAi-Based Gene Therapy. Molecular Therapy Nucleic Acids. VOLUME 16, P26-37, JUNE 07, 2019

Barker Holly V., Niblock Michael, Lee Youn-Bok, Shaw Christopher E., Gallo Jean-Marc. (2017) RNA Misprocessing in C9orf72-Linked Neurodegeneration. Frontiers in Cellular Neuroscience. 11:195. DOI=10.3389/fncel.2017.00195

Yin S. et al. (2017) Evidence that C9ORF72 Dipeptide Repeat Proteins Associate with U2 snRNP to Cause Mis-splicing in ALS/FTD Patients. Cell Reports. VOLUME 19, ISSUE 11, P2244-2256, JUNE 13, 2017

Zhang K. et al., The C9orf72 repeat expansion disrupts nucleocytoplasmic transport. Nature. 2015; 525: 56-61

Rodrigo Lopez-Gonzalez et al. Poly(GR) in C9ORF72-Related ALS/FTD Compromises Mitochondrial Function and Increases Oxidative Stress and DNA Damage in iPSC-Derived Motor Neurons. Neuron. 2016 Oct 19;92(2):383-391. doi: 10.1016/j.neuron.2016.09.015. Epub 2016 Oct 6.

Donnelly C. J. et al. (2013) RNA Toxicity from the ALS/FTD C9ORF72 Expansion Is Mitigated by Antisense Intervention. Neuron. Volume 80, Issue 2, 16 October 2013, Pages 415-428

Belzil, V.V., Bauer, P.O., Prudencio, M. et al. Reduced C9orf72 gene expression in c9FTD/ALS is caused by histone trimethylation, an epigenetic event detectable in blood. Acta Neuropathol 126, 895–905 (2013). https://doi.org/10.1007/s00401-013-1199-1

Hardiman, O., Al-Chalabi, A., Chio, A. et al. Amyotrophic lateral sclerosis. Nat Rev Dis Primers 3, 17071 (2017). https://doi.org/10.1038/nrdp.2017.71

Koppers, M., Blokhuis, A.M., Westeneng, H.-J., Terpstra, M.L., Zundel, C.A.C., Vieira de Sá, R., Schellevis, R.D., Waite, A.J., Blake, D.J., Veldink, J.H., van den Berg, L.H. and Pasterkamp, R.J. (2015), C9orf72 ablation in mice does not cause motor neuron degeneration or motor deficits. Ann Neurol., 78: 426-438. doi:10.1002/ana.24453

J. G. O'ROURKE et al. C9orf72 is required for proper macrophage and microglial function in mice. SCIENCE18 MAR 2016 : 1324-1329

AARON BURBERRY et al. Loss-of-function mutations in the C9ORF72 mouse ortholog cause fatal autoimmune disease. SCIENCE TRANSLATIONAL MEDICINE13 JUL 2016 : 347RA93

Atanasio, A., Decman, V., White, D. et al. C9orf72 ablation causes immune dysregulation characterized by leukocyte expansion, autoantibody production and glomerulonephropathy in mice. Sci Rep 6, 23204 (2016). https://doi.org/10.1038/srep23204

Amick J, Roczniak-Ferguson A, Ferguson SM. 2016. C9orf72 binds SMCR8, localizes to lysosomes, and regulates mTORC1 signaling. Mol Biol Cell 27: 3040–3051.

Sellier C, Campanari ML, Julie Corbier C, Gaucherot A, Kolb-Cheynel I, Oulad-Abdelghani M, Ruffenach F, Page A, Ciura S, Kabashi E, et al. 2016. Loss of C9ORF72 impairs autophagy and synergizes with polyQ Ataxin-2 to induce motor neuron dysfunction and cell death. EMBO J 35: 1276–1297.

Sullivan PM, Zhou X, Robins AM, Paushter DH, Kim D, Smolka MB, Hu F. 2016. The ALS/FTLD associated protein C9orf72 associates with SMCR8 and WDR41 to regulate the autophagy-lysosome pathway. Acta Neuropathol Commun 4: 51.

Ugolino J, Ji YJ, Conchina K, Chu J, Nirujogi RS, Pandey A, Brady NR, Hamacher-Brady A, Wang J. 2016. Loss of C9orf72 enhances autophagic activity via deregulated mTOR and TFEB signaling. PLoS Genet 12: e1006443.

Yang M, Liang C, Swaminathan K, Herrlinger S, Lai F, Shiekhattar R, Chen JF. 2016. A C9ORF72/SMCR8-containing complex regulates ULK1 and plays a dual role in autophagy. Sci Adv 2: e1601167.

Qiang Shao, Mei Yang, Chen Liang, Li Ma, Wei Zhang, Zhiwen Jiang, Jun Luo, Jae-Kyung Lee, Chengyu Liang & Jian-Fu Chen (2019) C9orf72 and smcr8 mutant mice reveal MTORC1 activation due to impaired lysosomal degradation and exocytosis, Autophagy, DOI: 10.1080/15548627.2019.1703353

Wen X. et al. (2017) Pathogenic determinants and mechanisms of ALS/FTD linked to hexanucleotide repeat expansions in the C9orf72 gene. Neuroscience Letters. Volume 636, 1 January 2017, Pages 16-26

De Jager, P.L., Yang, H. & Bennett, D.A. Deconstructing and targeting the genomic architecture of human neurodegeneration. Nat Neurosci 21, 1310–1317 (2018). https://doi.org/10.1038/s41593-018-0240-z

Gijselinck I., on behalf of the BELNEU CONSORTIUM13, Van Mossevelde S., et al. The C9orf72 repeat size correlates with onset age of disease, DNA methylation and transcriptional downregulation of the promoter. Molecular Psychiatry. 2016;21(8):1112–1124. doi: 10.1038/mp.2015.159.

Jackson, J.L., Finch, N.A., Baker, M.C. et al. Elevated methylation levels, reduced expression levels, and frequent contractions in a clinical cohort of C9orf72 expansion carriers. Mol Neurodegeneration 15, 7 (2020). https://doi.org/10.1186/s13024-020-0359-8

CHAPTER 2

A C9ORF72/SMCR8-containing complex regulates ULK1 and plays a dual role in autophagy

Mei Yang*, Chen Liang*, Kunchithapadam Swaminathan, Stephanie Herrlinger, Fan Lai, Ramin Shiekhattar and Jian-Fu Chen. Science Advances S02 SEP 2016 : E1601167 (*Co-first author).
Reprinted here with permission of the publisher.
URL: https://advances.sciencemag.org/content/2/9/e1601167

Abstract

The intronic GGGGCC hexanucleotide repeat expansion in chromosome 9 open reading frame 72 (C9ORF72) is a prevalent genetic abnormality identified in both frontotemporal dementia (FTD) and amyotrophic lateral sclerosis (ALS). Smith-Magenis syndrome chromosomal region candidate gene 8 (SMCR8) is a protein with unclear functions. We report that C9ORF72 is a component of a multiprotein complex containing SMCR8, WDR41, and ATG101 (an important regulator of autophagy). The C9ORF72 complex displays guanosine triphosphatase (GTPase) activity and acts as a guanosine diphosphate–guanosine 5′-triphosphate (GDP-GTP) exchange factor (GEF) for RAB39B. We created Smcr8 knockout mice and found that Smcr8 mutant cells exhibit impaired autophagy induction, which is similarly observed in C9orf72 knockdown cells. Mechanistically, SMCR8/C9ORF72 interacts with the key autophagy initiation ULK1 complex and regulates expression and activity of ULK1. The complex has an additional role in regulating later stages of autophagy. Whereas autophagic flux is enhanced in C9orf72 knockdown cells, depletion of Smcr8 results in a reduced flux with an abnormal expression of lysosomal enzymes. Thus, C9ORF72 and SMCR8 have similar functions in modulating autophagy induction by regulating ULK1 and play distinct roles in regulating autophagic flux.

Introduction

Frontotemporal dementia (FTD) and amyotrophic lateral sclerosis (ALS) are neurodegenerative disorders leading to dementia and loss of motor coordination (1, 2). The aberrant regulation of RNA and protein metabolism has been suggested to underlie the pathogenesis of these diseases (3). An expanded hexanucleotide repeat (GGGGCC) in a noncoding region of chromosome 9 open reading frame 72 (C9ORF72) has been identified as the most common cause of familial FTD and ALS (4–7). Proposed mechanisms of disease onset include RNA toxicity due to accumulation of transcripts containing the GGGGCC repeat, accumulation of aberrantly expressed peptides, and C9ORF72 loss of function (8–17). Knockout of C9orf72 in mice does not result in neurodegeneration but instead causes defects in macrophage and microglial function (18–20), suggesting that loss of function of C9orf72 alone is not sufficient to cause FTD-ALS. However, C9ORF72 mRNA levels are reduced in FTD-ALS patients, and microglial dysfunction is tightly connected with FTD-ALS pathogenesis (4, 6, 18, 21, 22). These studies raise the possibility that haploinsufficiency of C9ORF72 could contribute to FTD-ALS diseases. It is important to understand the cellular functions of C9ORF72 and its mechanisms of action.

Autophagy is an evolutionarily conserved process characterized by engulfing cytoplasmic proteins or organelles into double-membrane vesicles called autophagosomes, which fuse with lysosomes to form autolysosomes primed for degradation (23–25). Autophagy is essential for cellular homeostasis because it

removes aggregates of misfolded proteins and/or defective organelles, provides energy, and recycles cellular components (25). Autophagy is a highly regulated and multistep process (24, 25), and its deregulation has been implicated in a variety of neurodegenerative diseases including FTD, ALS, Parkinson's, Alzheimer's, and Huntington's disease (26, 27). ULK1, a mammalian homolog of autophagy-related 1 (Atg1), forms a protein complex with FIP200, ATG13, and ATG101 to control autophagy initiation. After the initiation, Atg proteins are recruited to a membrane structure called the phagophore, which expands and fuses upon itself to form the autophagosome. The autophagosome is directed to and fuses with a lysosome, where the enclosed materials are degraded. Subsequently, the nutrients are released back into the cytosol for reuse. Accumulating evidence suggests that autophagy impairment at distinct regulatory steps may have different consequences for the pathogenesis of neurodegenerative diseases (26, 27). Therefore, it is crucial to understand the nature of defects in autophagy in individual neurodegenerative diseases.

Rab guanosine triphosphatases (GTPases) encode information about the state of membrane domains to control specific membrane trafficking events (28). Rabs are activated by specific guanine nucleotide exchange factors (GEFs). One of the emerging families of GEFs contains DENN (differentially expressed in normal and neoplastic cell) domains (29, 30). DENN domain–containing GEFs catalyze the dissociation of guanosine diphosphate (GDP) from the Rab GTPase followed by guanosine 5′-triphosphate (GTP) exchange. The GTP-bound Rab is then activated and recruits its effectors to regulate membrane trafficking. Bioinformatics studies predict that C9ORF72

contains DENN domains (31, 32), suggesting its potential functions in membrane trafficking as a GEF factor. Indeed, it has been reported that C9ORF72 is associated with RAB1, RAB5, RAB7, and RAB11, and is involved in endocytosis and autophagy (33). A recent study shows that C9ORF72 functions as a GEF for RAB8A and RAB39B, and its depletion has a partial deleterious effect on autophagy (34). Despite these progresses, the specific steps C9ORF72 regulates in autophagy and the molecular mechanisms by which C9ORF72 confers this regulation remain unclear.

To gain insights into the biology of the C9ORF72 protein, we isolated C9ORF72-containing complexes from human cells and characterized their functions. We found that C9ORF72 forms a protein complex with Smith-Magenis syndrome chromosomal region candidate gene 8 (SMCR8). Although it has been implicated in autophagy (35), the experimental evidence of SMCR8 functions is lacking. SMCR8 is also predicted to contain DENN domains and exhibits some homology with C9ORF72 (31, 32). We created Smcr8 knockout mice and found that mutant cells exhibit impaired autophagy induction, which is likewise observed in C9orf72 knockdown cells. Our mechanistic studies show that C9ORF72/SMCR8 interacts with the key autophagy initiation ULK1 complex, and the interaction is enhanced under starvation conditions. C9ORF72/SMCR8 regulates the expression and activity of ULK1. Furthermore, we identified unique roles for this complex at the later stage of autophagy. Whereas autophagic flux is enhanced in C9orf72 knockdown cells, depletion of Smcr8 leads to a reduced flux with an abnormal expression of lysosomal enzymes. Thus, C9ORF72 and SMCR8 have similar functions in modulating autophagy induction by regulating ULK1 and play distinct roles in regulating autophagic flux.

Materials and Methods

Affinity purification of Flag-C9ORF72, Flag-SMCR8, and Flag-WDR41

Expression constructs for Flag-C9ORF72, Flag-SMCR8, and Flag-WDR41 were individually cotransfected with a puromycin resistance plasmid into HEK293 cells. Protein complexes were purified (50 to 150 mg) from cytoplasmic extract (S100) with anti-Flag M2 affinity gel (Sigma). Two washes were performed using buffer A [20 mM tris-HCl (pH 7.9), 0.5 M KCl, 10% glycerol, 1 mM EDTA, 5 mM dithiothreitol (DTT), 0.2 mM phenylmethylsulfonyl fluoride (PMSF), 0.5% NP-40] followed by one wash with buffer B [20 mM tris-HCl (pH 7.9), 0.1 M KCl, 10% glycerol, 1 mM EDTA, 5 mM DTT, 0.2 mM PMSF]. Then, the affinity column was eluted with Flag peptide (400 μg/ml). Proteins were further separated with Superose 6 gel filtration chromatography. Fractions were examined by SDS-PAGE analysis, and fractions containing C9ORF72/SMCR8 were combined and concentrated with Millipore Amicon Ultra (100K). Purified proteins were snap-frozen in liquid nitrogen and stored at −80°C.

Generation of $Smcr8^{\beta geo/\beta geo}$ mutant mice

The $Smcr8^{tm1(KOMP)Vlcg}$ ES cells were obtained from the University of California, Davis, Knockout Mouse Project Repository. Smcr8 locus is partially replaced by a cassette containing lacZ-polyA followed by a loxP-flanked hUbCpro-neo-polyA sequence. The Mouse Genetic Core Facility at National Jewish Health at Denver, CO, performed the ES cell injections into C57BL/6N blastocysts. The chimeric offsprings were mated to 129S1/SvImJ mice for germline transmission; germline-transmitted heterozygous females were crossed with CMV-Cre males to remove the Neo cassette. The PCR

primers used for genotyping are as follows: LacF, acttgctttaaaaaacctcccaca; Smcr8-R, tgaacgaagactgctgtgtttaccc; Smcr8-wtR, gtcagtgttttccactccgaagtcc; and Smcr8-wtF, agaagcctatgcggataatgagggg. All animals were handled according to protocols approved by the Institutional Animal Care and Use Committee at the University of Georgia, Athens.

Constructs

For RFP-SMCR8, the SMCR8 gene was cloned into the pTag-RFP-N vector using the primers ggctcgagatgatcagcgcccctgac and ccgaattcggattttatacaaaaagct. For RFP-WDR41, the WDR41 gene was cloned into the pTag-RFP-N vector using the primers ggctcgagatgttgcgatggctgatc and ccgaattcggacagcaaggtataagtc. For the GFP-C9ORF72, the C9ORF72 gene was cloned into the pCAG–enhanced GFP vector using the primers gaattcatgtcgactctttgccca and ggtaccgtaaaagtcattagaacatc. For His-RAB39B, the RAB39B gene was cloned into the His vector using the primers aactcgaggaggccatctggctgtacca and ttaagcttctagcacaaacatctcctct. C9orf72 shRNA constructs were derived from the pLKO.1 vector using the targeting sequence gtgcagagaaagtaaataa and ggcctacactctttcatct. SMCR8 shRNA constructs were derived from the pLKO.1 vector using the targeting sequences ttacttctctttgcggattat and caagagctctcggccgaattt.

Antibodies

The following antibodies were used: rabbit anti-C9ORF72 (sc-138763, Santa Cruz Biotechnology), rabbit anti-SMCR8 (ab121682, Abcam), rabbit anti-WDR41 (sc-137922, Santa Cruz Biotechnology), rabbit anti-ATG101 (SAB4200175, Sigma), rabbit anti-ATG13 (13468, Cell Signaling), rabbit anti-ULK1 (8054, Cell Signaling), rabbit anti–phospho-ULK1 (6888, Cell Signaling), rabbit anti-p62 (5114, Cell Signaling), rabbit anti-RFP (R10367, Invitrogen), mouse anti-LC3 (0231-100/LC3-5F10, Nanotools), rabbit anti-LC3 (PM036, MBL), mouse anti–cathepsin D (AF1029, R&D Systems), rat anti–cathepsin L (MAB9521, R&D Systems).

GEF assay

For loading with GDP, 1 μM His-RAB39B protein in 110 mM NaCl, 50 mM tris-HCl (pH 8.0), 1 mM EDTA, 0.8 mM DTT, and 0.005% Triton X-100 was incubated with 50 μM BODIPY-GDP (Invitrogen) for 60 min at 30°C. Then, 0.1 μM preloaded RAB39B proteins were incubated with 7.5 nM C9ORF72 complex or control without C9ORF72 complex in the buffer containing 110 mM NaCl, 50 mM tris-HCl (pH 8.0), 12 mM MgCl2, 0.8 mM DTT, and 2 mM GDP solution for 7 min. As a positive control, preloaded RAB39B was incubated with 20 mM EDTA in the above solution. The fluorescence intensity was recorded with Synergy H4 Hybrid Multi-Mode Microplate Reader. The fluorescence intensity after equilibration with excess EDTA was defined as 100% exchange.

MEF isolation

MEFs were isolated from E15.5 wild-type and Smcr8 mutant embryos, as described (63), and cultured in Dulbecco's modified Eagle's medium (DMEM) with 15% fetal bovine serum (FBS) and penicillin/streptomycin (50 μg/ml).

Cell culture and lentivirus infection

To knock down SMCR8 in HEK293 cells or C9orf72 in N2A cells, cells were cultured in DMEM with 10% FBS plus penicillin/streptomycin (50 μg/ml). Around 60% confluent, cells were infected by lentiviruses expressing SMCR8 or C9orf72 shRNA followed by puromycin (2 μg/ml) selection for 72 hours before experiments. To examine autophagsome numbers or autophagic flux, GFP-LC3 or mCherry-GFP-LC3 plasmids were transfected into HEK293 or N2A cells using jetPRIME transfection reagents after puromycin (2 μg/ml) selection for 48 hours. Twenty-four hours after plasmid transfection, cells were fixed with 4% paraformaldehyde followed by immunostaining using antibodies against GFP or mCherry. For starvation, ~80% confluent, MEFs were infected by lentiviruses expressing C9orf72 shRNA followed by puromycin (2 μg/ml) selection for 72 hours before experiments. Smcr8 mutant or C9orf72 knockdown MEFs were cultured in DMEM with 15% FBS, washed with PBS, and then cultured in amino acid–free DMEM (United States Biological) for 3.5 hours before immunostaining using antibodies against LC3 (PM036, MBL). To induce autophagy with rapamycin, Smcr8 mutant or C9orf72 knockdown MEFs cultured in DMEM with 15% FBS were treated with rapamycin (0.1 μM) for 3.5 hours before protein lysate collection. To monitor the effects of blocking lysosomal degradation, Smcr8 mutant or C9orf72 knockdown MEFs were

treated with lysosome inhibitors (LP) (100 μM each) for 3.5 hours before protein lysate collection.

Immunoprecipitation

HEK293 or N2A cells were transfected with plasmids, as indicated in the figures, and cultured for 36 hours before protein lysate collection. Cells were lysed in lysis buffer [50 mM tris-HCl (pH 7.4), 150 mM NaCl, 1 mM EDTA, 1% Triton X-100, and 1 tablet protease inhibitor (Roche) per 10 ml]. Cell debris was pelleted at 12,500 rpm for 10 min at 4°C, and the supernatant was incubated with primary antibodies overnight at 4°C. The lysates with antibodies were incubated with M2 or anti-GFP beads for 2 hours, followed by washing of the immunoprecipitates three times with lysis buffer and elution of bound proteins in SDS-PAGE sampling buffer at 100°C for 10 min. Western blots were performed using the antibodies described above.

Results

C9ORF72 forms a protein complex with SMCR8, WDR41, and ATG101

We developed a human embryonic kidney (HEK) 293 cell–derived stable cell line expressing Flag-C9ORF72 protein. The cytoplasmic extract enriched for the Flag-C9ORF72 protein was affinity-purified using Flag resin to examine C9ORF72-associated proteins. A Flag–green fluorescent protein (GFP) HEK293 stable cell line was used as a control. Flag-C9ORF72 affinity eluate was subjected to SDS–polyacrylamide gel electrophoresis (SDS-PAGE) followed by silver staining (Fig. 1A). The C9ORF72 eluate was enriched for several proteins in association with C9ORF72. The individual bands were extracted from the gel and subjected to mass spectrometry. This analysis revealed the identification of SMCR8, WDR41, and ATG101 proteins with similar peptide coverage (~60%) to that of C9ORF72, reflecting a near-stoichiometric presence (Fig. 2.1A and table 2.S1). The ULK1/FIP200/ATG13/ATG101 protein complex controls autophagy initiation (36–38). ATG101 is a binding partner of ATG13, interacts with ULK1, and regulates autophagy (39, 40). Mass spectrometry analysis of C9ORF72-associated proteins identified ATG13 and ULK1 with the coverage of ~26 and ~32%, respectively (table 2.S1). Proteins at 68, 55, and 50 kD were respectively identified as SKB1, α-tubulin, and MEP50, which are common contaminants of Flag affinity purification (Fig. 2.1A, Flag-GFP, shown as asterisks). Together, these results suggest that C9ORF72, SMCR8, WDR41, and ATG101 form a protein complex, which is associated with the ULK1 complex and is potentially involved in autophagy.

Next, we subjected the cytoplasmic Flag-C9ORF72 affinity eluate to size exclusion chromatography. After analysis of column fractions using silver stain and

Figure. 2.1. Isolation of C9ORF72-associated proteins.

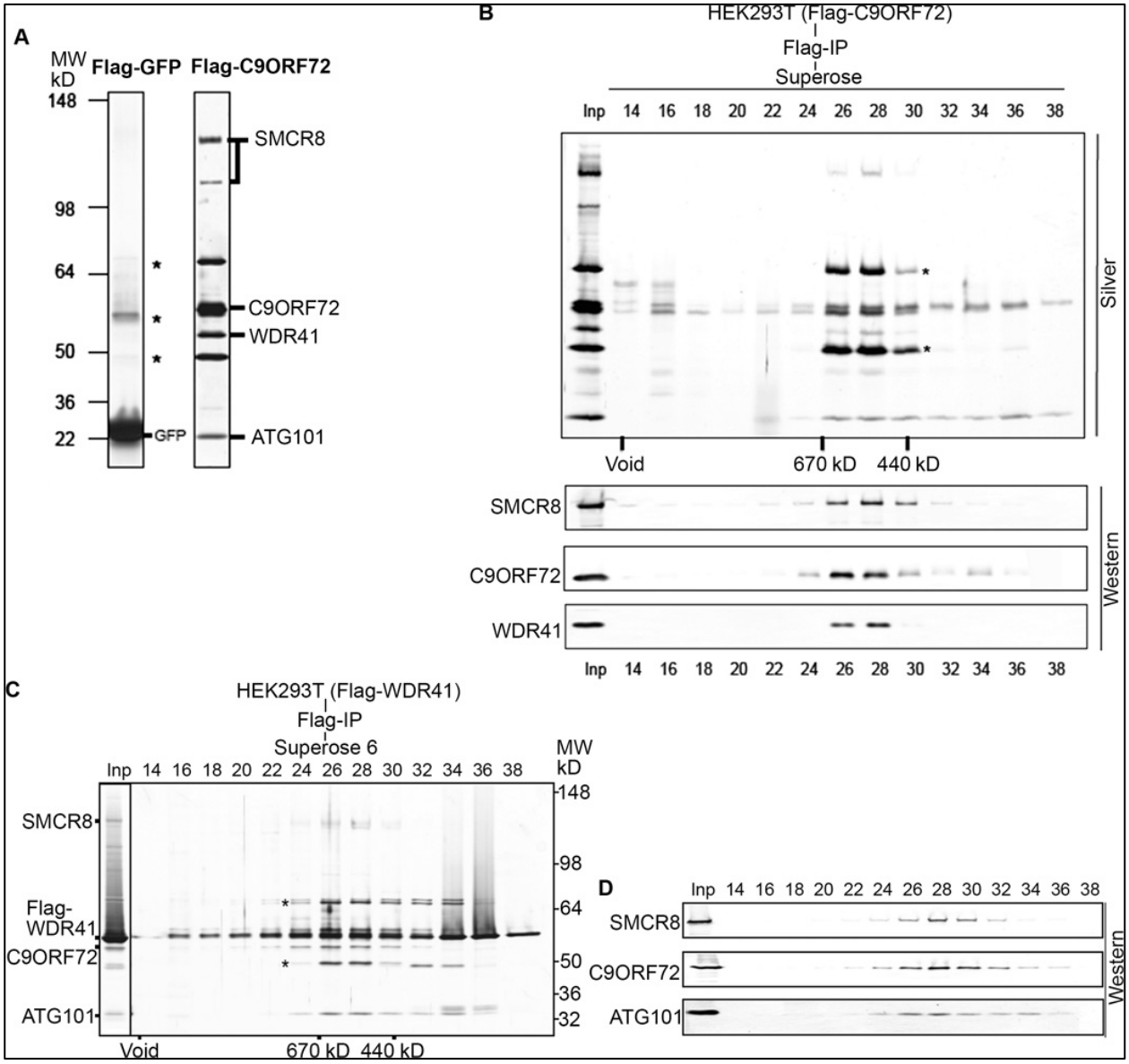

(A) Silver staining analysis of Flag affinity–purified fractions from cytoplasmic extracts of Flag-GFP and Flag-C9ORF72 HEK293 cell lines. Asterisks indicate common contaminants of Flag purification (SKB1, α-tubulin, and MEP50). Flag-C9ORF72–associated proteins as identified by mass spectrometry are indicated. MW, molecular weight; IP, immunoprecipitation. (B) Superose 6 gel filtration fractions from C9ORF72 cytoplasmic Flag affinity purification. Fractions were resolved by 4 to 12% SDS-PAGE and analyzed by silver staining (top) and Western blot with corresponding antibodies (bottom). The gel filtration purification scheme and fraction numbers are indicated on the top. (C and D) Purification of the WDR41-associated proteins from a HEK293 stable cell line expressing Flag-WDR41. Gel filtration fractions and Flag eluates were resolved on a 4 to 12% SDS-PAGE gel, followed with silver staining (left) and Western blot with

corresponding antibodies (right). The gel filtration purification scheme and fraction numbers are indicated on the top. WDR41-associated proteins and molecular markers are indicated.

Western blot analysis, C9ORF72 protein coeluted with SMCR8, WDR41, and ATG101 in fractions 26 to 30, reflecting a complex of ~600 kD (Fig. 2.1B). A fraction of Flag-C9ORF72 also eluted at a lower molecular mass; SMCR8 and WDR41 did not appear to comigrate with this fraction of C9ORF72 (Fig. 2.1B). To further confirm the presence of C9ORF72 protein in a large protein complex in the cytoplasm, we developed HEK293-derived stable cell lines expressing Flag-WDR41 or Flag-SMCR8 protein. Flag affinity purification from cytoplasmic fractions followed by gel filtration chromatography revealed the presence of a similar-sized protein complex containing Flag-WDR41, SMCR8, C9ORF72, and ATG101 in fractions 26 through 30, corresponding to a complex of ~600 kD (Fig. 2.1C). Western blot analysis confirmed the coexistence of SMCR8, C9ORF72, and ATG101 in fractions 26 to 30 (Fig. 2.1D). A similar protein complex was also identified using a HEK293 cell line expressing the Flag-SMCR8 protein (fig. S2.1). Thus, our biochemical purification studies show that C9ORF72 forms a protein complex with SMCR8, WDR41, and ATG101.

The C9ORF72 complex exhibits a GTPase activity and acts as a GEF for RAB39B

Previous bioinformatics analyses of protein motifs in C9ORF72 and SMCR8 identified a conserved DENN domain region in both proteins (31, 32). DENN domain–containing proteins are suggested to function as GEFs to activate Rab GTPases and regulate membrane trafficking (28–30). We reasoned that a Rab GTPase might loosely associate with the C9ORF72 protein complex. To test this hypothesis, we decided to use the protein complex from the fractions of the Flag-WDR41 gel filtration. WDR41 contains a WD-repeat domain, which often functions as a scaffold for protein interaction (41). Because of this, we reasoned that Flag-WDR41 could be more effective to pull the

Figure. 2.2. The C9ORF72 complex displays a GTPase activity and acts as a GEF for RAB39B.

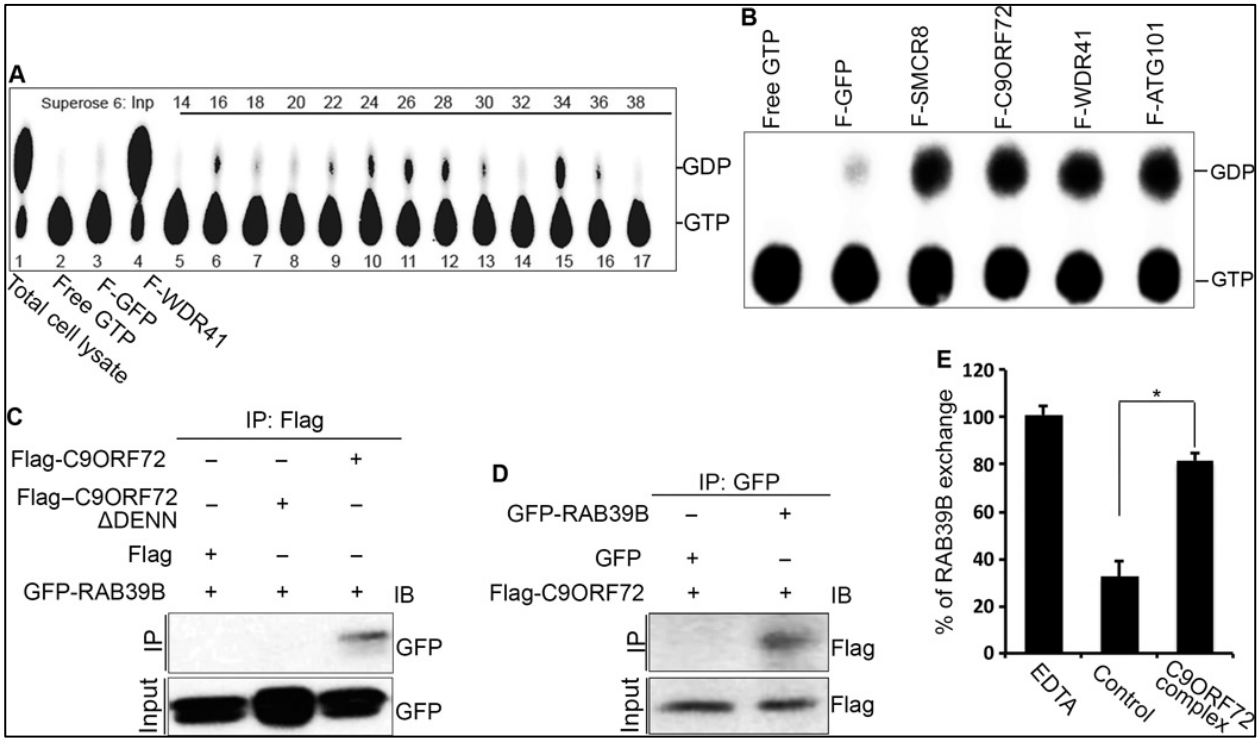

(A) GTPase assays were performed using WDR41 gel filtration fractions with [α-32P]GTP. The guanine nucleotides were separated by thin-layer chromatography plate. The positions of [α-32P]GTP and [α-32P]GDP are indicated on the right. (B) GTPase assay with Flag affinity–purified eluates from different Flag-tagged proteins in the C9ORF72 complex. Free [α-32P]GTP and Flag-GFP elutes were treated as controls. [α-32P]GTP and [α-32P]GDP are indicated on the right. (C and D) GFP-RAB39B, Flag-C9ORF72, or DENN domain–depleted C9ORF72ΔDENN was transfected into N2A cells. C9ORF72 proteins or RAB39B proteins were immunoprecipitated with M2 beads (anti-Flag) (C) or anti-GFP beads (D) followed by Western blot analyses using antibodies as listed. IB, immunoblot. (E) GEF assay of C9ORF72 protein complex and RAB39B. Purified His-tagged RAB39B proteins were preloaded with fluorescence-labeled BODIPY-GDP followed by addition of control or C9ORF72 protein complex. Fractions without C9ORF72 complex serve as the negative control. C9ORF72 complex promotes the release of GDP from RAB39B, suggesting its GEF activity against RAB39B.

associated GTPase activity compared to using Flag-C9ORF72 or Flag-SMCR8 fractions. We subjected the fractions of the Flag-WDR41 gel filtration to a GTPase assay (Fig. 2.2A). This study showed a peak of GTPase activity eluting in fractions 26 and 28 (Fig. 2.2A), coincident with the peak of the C9ORF72/SMCR8-containing complex (Fig. 2.1, B to D). We also found GTPase activity in a smaller molecular weight complex (fraction 34), reflecting an interaction between WDR41 protein and a putative Rab GTPase in a lower molecular range (Fig. 2.2A). To further confirm the GTPase activities associated with C9ORF72 protein complex, we generated stable Flag cell lines for ATG101 in HEK293 cells. Analysis of Flag affinity eluates from these stable cell lines similarly showed the presence of a specific and robust GTPase activity associating with C9ORF72-containing complexes (Fig. 2.2B). These data suggest that the C9ORF72 complex displays a GTPase activity.

To identify potential Rab GTPases associated with the C9ORF72 complex, we performed co-IP studies. Among the six candidate GTPases examined, including RAB33, RAB35, RAB39A, RAB39B, RAB31, and RAB24, we found that RAB31, RAB33, and RAB39B exhibit interactions with C9ORF72 (fig. S2.2A). Because mutations in RAB39B cause intellectual disability and early-onset Parkinson's diseases (42, 43), we decided to focus on RAB39B for further investigations. Reciprocal co-IP analyses confirmed that C9ORF72 interacts with RAB39B (Fig. 2.2, C and D). In contrast, we failed to detect the interaction between SMCR8 and RAB39B under the same experimental conditions (fig. S2.2B). Emerging evidence suggests that DENN domains directly interact with Rab GTPases (29). To test whether the DENN domain of C9ORF72 is required for its interactions with RAB39B, we deleted the DENN domain

and found that the interaction between C9ORF72 and RAB39B is abolished (Fig. 2.2C). These studies suggest that C9ORF72 interacts with RAB39B in a DENN domain–dependent manner. To determine whether the C9ORF72/SMCR8 complex functions as a GEF for RAB39B, we performed an in vitro activity assay (44). The His-tagged RAB39B protein was purified and preloaded with fluorescence-labeled BODIPY-GDP. Measurement of the release rate of BODIPY-GDP shows that the C9ORF72 protein complex strongly promotes GDP release from RAB39B (Fig. 2.2E), indicating that the C9ORF72/SMCR8 complex functions as a GEF for RAB39B.

C9ORF72 interacts with SMCR8 in a DENN domain–dependent manner

To examine whether C9ORF72 interacts with SMCR8 and WDR41 in cells other than HEK293, we performed co-IP studies in N2A cells, a mouse neuroblastoma cell line. Experimental results confirmed the interaction between C9ORF72 and SMCR8 or WDR41 in N2A cells (Fig. 2.3, A and B). Because DENN domains directly interact with Rab GTPases, in addition to serving as GEF enzymes (29), we examined the importance of DENN domains in protein interactions within the C9ORF72 complex. Deletion of the DENN domain in SMCR8 abolished its interaction with C9ORF72, but not with WDR41 (Fig. 2.3C). In contrast, both SMCR8's and WDR41's interactions with C9ORF72 are lost upon the deletion of C9ORF72 DENN domain (Fig. 2.3D). It is possible that DENN-depleted C9ORF72 or SMCR8 cannot fold correctly. These results suggest that the DENN domains are essential for the interaction between C9ORF72 and SMCR8.

Next, we examined whether C9orf72 colocalizes with Smcr8 or Wdr41. Because commercially available antibodies failed to detect the endogenous localization of

Figure. 2.3. C9ORF72 interacts with SMCR8 in a DENN domain–dependent manner.

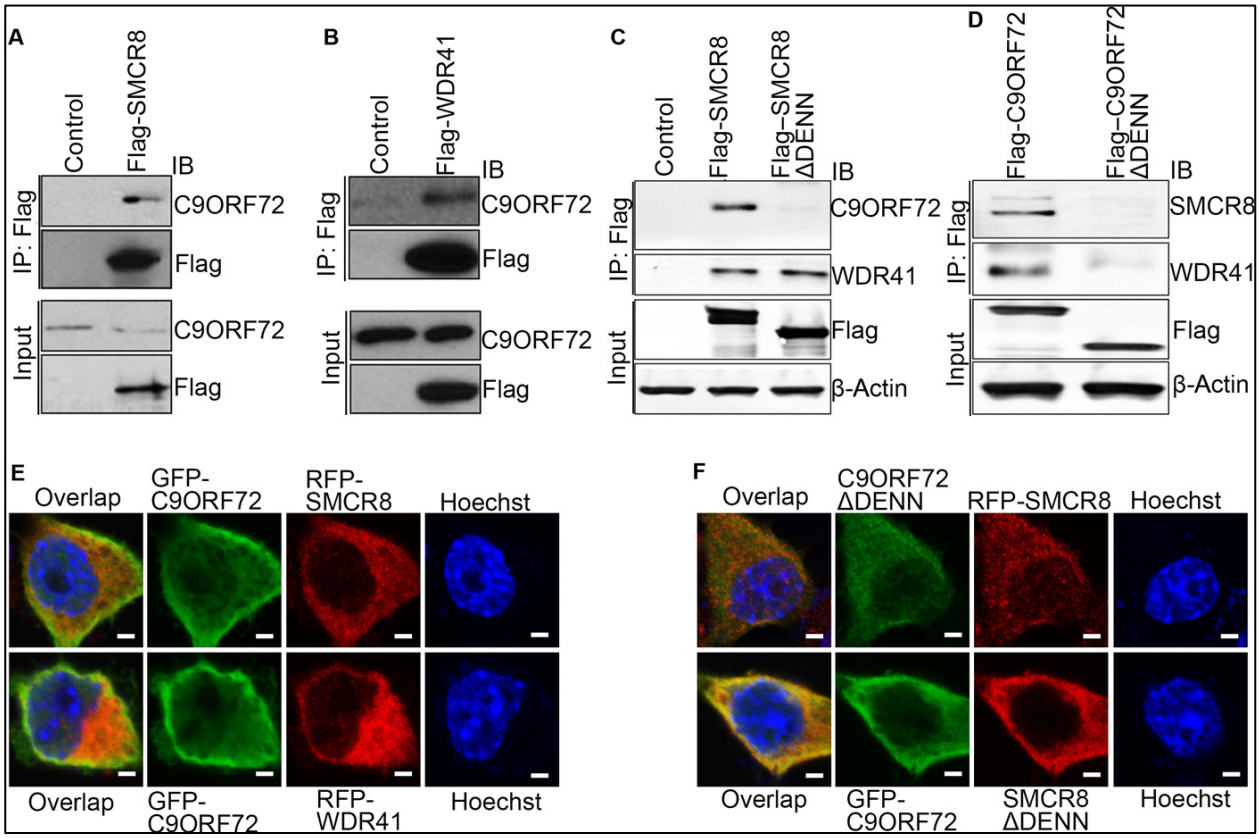

(A and B) Flag-tagged SMCR8 or WDR41 was transfected into N2A cells. SMCR8 or WDR41 proteins were immunoprecipitated with M2 beads (anti-Flag) followed by Western blot analysis using antibodies against endogenous C9ORF72. (C) Flag-tagged full-length or DENN domain–deleted SMCR8 was transfected into HEK293 cells. SMCR8 proteins were immunoprecipitated with M2 beads (anti-Flag) followed by Western blot analysis using antibodies against C9ORF72 or WDR41. (D) Flag-tagged full-length or DENN domain–deleted C9ORF72 constructs were transfected into HEK293 cells. C9ORF72 proteins were immunoprecipitated with M2 beads (anti-Flag) followed by Western blot analysis using antibodies against SMCR8 or WDR41. (E) GFP-tagged C9ORF72 was cotransfected with red fluorescent protein (RFP)–tagged SMCR8 or WDR41 into N2A cells. Confocal micrographs of N2A cells stained with antibodies against GFP (C9ORF72; green) and RFP (SMCR8 or WDR41; red). Hoechst stains the nuclei (blue). Scale bars, 10 μm. (F) GFP-tagged DENN domain–depleted C9ORF72 was cotransfected with RFP-tagged SMCR8 into N2A cells (upper panels). GFP-tagged C9ORF72 was cotransfected with RFP-tagged DENN domain–depleted SMCR8 into N2A cells (lower panels). Confocal micrographs of N2A cells stained with antibodies against GFP (C9ORF72ΔDENN or C9ORF72; green) and RFP (SMCR8 or SMCR8ΔDENN; red). Hoechst stains the nuclei (blue). Scale bars, 10 μm.

C9orf72 and Smcr8 in mouse cells, we constructed GFP-tagged C9ORF72 as well as RFP-tagged SMCR8 and WDR41. In addition to the nucleus, C9ORF72 is predominantly detected in the cytoplasm of N2A cells (Fig. 2.3E). Immunostaining results show that C9ORF72 is colocalized with both SMCR8 and WDR41 in the cytoplasm of N2A cells (Fig. 2.3E). To determine whether loss of the interaction between C9ORF72 and SMCR8 in the co-IP studies above is due to the aberrant localization of DENN domain depleted C9ORF72 or SMCR8, we examined cellular localization of C9ORF72ΔDENN and SMCR8ΔDENN. We found that DENN domain depletion does not significantly change their cellular distributions (Fig. 2.3F). These studies suggest that C9ORF72 colocalizes with SMCR8 and WDR41, and C9ORF72 interacts with them in a DENN domain–dependent manner.

Autophagy induction is compromised in Smcr8-deficient cells

Autophagy is known to be the basic mechanism of delivering cytoplasmic contents to the lysosomes for degradation (24, 25). The ULK1/FIP200/ATG13 protein complex controls autophagy initiation (36–38). Because C9ORF72/SMCR8 is associated with ULK1/ATG13 in our mass spectrometry analysis of C9ORF72-associated proteins (table 2.S1), we examined Smcr8's potential involvement in autophagy. We generated two SMCR8 lentiviral short hairpin RNA (shRNA) constructs. Western blot and reverse transcription polymerase chain reaction (RT-PCR) analyses confirmed that SMCR8 shRNA1 and shRNA2 display ~85 to 90% knockdown efficiency with high specificities (fig. 2.S3, A to C). Microtubule-associated protein 1 light chain 3 (LC3) protein expression has been widely used to monitor autophagy. LC3-I is a proteolytically processed form and is finally modified into the phosphatidylethanolamine (PE)–

Figure. 2.4. Autophagy induction is compromised in Smcr8-deficient cells.

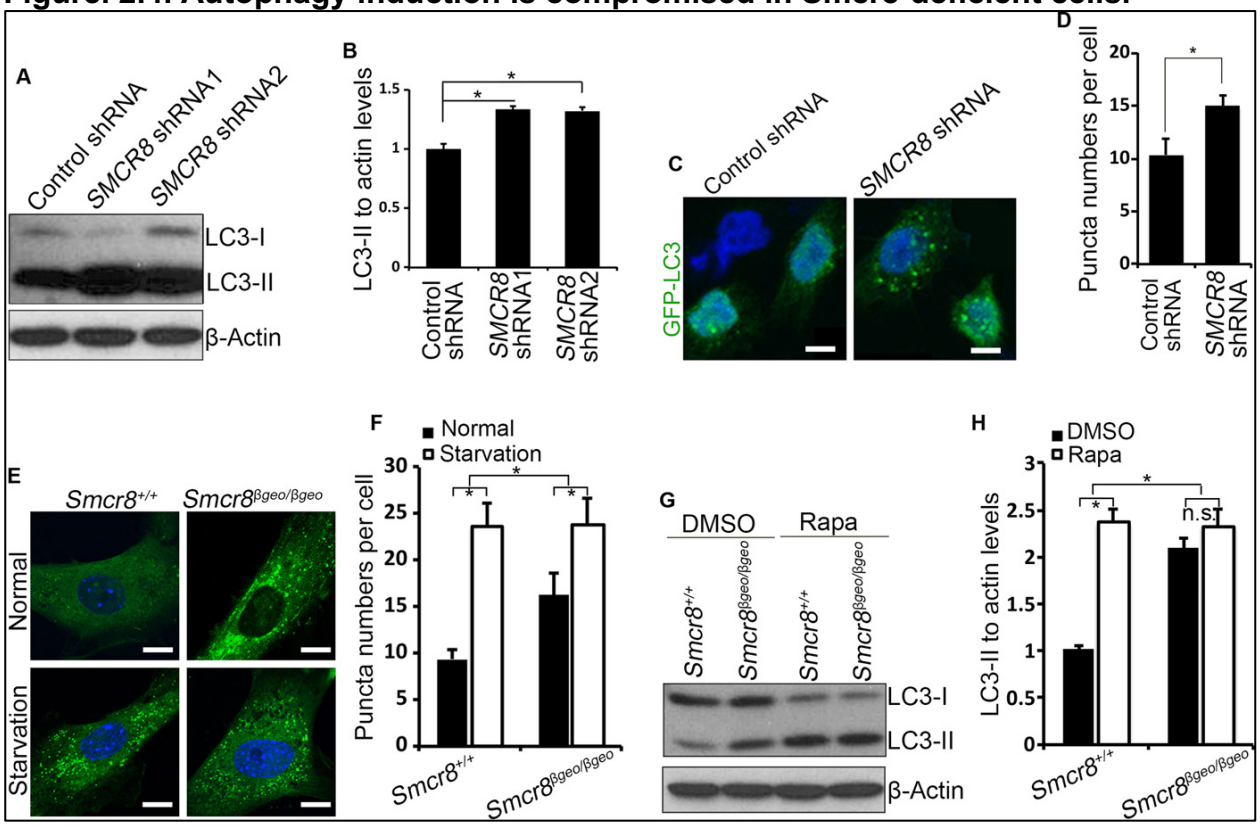

(A) HEK293 cells infected with lentiviruses expressing control shRNA, SMCR8 shRNA1, or SMCR8 shRNA2 were cultured 72 hours before protein lysate collection. The cell lysates were subjected to Western blot analyses using antibodies as indicated. (B) Quantification of LC3-II/actin ratio. Error bars represent SEM of three measurements from three independent experiments; *P < 0.05 (Student's t test). (C) Confocal imaging of GFP-LC3 expression in SMCR8 knockdown HEK293 cells using antibodies against GFP. Hoechst stains the nuclei (blue). Scale bars, 10 μm. (D) Quantification of GFP-LC3–positive puncta per cell in (C). Error bars represent SEM of three independent experiments; ~100 GFP-positive cells were randomly selected for each experiment. *P < 0.05 (Student's t test). (E) Confocal microscope images of wild-type and Smcr8 mutant MEFs stained with antibodies against LC3 (green) under normal or starvation conditions. Hoechst stains the nuclei (blue). Scale bars, 10 μm. (F) Quantification of LC3-positive puncta per cell in (E). Error bars represent SEM of three independent experiments; ~100 cells were randomly selected for each experiment. *P < 0.05 (Student's t test). Two-way analysis of variance (ANOVA) detects a significant decrease in the magnitude of up-regulation of LC3-positive puncta after starvation in Smcr8 mutant MEFs compared to that in wild-type MEFs (P < 0.05). (G) Western blot analysis of LC3 expression. Wild-type or Smcr8 mutant MEFs were treated with dimethyl sulfoxide (DMSO) or rapamycin (0.1 μM) for 3.5 hours before protein lysate collection. β-Actin serves as the loading control. (H) Quantification of LC3-II/actin ratio from (G). Error bars represent SEM of three measurements from three independent experiments; *P < 0.05 (Student's t test). n.s. represents no significant difference in LC3-II expression between DMSO and rapamycin treatment in Smcr8 mutant MEFs. Two-way ANOVA

detects a significant decrease in the magnitude of LC3-II up-regulation after rapamycin treatment in the Smcr8 mutant MEFs compared to wild-type MEFs ($P < 0.05$).

conjugated form, LC3-II (45). Knockdown of SMCR8 results in a significant increase in LC3-II protein levels relative to actin (Fig. 2.4, A and B). LC3 or GFP-tagged LC3 has been used to monitor autophagy at cellular levels by examining LC3-positive puncta (45). We examined autophagosome formation by staining GFP-LC3–positive puncta and found that there is a significant increase in puncta numbers per cell in SMCR8 knockdown cells compared to controls (Fig. 2.4, C and D). These data suggest that SMCR8 is involved in autophagy.

To further understand Smcr8's functions, we created a mouse model using embryonic stem (ES) cells in which the Smcr8 gene has been disrupted by the β-geo reporter gene. We isolated mouse embryonic fibroblasts (MEFs) from Smcr8 mutant embryos. RT-PCR and Western blot analyses confirmed the depletion of Smcr8 at both mRNA and protein levels. Increased LC3-II levels in Smcr8-deficient cells could be due to increased autophagy induction or a block of autophagsome maturation. Amino acid starvation blocks mammalian target of rapamycin (mTOR) signaling and therefore induces autophagy by releasing mTOR signaling–mediated inhibition (25, 46). To determine whether autophagy induction is enhanced in Smcr8 mutant cells, we performed amino acid starvation experiments in MEFs. Immunostaining results show that LC3-positive puncta numbers are increased in Smcr8 mutant cells compared to controls (Fig. 2.4, E and F), which is consistent with SMCR8 shRNA knockdown studies (Fig. 2.4, C and D). Whereas puncta numbers per cell are increased in both wild-type and mutant MEFs under starvation, the magnitude of increase is significantly less in Smcr8 mutant MEFs compared to that in wild-type MEFs (Fig. 2.4, E and F), suggesting that autophagy induction is compromised in Smcr8 mutant cells. To further examine

autophagy induction, we used rapamycin treatment to induce autophagy followed by Western blot analysis of LC3 expression. Rapamycin treatment results in autophagy induction reflected by induced expression of LC3-II in wild-type MEFs (Fig. 2.4, G and H). However, LC3-II levels are not significantly increased in Smcr8 mutant MEFs after rapamycin treatment (Fig. 2.4, G and H). Together, these results suggest that autophagy induction is compromised in Smcr8 mutant cells.

C9orf72 knockdown disrupts autophagy induction

Previous studies have implicated C9ORF72 in autophagy, but which step it regulates in autophagy remains unclear (33). To determine whether C9orf72 performs similar functions as Smcr8 in regulating autophagy induction, we generated two lentiviral C9orf72 shRNA constructs, which both effectively knock down C9orf72 expression (fig. S3D). We did not observe functional differences between these two shRNAs; therefore, we used C9orf72 shRNA1 in our studies. To determine how C9orf72 regulates autophagy, we performed Western blot analyses in MEFs. We found that the LC3-II/actin level is significantly reduced in C9orf72 knockdown cells (Fig. 2.5, A and B), suggesting a reduced number of autophagsomes. Reduced autophagsomes could be due to a decrease in autophagy induction or an enhanced autophagic flux. To determine whether C9orf72 regulates autophagy initiation, we used rapamycin to induce autophagy in MEFs. Rapamycin treatment results in a significant increase in LC3-II levels in control cells but not in C9orf72 knockdown cells (Fig. 2.5, A and B). Next, we examined LC3-positive puncta numbers. Control MEFs exhibit a significant increase in puncta numbers per cell under starvation conditions (Fig. 2.5, C and D). In contrast, C9orf72 knockdown MEFs exhibit normal puncta numbers under starvation compared to

Figure. 2.5. C9orf72 knockdown disrupts autophagy induction.

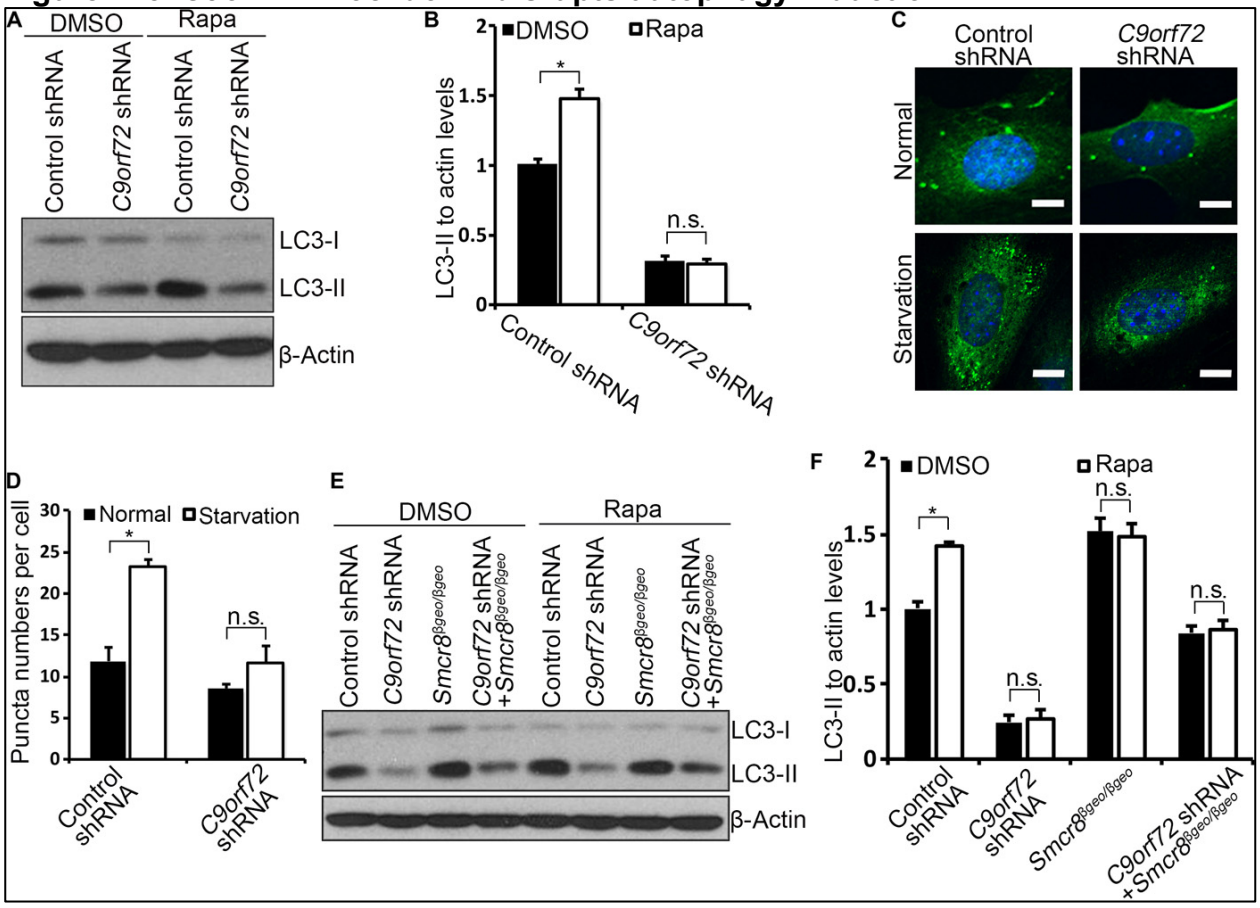

(A) Western blot analysis of LC3 expression. MEF cells infected with lentiviruses expressing control or *C9orf72* shRNA were treated with DMSO or rapamycin (0.1 μM) for 3.5 hours before protein lysate collection. β-Actin serves as the loading control. (B) Quantification of LC3-II/actin ratio. Error bars represent SEM of three measurements from three independent experiments; **P* < 0.05 (Student's *t* test). n.s. represents no significant difference in LC3-II expression between DMSO and rapamycin treatment in *C9orf72* knockdown MEFs. Two-way ANOVA detects a significant decrease in the magnitude of LC3-II up-regulation after rapamycin treatment in the *C9orf72* knockdown MEFs compared to that in wild-type MEFs (*P* < 0.05). (C) Confocal imaging of MEFs stained with antibodies against LC3 (green). MEF cells were infected with lentiviruses expressing control or *C9orf72*shRNA followed by starvation. Hoechst stains the nuclei (blue). Scale bars, 10 μm. (D) Quantification of LC3-positive puncta per cell in (C). Error bars represent SEM of three independent experiments; ~100 cells were randomly selected for each experiment. **P* < 0.05 (Student's *t* test). (E) Western blot analysis of LC3 expression. Wild-type or *Smcr8*mutant MEF cells were infected with lentiviruses expressing control or *C9orf72* shRNA as indicated followed by DMSO or rapamycin (0.1 μM) treatment for 3.5 hours before protein lysate collection. β-Actin serves as the loading control. (F) Quantification of LC3-II/actin ratio. Error bars represent SEM of three measurements from three independent experiments; **P* < 0.05 (Student's *t* test). n.s. represents no significant difference in LC3-II expression between DMSO and rapamycin treatment. Two-way ANOVA detects a significant decrease in the magnitude

of LC3-II up-regulation after rapamycin treatment in the *C9orf72* knockdown, *Smcr8* mutant, and *C9orf72/Smcr8* double depletion MEFs compared to that in wild-type MEFs ($P < 0.05$).

normal culture conditions (Fig. 2.5, C and D). Together, these results suggest that autophagy induction is impaired in C9orf72 knockdown cells. Last, we examined autophagy induction in both C9orf72- and Smcr8-deficient cells. Rapamycin treatment failed to promote autophagy induction in C9orf72, Smcr8, or C9orf72/Smcr8 double-deficient MEFs, although autophagy is significantly induced in wild-type MEFs (Fig. 2.5, E and F). Together, these studies suggest that autophagy induction is compromised in C9orf72, Smcr8, and C9orf72/Smcr8 double-depleted cells.

The C9ORF72/SMCR8 complex regulates ULK1

In mammalian cells, ULK1 forms a protein complex with FIP200/ATG13 regardless of nutrient status (36). During normal nutrient conditions, mTOR complex 1 phosphorylates Ser757 on ULK1, which results in repressing autophagy initiation (37, 38, 47). Under starvation, mTOR-mediated inhibition of autophagy is released, resulting in autophagy induction. Because our mass spectrometry data show that C9ORF72/SMCR8 is associated with ULK1 (table 2.S1), we hypothesized that C9ORF72/SMCR8 regulates autophagy induction by affecting the expression or activity of ULK1. To test this hypothesis, we attempted to confirm the interaction between the C9ORF72/SMCR8 complex and ULK1/ATG13. We expressed C9ORF72 or SMCR8 alone or in combination in HEK293 cells. Endogenous ULK1 and ATG13 are coimmunoprecipitated with C9ORF72 when it is expressed together with SMCR8, but this co-IP is drastically reduced when C9ORF72 is expressed alone (Fig. 2.6A). Furthermore, the interaction between C9ORF72/SMCR8 and ULK1/ATG13 is enhanced under amino acid starvation conditions (Fig. 2.6A). Together, these results suggest that C9ORF72/SMCR8 interacts with the ULK1/ATG13 complex, which is facilitated by starvation conditions.

Figure. 2.6. The C9ORF72/SMCR8 complex regulates ULK1.

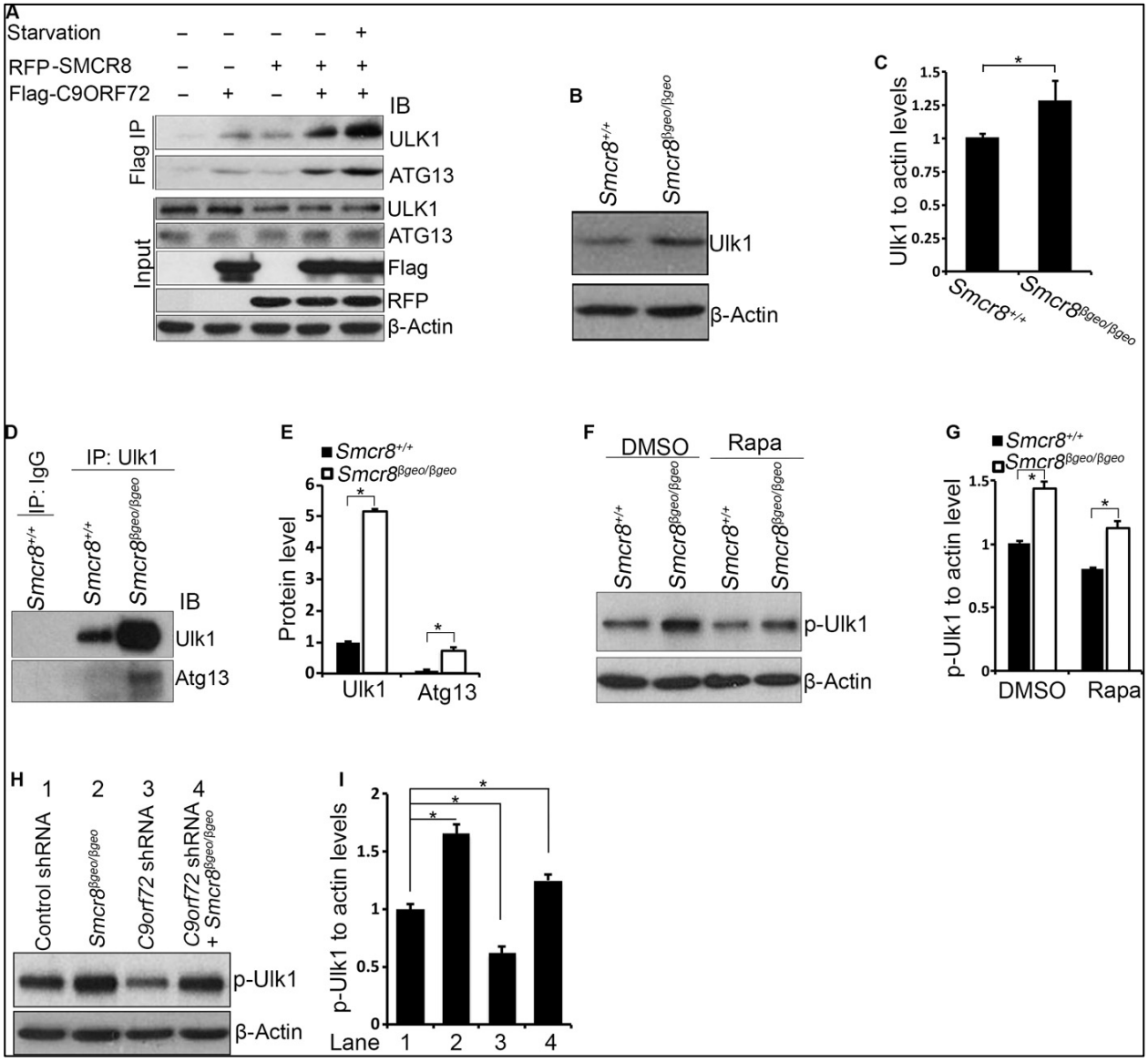

(A) The interaction between C9ORF72/SMCR8 complex with ULK1 is enhanced under starvation conditions. Flag-C9ORF72 and RFP-SMCR8 were transfected into HEK293 cells with or without amino acid starvation for 1 hour before protein lysate collection. C9ORF72 protein was immunoprecipitated with M2 beads (anti-Flag) followed by Western blot analyses using antibodies as listed. (B) Western blot analysis of Ulk1 expression in wild-type or Smcr8 mutant MEFs. β-Actin serves as the loading control. (C) Quantification of Ulk1 expression relative to actin. Error bars represent SEM of three measurements from three independent experiments; *P < 0.05 (Student's t test). (D) Ulk1 protein in wild-type or Smcr8 mutant MEFs was immunoprecipitated with Ulk1 antibodies followed by Western blot analyses. IgG, immunoglobulin G. (E) Quantification of relative Ulk1 and Atg13 protein levels. Error bars represent SEM of three measurements from three independent experiments; *P < 0.01 (Student's t test). (F) Western blot analysis of phospho-Ulk1 (p-Ser757) expression. Wild-type or Smcr8

mutant MEFs were treated with DMSO or rapamycin (0.1 μM) for 3.5 hours before protein lysate collection. (G) Quantification of phospo-Ulk1 (p-Ulk1)/actin ratio. Error bars represent SEM of three measurements from three independent experiments; *P < 0.05 (Student's t test). (H) Western blot analysis of phospho-Ulk1 (p-Ser757) expression. Wild-type or Smcr8 mutant MEFs were infected with lentiviruses expressing control or C9orf72 shRNA constructs. β-Actin serves as the loading control. (I) Quantification of relative levels of phospho-Ulk1. Error bars represent SEM of three measurements from three independent experiments; *P < 0.05 (Student's t test).

To determine whether Ulk1 protein level is altered in Smcr8 mutant cells, we performed Western blot analyses and found that Ulk1 protein is significantly enhanced in mutant MEFs (Fig. 2.6, B and C). IP of endogenous Ulk1 in Smcr8 mutant cells shows markedly enhanced protein levels of Ulk1 and Atg13 (Fig. 2.6, D and E). It is possible that Smcr8 masks the epitope that Ulk1 antibody recognizes; therefore, Smcr8 depletion results in a more efficient IP of Ulk1. Together, these results suggest that Smcr8 is required for normal levels of Ulk1 and Atg13. Phosphorylation of Ser757 on Ulk1 controls autophagy initiation (37, 38, 47). The increased protein level of Ulk1 and defective autophagy induction in Smcr8 mutant cells prompted us to test whether Ulk1 phosphorylation is also altered in mutant MEFs. Indeed, phosphorylated Ulk1 (phospho-Ulk1) is significantly enhanced in Smcr8 mutant MEFs (Fig. 2.6, F and G). In rapamycin-treated cells, phospho-Ulk1 levels are also significantly increased (Fig. 2.6, F and G), which is consistent with the impaired autophagy induction in Smcr8 mutant cells (Fig. 2.4, E to H). Next, we examined phospho-Ulk1 expression in C9orf72 knockdown cells. In contrast to the up-regulation of phospho-Ulk1 in Smcr8 mutant MEFs, C9orf72 knockdown results in a decrease in phospho-Ulk1; C9orf72/Smcr8 double depletion leads to an intermediate level of phospho-Ulk1 in MEFs (Fig. 2.6, H and I). Together, these results suggest that the C9ORF72 and SMCR8 regulate autophagy induction by modulating ULK1 through distinct mechanisms.

Autophagic flux is defective in Smcr8-deficient cells

Autophagy induction is reduced (Fig. 2.4, E to H), but the autophagsome numbers are increased in Smcr8 mutant cells reflected by increased LC3-II levels (Figs. 2.4, G and H, and 2.5, E and F), suggesting that autophagsome maturation is defective

Figure. 2.7. Autophagic flux is defective in Smcr8-deficient cells.

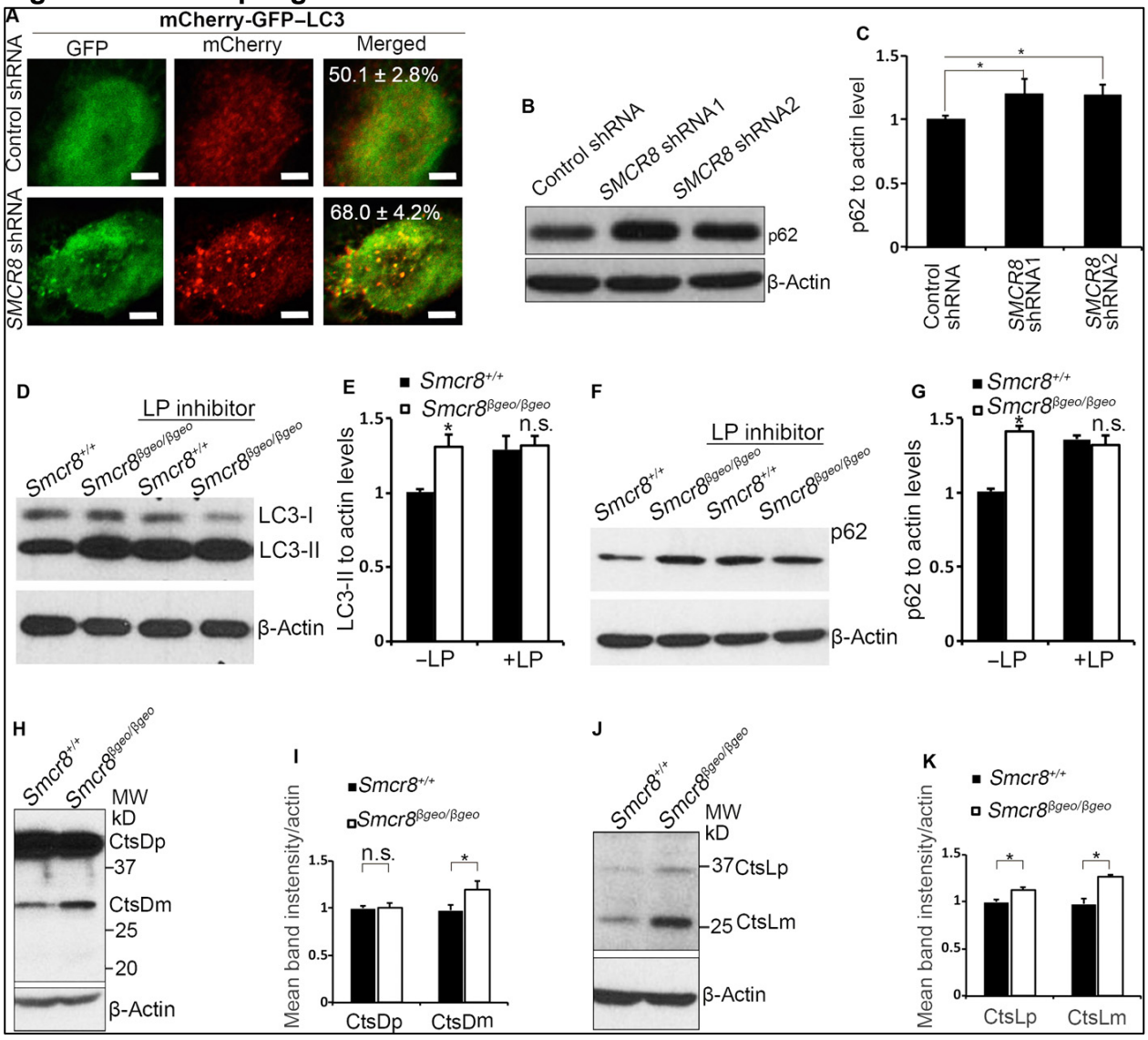

(A) Confocal imaging of HEK293 cells infected by lentiviruses expressing control or SMCR8 shRNA. Double-tagged LC3 (mCherry-GFP-LC3) protein was used to indicate autophagic flux. The percentage of yellow dots, which maintains both GFP and mCherry signal, out of total red dots is listed in the merged figures. Values represent SEM of three independent experiments; ~50 cells were randomly selected for each statistical analysis. *P < 0.05 (Student's t test). (B) Western blot analysis of p62 expression. β-Actin serves as the loading control. (C) Quantification of p62 protein levels relative to actin. Error bars represent SEM of three measurements from three independent experiments; *P < 0.05 (Student's t test). (D and F) Western blot analyses of LC3 (D) or p62 (F) expression in MEFs. MEFs were cultured in normal conditions or treated with lysosome inhibitors LP (100 μM each) for 3.5 hours before protein lysate collection. β-Actin serves as the loading control. (E and G) Quantification of LC3-II levels relative to actin (E) and p62 levels relative to actin (G). Error bars represent SEM of three measurements from three independent experiments; *P < 0.05 (Student's t test). n.s. represents no significant difference of LC3-II or p62 expression. Two-way ANOVA

detects a significant decrease in the magnitude of LC3-II or p62 up-regulation after LP treatment in Smcr8 mutant MEFs compared to that in wild-type MEFs ($P < 0.05$). (H and J) Western blot analysis of cathepsin D (H) or cathepsin L (J) expression. β-Actin serves as the loading control. CtsDp, procathepsin D; CtsDm, mature cathepsin D; CtsLp, procathepsin L; CtsLm, mature cathepsin L. (I and K) Quantification of cathepsins D or L expression. Error bars represent SEM of three measurements from three independent experiments; *$P < 0.05$ (Student's t test); n.s. represents no significant difference detected.

in Smcr8-deficient cells. Autophagosome accumulation could be due to a blockage of autophagic flux (24, 25). We used double-tagged LC3 proteins (mCherry-GFP-LC3) to monitor autophagic flux. Simultaneous expression of mCherry and GFP results in yellow signals under physiological pH, whereas an acidic environment in the autolysosome quenches the GFP signal and results in exclusively red signals (24, 45). We found that the yellow dot/total red dot ratio is 50.1 ± 2.8% in control cells, whereas the yellow dot/total red dot ratio is higher at 68.0 ± 4.2% in SMCR8 knockdown cells (Fig. 2.7A), suggesting that relatively less GFP signal is quenched in knockdown cells. These results indicate that autophagsome maturation is compromised in Smcr8-deficient cells, which is consistent with LC3-II accumulation in Smcr8-deficient cells (Figs. 2.4, A, B, G, and H, and 2.7, D and E). Next, we examined a well-defined autophagy substrate, p62 (48). Consistent with an impaired degradation function of autophagsome, p62 is significantly accumulated in Smcr8-deficient cells (Fig. 2.7, B, C, F, and G). Together, these results suggest that Smcr8 depletion results in a defective autophagic flux.

Lysosomal degradation is mainly mediated by cysteine and aspartyl protease, which are inhibited by leupeptin and pepstatin, respectively. If an increased LC3-II level is due to the enhancement of autophagy induction, blocking lysosomal degradation using leupeptin and pepstatin A (LP) should result in a further increase of LC3-II levels. However, if an increased LC3-II level is because of defective autophagsome maturation, blocking lysosomal degradation using LP will not further increase LC3-II levels (45). To confirm that increased LC3-II levels are due to defective autophagsome maturation and not autophagy induction enhancement in Smcr8 mutant cells, we treated MEFs for 3.5 hours with lysosomal inhibitors (LP). This treatment leads to a significant accumulation

of endogenous LC3-II, reflecting blockage of LC3-II degradation after lysosomal inhibitor (LP) treatment in control cells (Fig. 2.7D). However, there is no significant further increase of LC3-II levels in Smcr8 mutant cells (Fig. 2.7, D and E). Consistent with a blockage of autophagsome maturation, LP treatment fails to cause further accumulation of p62 in Smcr8 mutant cells (Fig. 2.7, F and G). Together, these results suggest that Smcr8 depletion results in defective autophagsome maturation and impaired autophagosome degradation.

The defective autophagsome maturation could be due to a block in autophagsome-lysosome fusion or lysosomal degradation. We failed to detect a significant alteration in autophagosome-lysosome fusions in Smcr8 mutant MEFs. Therefore, we examined lysosomal degradation. Cathepsins D and L are widely used as reporter molecules for trafficking and maturation of lysosomal hydrolases (49, 50). Cathepsins D and L are synthesized as preprocathepsins D and L, which are converted into procathepsins D and L in the endoplasmic reticulum (ER) after signaling peptides are removed. Procathepsin D (52 kD) and procathepsin L (36 kD) are generated in the ER transit from the trans-Golgi and are transported to late endosomes and lysosomes. Encountering the acidic environment in lysosomes, procathepsin D undergoes further proteolytic processing into a 44-kD form and finally into the 32-kD mature form. Procathepsin L is processed into a 24-kD mature form (49, 50). In wild-type MEFs, the procathepsin D 52-kD band was barely visible, and the dominant signals were from 44-kD procathepsin D and 32-kD mature cathepsin D bands (Fig. 2.7H). In Smcr8 mutant MEFs, the mature cathepsin D level is significantly increased (Fig. 2.7, H and I). For cathepsin L, both procathepsin L and mature cathepsin L levels were significantly

increased in Smcr8 mutant MEFs (Fig. 2.7, J and K). The increased amounts of cathepsins D and L in Smcr8 mutant cells indicate either an increase in their synthesis or a decrease in their degradation, which is often observed when lysosomal function is disrupted (51–53). Together, the defective autophagic flux could be due to a block of lysosomal degradation in Smcr8 mutant cells.

C9orf72 knockdown results in an increase in autophagic flux

Because C9ORF72 and SMCR8 are within a protein complex, we asked whether autophagic flux is also compromised in C9orf72 knockdown cells. We used double-tagged LC3 proteins (mCherry-GFP-LC3) to monitor autophagic flux (45). Surprisingly, C9orf72 knockdown results in a significant decrease in the ratio of yellow to red puncta (Fig. 2.8, A and B). These results suggest that autophagic flux is enhanced in C9orf72 knockdown cells, which is opposite to the reduced autophagic flux in Smcr8-depleted cells (Fig. 2.7A). Next, we measured p62 expression and found that p62 is not significantly changed in C9orf72 knockdown cells compared to controls (Fig. 2.8, C and D). Whereas increased autophagic flux may lead to more efficient degradation of autophagy substrate p62, autophagy induction is compromised in C9orf72 knockdown cells (Fig. 2.5), which leads to more p62 accumulation. The combined alterations in autophagy induction and autophagic flux may result in normal p62 expression levels in C9orf72 knockdown cells. The protein level of p62 is slightly increased in C9orf72/Smcr8 double-depleted cells (Fig. 2.8, C and D). Together, these results suggest that autophagic flux is enhanced in C9orf72-deficient cells.

Altered autophagic flux and degradation could be due to changes in lysosomal integrity. Next, we examined lysosomal integrity by monitoring the expression of

Fig. 2.8. C9orf72 knockdown results in an increase in autophagic flux.

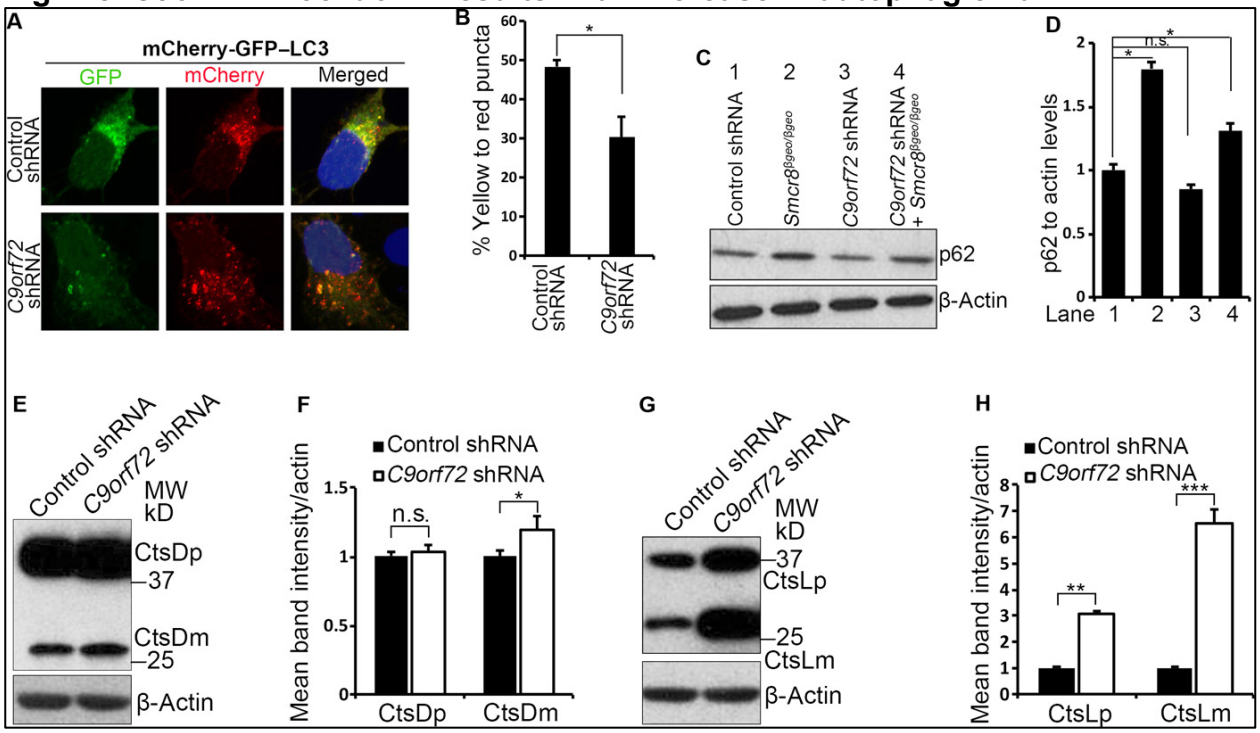

(A) Confocal imaging of GFP-mCherry expression in N2A cells infected with lentiviruses expressing control or C9orf72 shRNA. (B) Quantification of the percentage of yellow dots, which maintains both GFP and mCherry signal, out of total red dots. Values represent SEM of three independent experiments; ~50 cells were randomly selected for each statistical analysis. *P < 0.05 (Student's t test). (C) Western blot analyses of p62 expression. Wild-type or Smcr8 mutant MEFs were infected with lentiviruses expressing control or C9orf72 shRNA followed by 72 hours of culture before protein lysate collection. β-Actin serves as the loading control. (D) Quantification of p62 levels relative to actin. Error bars represent SEM of three measurements from three independent experiments; *P < 0.05 (Student's t test). n.s. represents no significant difference detected. (E and G) Western blot analysis of cathepsin D (E) or cathepsin L (G) expression in the control or C9orf72 knockdown MEFs. β-Actin serves as the loading control. (F and H) Quantification of cathepsins D or L expression. Error bars represent SEM of three measurements from three independent experiments; *P < 0.05, ***P < 0.001 (Student's t test); n.s. represents no significant difference detected.

cathepsins D and L. In C9orf72 knockdown MEFs, the mature cathepsin D level is slightly increased, whereas its precursor level appears normal (Fig. 2.8, E and F). In contrast, both procathepsin L and mature cathepsin L levels were significantly increased in C9orf72 knockdown MEFs (Fig. 2.8, G and H). Together, these results suggest that enhanced autophagic flux could be due to an increased lysosomal degradation in C9orf72 knockdown cells.

Discussion

To gain insights into the biology of the C9ORF72 protein, we isolated C9ORF72-containing complexes from human cells and characterized their functions. We found that C9ORF72 forms a protein complex with SMCR8, WDR41, and ATG101. Here, we investigated C9ORF72/SMCR8's functions in regulating autophagy and its action mechanisms.

Our studies provide novel insights into C9ORF72/SMCR8's functions and its action mechanisms. First, in addition to forming a protein complex as reported (34, 54), we found that C9ORF72, SMCR8, WDR41, and ATG101 proteins exhibit similar peptide coverage (~60%) based on mass spectrometry analysis, reflecting a near-stoichiometric presence. In addition, C9ORF72 interacts with SMCR8 and WDR41 in a DENN domain–dependent manner. Starvation condition facilitates the interaction between C9ORF72/SMCR8 and ULK1. Our gel filtration identifies ATG101 as a component within the C9ORF72 complex, which could further aid in understanding this protein complex's functions. ULK1/ATG13/FIP200/ATG101 complex acts as a key upstream factor to initiate autophagy (37, 38). It has been reported that Atg101 is essential for

autophagy initiation; Atg101 binds to Atg13 and is required for its protein stabilization; Atg101 is responsible for recruiting downstream factors to the autophagosome formation sites (39, 40, 55). Future studies should reveal if and how the C9ORF72/SMCR8 complex regulates ATG101/ATG13 protein stabilization and ATG101's functions in recruiting downstream autophagy factors. Second, the C9ORF72/SMCR8 complex has dual functions in autophagy by modulating both autophagy initiation and autophagic flux. Autophagy induction is compromised in Smcr8 mutant cells. SMCR8 is associated with and regulates the autophagy initiation factor ULK1. These data suggest that SMCR8 has a direct role in regulating autophagy initiation. However, it remains possible that a high baseline in autophagsome number is due to defective lysosomal degradation, which ultimately results in aberrant autophagy induction. Third, C9ORF72 and SMCR8 have overlapping and distinct functions, although they are within the same protein complex. C9orf72 or Smcr8 depletion results in impaired autophagy induction. However, phospho-Ulk1 expression is enhanced in Smcr8 mutant MEFs and is decreased in C9orf72 knockdown MEFs, suggesting that they have different mechanisms to regulate autophagy initiation. In addition, studies using double-tagged LC3 protein show that autophagic flux is enhanced in C9orf72 knockdown cells and is reduced in Smcr8 mutant cells. One potential explanation as to why C9ORF72 and SMCR8 have distinct functions in autophagy is because they interact with and activate different downstream Rab GTPases. Indeed, we found that C9ORF72 interacts with and activates RAB39B, but SMCR8 does not interact with RAB39B under the same experimental conditions. Future studies should further reveal

the mechanisms underlying these overlapping and distinct functions of C9ORF72/SMCR8.

Our studies have important implications for C9ORF72-related neurodegeneration diseases. It has been reported that C9orf72 depletion alone in mice is not sufficient to cause motor neuron diseases (13, 19). The fact that C9ORF72 and SMCR8 form a protein complex and have overlapping functions in autophagy raises the possibility that Smcr8 has compensatory effects on C9orf72 loss of function. Future studies should examine whether double knockout of C9orf72 and Smcr8 causes autophagy defects in neurons. Given the importance of autophagy in the central nervous system (25, 56, 57), it is also important to determine whether double-knockout C9orf72/Smcr8 causes neurodegeneration due to defective autophagy in neurons. Multiple independent studies show that C9orf72 ablation in mice results in defective immune functions. It will be interesting to determine whether Smcr8 mutant mice also exhibit dysregulation of immune functions, which could be exacerbated in the C9orf72/Smcr8 double-knockout background. Because neurodegeneration is influenced by innate immune system and inflammation (58, 59), future studies should reveal if and how dysregulation of C9ORF72/SMCR8-mediated immune functions contributes to neurodegenerative diseases.

There are several reports about the C9ORF72 protein complex and its involvement in autophagy (34, 54, 60, 61). Our studies have revealed novel information about C9ORF72/SMCR8 complex functions compared to these recent studies. We found that ATG101 is a major component of C9ORF72 protein complex, which leads to the finding that C9ORF72 positively regulates ULK1 and autophagy initiation.

Furthermore, we showed that C9orf72 plays a role in autophagic flux. Most notably, our studies using MEFs from Smcr8 knockout mice demonstrate that Smcr8 has dual roles in autophagy initiation and autophagic flux. Overall, our studies suggest that C9ORF72 and SMCR8 have distinct and overlapping functions at different steps of autophagy. It has been reported that a long form of C9ORF72 (C9-L) and not the short form of C9ORF72 (C9-S) interacts with SMCR8 and WDR41 (61, 62). C9-L, but not C9-S, is decreased in the frontal cortex of patients with FTD (61). Our gel filtration results show that a longer, but not shorter, form of C9ORF72 comigrates with SMCR8, WDR41, and ATG101 (Fig. 2.1B), suggesting that the longer form of C9ORF72 regulates autophagy. Future studies should determine whether C9-L and C9-S have different cellular functions relevant to the FTD diseases. Our co-IP experiments failed to detect the interaction between SMCR8 and RAB39B. However, Sellier et al. (34) showed an interaction between SMCR8 and RAB39B, and the presence of SMCR8 is essential for the complex to interact with RAB39B. These discrepancies could be because we performed studies in the N2A cells, whereas their co-IP was done in the HEK293 cells. Future studies should determine whether C9ORF72 and SMCR8 have differential interactions with other Rab GTPases and their functional importance.

Acknowledgments

We thank J.-F.C.'s laboratory colleagues for the stimulating discussions. We thank J. Eggenschwiler, N. Manley, B. Condie, D. Menke, and J. Lauderdale for the use of their equipment. We also thank the Oncogenomics Core Facility at the Sylvester Comprehensive Cancer Center for their services.

Supplemental Figure 2.S1. Isolation of SMCR8-associated proteins.

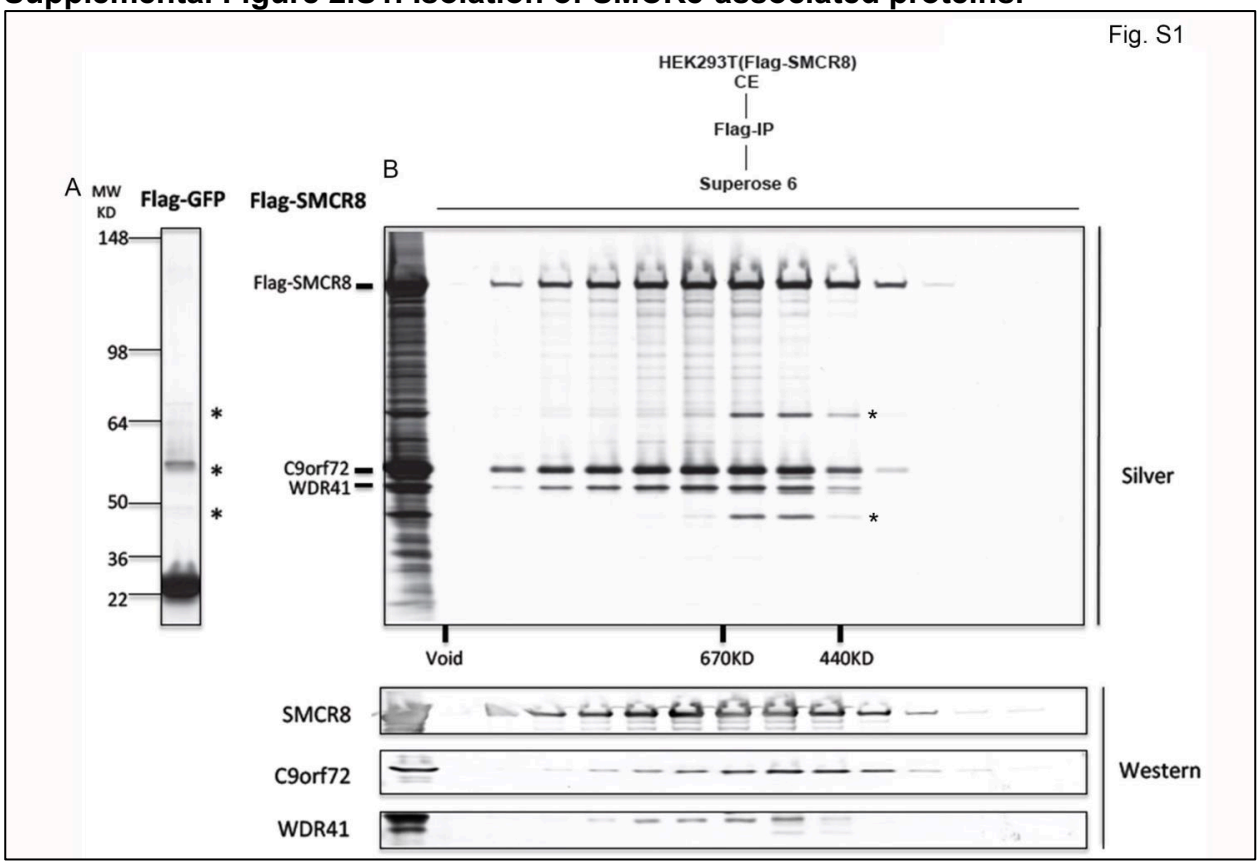

(A and B) Silver staining analysis of Flag affinity purified fractions from cytoplasmic extracts of Flag-GFP and Flag-SMCR8 HEK293 cell lines. Asterisks indicate common contaminants of Flag purification (SKB1, α-tubulin and MEP50). Flag-SMCR8 associated proteins as identified by mass spectrometry are indicated. (B) Superose 6 gel filtration fractions from SMCR8 cytoplasmic flag affinity purification. Fractions were resolved by 4-12% SDS-PAGE and analyzed by silver staining (Top) and western blot with corresponding antibodies (Bottom).

Supplemental Figure 2.S2. Identify C9orf72- or SMCR8-associated Rab GTPases.

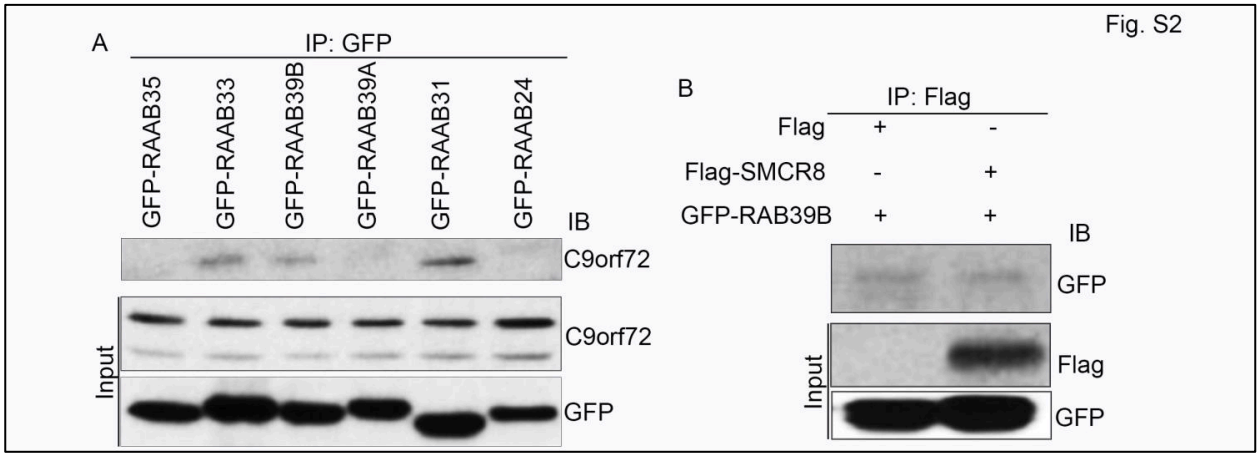

(A) Individual GFP-tagged Rab GTPase constructs were transfected into N2A cells. GTPase proteins were immunoprecipitated (IP) with GFP beads followed by western blot analyses using antibodies against C9orf72. (B) Flag-tagged SMCR8 and GFP-tagged RAB39B were transfected into N2A cells. SMCR8 proteins were immunoprecipitated (IP) with m2 beads (anti-Flag) followed by western blot analyses using antibodies against GFP.

Supplemental Figure 2.S3. Characterization of SMCR8 and C9orf72 shRNA constructs.

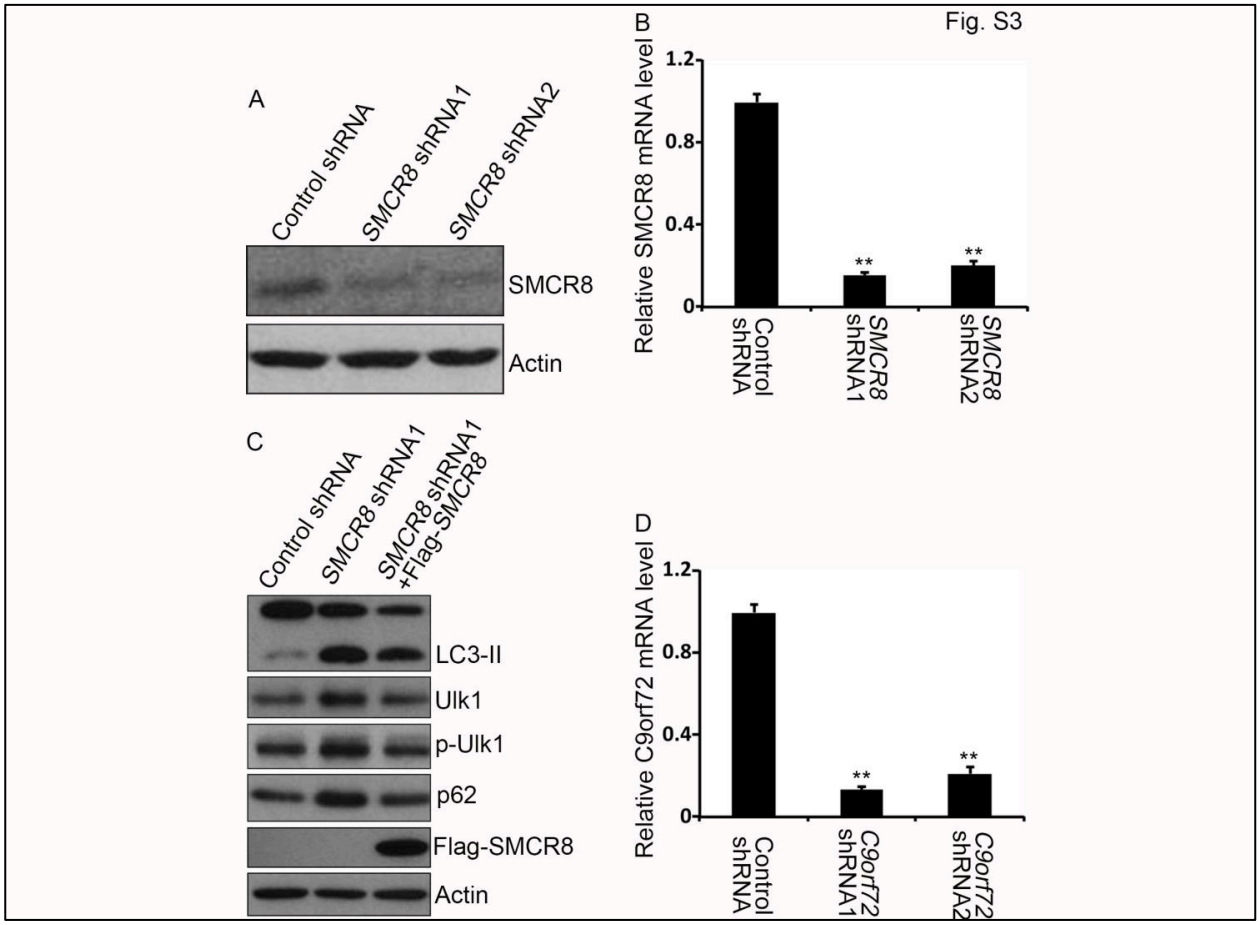

(A) Western blot analysis of SMCR8 expression in HEK293 cells transfected with control, SMCR8 shRNA1, or SMCR8 shRNA2 constructs. β-actin serves as the loading control. (B) RT-PCR analysis of SMCR8 mRNA in HEK293 cells transfected with control, SMCR8 shRNA1, or SMCR8 shRNA2 constructs. (C) HEK293 cells transfected with control, SMCR8 shRNA1, or SMCR8 shRNA1 plus Flag-SMCR8 DNA followed by western blot analyses using antibodies as indicated. β-actin serves as the loading control. (D) RT-PCR analysis of C9orf72 mRNA in N2A cells infected with lentiviruses expressing control, C9orf72 shRNA1, or C9orf72 shRNA2.

Supplemental Table 2.S1. Polypeptide composition through Flag-C9ORF72 immunopurification by mass spectrometry.

Supplementary Table 1

ID	Description	Calculated MW	Coverage	Identified Unique Peptides
UR1H_Q8TEV9	__HOMO Smith-Magenis syndrome chromosomal region candidate gene 8 protein	105,022	81.1	399
UR1H_Q96LT7	__HOMO Uncharacterized protein C9orf72	54,328	74.6	259
UR1H_Q9BSB4	__HOMO Autophagy-related protein 101	25,003	63.8	21
UR1H_Q9HAD4	__HOMO WD repeat-containing protein 41	51,728	63.2	246
UR1H_O75385	__HOMO Serine/threonine-protein kinase ULK1	112,631	32.4	49
UR1H_E9PQZ8	__HOMO Autophagy-related protein 13	60,155	26.7	19

References

1. J. Bang, S. Spina, B. L. Miller, Frontotemporal dementia. Lancet 386, 1672–1682 (2015).

2. R. Rademakers, M. Neumann, I. R. Mackenzie, Advances in understanding the molecular basis of frontotemporal dementia. Nat. Rev. Neurol. 8, 423–434 (2012).

3. S.-C. Ling, M. Polymenidou, D. W. Cleveland, Converging mechanisms in ALS and FTD: Disrupted RNA and protein homeostasis. Neuron 79, 416–438 (2013).

4. I. Gijselinck, T. Van Langenhove, J. van der Zee, K. Sleegers, S. Philtjens, G. Kleinberger, J. Janssens, K. Bettens, C. Van Cauwenberghe, S. Pereson, S. Engelborghs, A. Sieben, P. De Jonghe, R. Vandenberghe, P. Santens, J. De Bleecker, G. Maes, V. Bäumer, L. Dillen, G. Joris, I. Cuijt, E. Corsmit, E. Elinck, J. Van Dongen, S. Vermeulen, M. Van den Broeck, C. Vaerenberg, M. Mattheijssens, K. Peeters, W. Robberecht, P. Cras, J.-J. Martin, P. P. De Deyn, M. Cruts, C. Van Broeckhoven, A C9orf72 promoter repeat expansion in a Flanders-Belgian cohort with disorders of the frontotemporal lobar degeneration-amyotrophic lateral sclerosis spectrum: A gene identification study. Lancet Neurol. 11, 54–65 (2012).

5. A. E. Renton, E. Majounie, A. Waite, J. Simón-Sánchez, S. Rollinson, J. R. Gibbs, J. C. Schymick, H. Laaksovirta, J. C. van Swieten, L. Myllykangas, H. Kalimo, A. Paetau, Y. Abramzon, A. M. Remes, A. Kaganovich, S. W. Scholz, J. Duckworth, J. Ding, D. W. Harmer, D. G. Hernandez, J. O. Johnson, K. Mok, M. Ryten, D. Trabzuni, R. J. Guerreiro, R. W. Orrell, J. Neal, A. Murray, J. Pearson, I. E. Jansen, D. Sondervan, H. Seelaar, D. Blake, K. Young, N. Halliwell, J. B. Callister, G. Toulson, A. Richardson, A. Gerhard, J. Snowden, D. Mann, D. Neary, M. A. Nalls, T. Peuralinna, L. Jansson, V.-M.

Isoviita, A.-L. Kaivorinne, M. Hölttä-Vuori, E. Ikonen, R. Sulkava, M. Benatar, J. Wuu, A. Chiò, G. Restagno, G. Borghero, M. Sabatelli; ITALSGEN Consortium, D. Heckerman, E. Rogaeva, L. Zinman, J. D. Rothstein, M. Sendtner, C. Drepper, E. E. Eichler, C. Alkan, Z. Abdullaev, S. D. Pack, A. Dutra, E. Pak, J. Hardy, A. Singleton, N. M. Williams, P. Heutink, S. Pickering-Brown, H. R. Morris, P. J. Tienari, B. J. Traynor, A hexanucleotide repeat expansion in C9ORF72 is the cause of chromosome 9p21-linked ALS-FTD. Neuron 72, 257–268 (2011).

6. M. DeJesus-Hernandez, I. R. Mackenzie, B. F. Boeve, A. L. Boxer, M. Baker, N. J. Rutherford, A. M. Nicholson, N. A. Finch, H. Flynn, J. Adamson, N. Kouri, A. Wojtas, P. Sengdy, G.-Y. R. Hsiung, A. Karydas, W. W. Seeley, K. A. Josephs, G. Coppola, D. H. Geschwind, Z. K. Wszolek, H. Feldman, D. S. Knopman, R. C. Petersen, B. L. Miller, D. W. Dickson, K. B. Boylan, N. R. Graff-Radford, R. Rademakers, Expanded GGGGCC hexanucleotide repeat in noncoding region of C9ORF72 causes chromosome 9p-linked FTD and ALS. Neuron 72, 245–256 (2011).

7. E. Majounie, A. E. Renton, K. Mok, E. G. P. Dopper, A. Waite, S. Rollinson, A. Chiò, G. Restagno, N. Nicolaou, J. Simon-Sanchez, J. C. van Swieten, Y. Abramzon, J. O. Johnson, M. Sendtner, R. Pamphlett, R. W. Orrell, S. Mead, K. C. Sidle, H. Houlden, J. D. Rohrer, K. E. Morrison, H. Pall, K. Talbot, O. Ansorge; Chromosome 9-ALS/FTD Consortium; French research network on FTLD/FTLD/ALS; ITALSGEN Consortium, D. G. Hernandez, S. Arepalli, M. Sabatelli, G. Mora, M. Corbo, F. Giannini, A. Calvo, E. Englund, G. Borghero, G. L. Floris, A. M. Remes, H. Laaksovirta, L. McCluskey, J. Q. Trojanowski, V. M. Van Deerlin, G. D. Schellenberg, M. A. Nalls, V. E. Drory, C.-S. Lu, T.-H. Yeh, H. Ishiura, Y. Takahashi, S. Tsuji, I. Le Ber, A. Brice, C. Drepper, N.

Williams, J. Kirby, P. Shaw, J. Hardy, P. J. Tienari, P. Heutink, H. R. Morris, S. Pickering-Brown, B. J. Traynor, Frequency of the C9orf72 hexanucleotide repeat expansion in patients with amyotrophic lateral sclerosis and frontotemporal dementia: A cross-sectional study. Lancet Neurol. 11, 323–330 (2012).

8. Z. Xu, M. Poidevin, X. Li, Y. Li, L. Shu, D. L. Nelson, H. Li, C. M. Hales, M. Gearing, T. S. Wingo, P. Jin, Expanded GGGGCC repeat RNA associated with amyotrophic lateral sclerosis and frontotemporal dementia causes neurodegeneration. Proc. Natl. Acad. Sci. U.S.A. 110, 7778–7783 (2013).

9. C. J. Donnelly, P.-W. Zhang, J. T. Pham, A. R. Haeusler, N. A. Mistry, S. Vidensky, E. L. Daley, E. M. Poth, B. Hoover, D. M. Fines, N. Maragakis, P. J. Tienari, L. Petrucelli, B. J. Traynor, J. Wang, F. Rigo, C. F. Bennett, S. Blackshaw, R. Sattler, J. D. Rothstein, RNA toxicity from the ALS/FTD C9ORF72 expansion is mitigated by antisense intervention. Neuron 80, 415–428 (2013).

10. Z. Tao, H. Wang, Q. Xia, K. Li, K. Li, X. Jiang, G. Xu, G. Wang, Z. Ying, Nucleolar stress and impaired stress granule formation contribute to C9orf72 RAN translation-induced cytotoxicity. Hum. Mol. Genet. 24, 2426–2441 (2015).

11. K. Mori, S.-M. Weng, T. Arzberger, S. May, K. Rentzsch, E. Kremmer, B. Schmid, H. A. Kretzschmar, M. Cruts, C. Van Broeckhoven, C. Haass, D. Edbauer, The C9orf72 GGGGCC repeat is translated into aggregating dipeptide-repeat proteins in FTLD/ALS. Science 339, 1335–1338 (2013).

12. T. Zu, Y. Liu, M. Bañez-Coronel, T. Reid, O. Pletnikova, J. Lewis, T. M. Miller, M. B. Harms, A. E. Falchook, S. H. Subramony, L. W. Ostrow, J. D. Rothstein, J. C. Troncoso, L. P. W. Ranum, RAN proteins and RNA foci from antisense transcripts in C9ORF72

ALS and frontotemporal dementia. Proc. Natl. Acad. Sci. U.S.A. 110, E4968–E4977 (2013).

13. C. Lagier-Tourenne, M. Baughn, F. Rigo, S. Sun, P. Liu, H.-R. Li, J. Jiang, A. T. Watt, S. Chun, M. Katz, J. Qiu, Y. Sun, S.-C. Ling, Q. Zhu, M. Polymenidou, K. Drenner, J. W. Artates, M. McAlonis-Downes, S. Markmiller, K. R. Hutt, D. P. Pizzo, J. Cady, M. B. Harms, R. H. Baloh, S. R. Vandenberg, G. W. Yeo, X.-D. Fu, C. F. Bennett, D. W. Cleveland, J. Ravits, Targeted degradation of sense and antisense C9orf72 RNA foci as therapy for ALS and frontotemporal degeneration. Proc. Natl. Acad. Sci. U.S.A. 110, E4530–E4539 (2013).

14. P. E. A. Ash, K. F. Bieniek, T. F. Gendron, T. Caulfield, W.-L. Lin, M. DeJesus-Hernandez, M. M. van Blitterswijk, K. Jansen-West, J. W. Paul III., R. Rademakers, K. B. Boylan, D. W. Dickson, L. Petrucelli, Unconventional translation of C9ORF72 GGGGCC expansion generates insoluble polypeptides specific to c9FTD/ALS. Neuron 77, 639–646 (2013).

15. S. Mizielinska, S. Grönke, T. Niccoli, C. E. Ridler, E. L. Clayton, A. Devoy, T. Moens, F. E. Norona, I. O. C. Woollacott, J. Pietrzyk, K. Cleverley, A. J. Nicoll, S. Pickering-Brown, J. Dols, M. Cabecinha, O. Hendrich, P. Fratta, E. M. C. Fisher, L. Partridge, A. M. Isaacs, C9orf72 repeat expansions cause neurodegeneration in Drosophila through arginine-rich proteins. Science 345, 1192–1194 (2014).

16. X. Wen, W. Tan, T. Westergard, K. Krishnamurthy, S. S. Markandaiah, Y. Shi, S. Lin, N. A. Shneider, J. Monaghan, U. B. Pandey, P. Pasinelli, J. K. Ichida, D. Trotti, Antisense proline-arginine RAN dipeptides linked to C9ORF72-ALS/FTD form toxic

nuclear aggregates that initiate in vitro and in vivo neuronal death. Neuron 84, 1213–1225 (2014).

17. I. Kwon, S. Xiang, M. Kato, L. Wu, P. Theodoropoulos, T. Wang, J. Kim, J. Yun, Y. Xie, S. L. McKnight, Poly-dipeptides encoded by the C9orf72 repeats bind nucleoli, impede RNA biogenesis, and kill cells. Science 345, 1139–1145 (2014).

18. J. G. O'Rourke, L. Bogdanik, A. Yáñez, D. Lall, A. J. Wolf, A. K. M. G. Muhammad, R. Ho, S. Carmona, J. P. Vit, J. Zarrow, K. J. Kim, S. Bell, M. B. Harms, T. M. Miller, C. A. Dangler, D. M. Underhill, H. S. Goodridge, C. M. Lutz, R. H. Baloh, C9orf72 is required for proper macrophage and microglial function in mice. Science 351, 1324–1329 (2016).

19. M. Koppers, A. M. Blokhuis, H.-J. Westeneng, M. L. Terpstra, C. A. C. Zundel, R. Vieira de Sá, R. D. Schellevis, A. J. Waite, D. J. Blake, J. H. Veldink, L. H. van den Berg, R. J. Pasterkamp, C9orf72 ablation in mice does not cause motor neuron degeneration or motor deficits. Ann. Neurol. 78, 426–438 (2015).

20. A. Atanasio, V. Decman, D. White, M. Ramos, B. Ikiz, H.-C. Lee, C.-J. Siao, S. Brydges, E. LaRosa, Y. Bai, W. Fury, P. Burfeind, R. Zamfirova, G. Warshaw, J. Orengo, A. Oyejide, M. Fralish, W. Auerbach, W. Poueymirou, J. Freudenberg, G. Gong, B. Zambrowicz, D. Valenzuela, G. Yancopoulos, A. Murphy, G. Thurston, K.-M. V. Lai, C9orf72 ablation causes immune dysregulation characterized by leukocyte expansion, autoantibody production, and glomerulonephropathy in mice. Sci. Rep. 6, 23204 (2016).

21. S. Mizielinska, T. Lashley, F. E. Norona, E. L. Clayton, C. E. Ridler, P. Fratta, A. M. Isaacs, C9orf72 frontotemporal lobar degeneration is characterised by frequent neuronal sense and antisense RNA foci. Acta Neuropathol. 126, 845–857 (2013).

22. A. J. Waite, D. Bäumer, S. East, J. Neal, H. R. Morris, O. Ansorge, D. J. Blake, Reduced C9orf72 protein levels in frontal cortex of amyotrophic lateral sclerosis and frontotemporal degeneration brain with the C9ORF72 hexanucleotide repeat expansion. Neurobiol. Aging 35, 1779.e5–1779.e13 (2014).

23. N. T. Ktistakis, S. A. Tooze, Digesting the expanding mechanisms of autophagy. Trends Cell Biol. 26, 624–635 (2016).

24. N. Mizushima, B. Levine, A. M. Cuervo, D. J. Klionsky, Autophagy fights disease through cellular self-digestion. Nature 451, 1069–1075 (2008).

25. N. Mizushima, M. Komatsu, Autophagy: Renovation of cells and tissues. Cell 147, 728–741 (2011).

26. R. L. Vidal, S. Matus, L. Bargsted, C. Hetz, Targeting autophagy in neurodegenerative diseases. Trends Pharmacol. Sci. 35, 583–591 (2014).

27. E. Wong, A. M. Cuervo, Autophagy gone awry in neurodegenerative diseases. Nat. Neurosci. 13, 805–811 (2010).

28. H. Stenmark, Rab GTPases as coordinators of vesicle traffic. Nat. Rev. Mol. Cell Biol. 10, 513–525 (2009).

29. A. L. Marat, H. Dokainish, P. S. McPherson, DENN domain proteins: Regulators of Rab GTPases. J. Biol. Chem. 286, 13791–13800 (2011).

30. S.-i. Yoshimura, A. Gerondopoulos, A. Linford, D. J. Rigden, F. A. Barr, Family-wide characterization of the DENN domain Rab GDP-GTP exchange factors. J. Cell Biol. 191, 367–381 (2010).

31. T. P. Levine, R. D. Daniels, A. T. Gatta, L. H. Wong, M. J. Hayes, The product of C9orf72, a gene strongly implicated in neurodegeneration, is structurally related to DENN Rab-GEFs. Bioinformatics 29, 499–503 (2013).

32. D. Zhang, L. M. Iyer, F. He, L. Aravind, Discovery of novel DENN proteins: Implications for the evolution of eukaryotic intracellular membrane structures and human disease. Front. Genet. 3, 283 (2012).

33. M. A. Farg, V. Sundaramoorthy, J. M. Sultana, S. Yang, R. A. K. Atkinson, V. Levina, M. A. Halloran, P. A. Gleeson, I. P. Blair, K. Y. Soo, A. E. King, J. D. Atkin, C9ORF72, implicated in amytrophic lateral sclerosis and frontotemporal dementia, regulates endosomal trafficking. Hum. Mol. Genet. 23, 3579–3595 (2014).

34. C. Sellier, M.-L. Campanari, C. Julie Corbier, A. Gaucherot, I. Kolb-Cheynel, M. Oulad-Abdelghani, F. Ruffenach, A. Page, S. Ciura, E. Kabashi, N. Charlet-Berguerand, Loss of C9ORF72 impairs autophagy and synergizes with polyQ Ataxin-2 to induce motor neuron dysfunction and cell death. EMBO J. 35, 1276–1297 (2016).

35. C. Behrends, M. E. Sowa, S. P. Gygi, J. W. Harper, Network organization of the human autophagy system. Nature 466, 68–76 (2010).

36. N. Hosokawa, T. Hara, T. Kaizuka, C. Kishi, A. Takamura, Y. Miura, S.-i. Iemura, T. Natsume, K. Takehana, N. Yamada, J.-L. Guan, N. Oshiro, N. Mizushima, Nutrient-dependent mTORC1 association with the ULK1–Atg13–FIP200 complex required for autophagy. Mol. Biol. Cell 20, 1981–1991 (2009).

37. J. Kim, M. Kundu, B. Viollet, K.-L. Guan, AMPK and mTOR regulate autophagy through direct phosphorylation of Ulk1. Nat. Cell Biol. 13, 132–141 (2011).
38. L. Shang, S. Chen, F. Du, S. Li, L. Zhao, X. Wang, Nutrient starvation elicits an acute autophagic response mediated by Ulk1 dephosphorylation and its subsequent dissociation from AMPK. Proc. Natl. Acad. Sci. U.S.A. 108, 4788–4793 (2011).
39. N. Hosokawa, T. Sasaki, S.-i. Iemura, T. Natsume, T. Hara, N. Mizushima, Atg101, a novel mammalian autophagy protein interacting with Atg13. Autophagy 5, 973–979 (2009).
40. C. A. Mercer, A. Kaliappan, P. B. Dennis, A novel, human Atg13 binding protein, Atg101, interacts with ULK1 and is essential for macroautophagy. Autophagy 5, 649–662 (2009).
41. D. Li, R. Roberts, WD-repeat proteins: Structure characteristics, biological function, and their involvement in human diseases. Cell. Mol. Life Sci. 58, 2085–2097 (2001).
42. G. R. Wilson, J. C. H. Sim, C. McLean, M. Giannandrea, C. A. Galea, J. R. Riseley, S. E. M. Stephenson, E. Fitzpatrick, S. A. Haas, K. Pope, K. J. Hogan, R. G. Gregg, C. J. Bromhead, D. S. Wargowski, C. H. Lawrence, P. A. James, A. Churchyard, Y. Gao, D. G. Phelan, G. Gillies, N. Salce, L. Stanford, A. P. L. Marsh, M. L. Mignogna, S. J. Hayflick, R. J. Leventer, M. B. Delatycki, G. D. Mellick, V. M. Kalscheuer, P. D'Adamo, M. Bahlo, D. J. Amor, P. J. Lockhart, Mutations in RAB39B cause X-linked intellectual disability and early-onset Parkinson disease with α-synuclein pathology. Am. J. Hum. Genet. 95, 729–735 (2014).
43. M. Giannandrea, V. Bianchi, M. L. Mignogna, A. Sirri, S. Carrabino, E. D'Elia, M. Vecellio, S. Russo, F. Cogliati, L. Larizza, H.-H. Ropers, A. Tzschach, V. Kalscheuer, B.

Oehl-Jaschkowitz, C. Skinner, C. E. Schwartz, J. Gecz, H. Van Esch, M. Raynaud, J. Chelly, A. P. M. de Brouwer, D. Toniolo, P. D'Adamo, Mutations in the small GTPase gene RAB39B are responsible for X-linked mental retardation associated with autism, epilepsy, and macrocephaly. Am. J. Hum. Genet. 86, 185–195 (2010).

44. B. Xiong, V. Bayat, M. Jaiswal, K. Zhang, H. Sandoval, W.-L. Charng, T. Li, G. David, L. Duraine, Y.-Q. Lin, G. G. Neely, S. Yamamoto, H. J. Bellen, Crag is a GEF for Rab11 required for rhodopsin trafficking and maintenance of adult photoreceptor cells. PLOS Biol. 10, e1001438 (2012).

45. D. J. Klionsky, K. Abdelmohsen, A. Abe, M. J. Abedin, H. Abeliovich, A. Acevedo Arozena,…E. Ziparo, C. E. Zois, T. Zoladek, W.-X. Zong, A. Zorzano, S. M. Zughaier, Guidelines for the use and interpretation of assays for monitoring autophagy (3rd edition). Autophagy 12, 1–222 (2016).

46. M. Laplante, D. M. Sabatini, mTOR signaling in growth control and disease. Cell 149, 274–293 (2012).

47. S. A. Kang, M. E. Pacold, C. L. Cervantes, D. Lim, H. J. Lou, K. Ottina, N. S. Gray, B. E. Turk, M. B. Yaffe, D. M. Sabatini, mTORC1 phosphorylation sites encode their sensitivity to starvation and rapamycin. Science 341, 1236566 (2013).

48. V. I. Korolchuk, A. Mansilla, F. M. Menzies, D. C. Rubinsztein, Autophagy inhibition compromises degradation of ubiquitin-proteasome pathway substrates. Mol. Cell 33, 517–527 (2009).

49. C. Progida, L. Cogli, F. Piro, A. De Luca, O. Bakke, C. Bucci, Rab7b controls trafficking from endosomes to the TGN. J. Cell Sci. 123, 1480–1491 (2010).

50. G. F. McIntyre, A. H. Erickson, Procathepsins L and D are membrane-bound in acidic microsomal vesicles. J. Biol. Chem. 266, 15438–15445 (1991).

51. M. Khundadze, K. Kollmann, N. Koch, C. Biskup, S. Nietzsche, G. Zimmer, J. C. Hennings, A. K. Huebner, J. Symmank, A. Jahic, E. I. Ilina, K. Karle, L. Schöls, M. Kessels, T. Braulke, B. Qualmann, I. Kurth, C. Beetz, C. A. Hübner, A hereditary spastic paraplegia mouse model supports a role of ZFYVE26/SPASTIZIN for the endolysosomal system. PLOS Genet. 9, e1003988 (2013).

52. F. M. Platt, B. Boland, A. C. van der Spoel, The cell biology of disease: Lysosomal storage disorders: The cellular impact of lysosomal dysfunction. J. Cell Biol. 199, 723–734 (2012).

53. M. A. Riederer, T. Soldati, A. D. Shapiro, J. Lin, S. R. Pfeffer, Lysosome biogenesis requires Rab9 function and receptor recycling from endosomes to the trans-Golgi network. J. Cell Biol. 125, 573–582 (1994).

54. P. M. Sullivan, X. Zhou, A. M. Robins, D. H. Paushter, D. Kim, M. B. Smolka, F. Hu, The ALS/FTLD associated protein C9orf72 associates with SMCR8 and WDR41 to regulate the autophagy-lysosome pathway. Acta Neuropathol. Commun. 4, 51 (2016).

55. H. Suzuki, T. Kaizuka, N. Mizushima, N. N. Noda, Structure of the Atg101–Atg13 complex reveals essential roles of Atg101 in autophagy initiation. Nat. Struct. Mol. Biol. 22, 572–580 (2015).

56. T. Hara, K. Nakamura, M. Matsui, A. Yamamoto, Y. Nakahara, R. Suzuki-Migishima, M. Yokoyama, K. Mishima, I. Saito, H. Okano, N. Mizushima, Suppression of basal autophagy in neural cells causes neurodegenerative disease in mice. Nature 441, 885–889 (2006).

57. M. Komatsu, S. Waguri, T. Chiba, S. Murata, J.-i. Iwata, I. Tanida, T. Ueno, M. Koike, Y. Uchiyama, E. Kominami, K. Tanaka, Loss of autophagy in the central nervous system causes neurodegeneration in mice. Nature 441, 880–884 (2006).

58. P. Ejlerskov, J. G. Hultberg, J. Wang, R. Carlsson, M. Ambjørn, M. Kuss, Y. Liu, G. Porcu, K. Kolkova, C. Friis Rundsten, K. Ruscher, B. Pakkenberg, T. Goldmann, D. Loreth, M. Prinz, D. C. Rubinsztein, S. Issazadeh-Navikas, Lack of neuronal IFN-β-IFNAR causes Lewy body- and Parkinson's disease-like dementia. Cell 163, 324–339 (2015).

59. N. P. Rocha, A. S. de Miranda, A. L. Teixeira, Insights into neuroinflammation in Parkinson's disease: From biomarkers to anti-inflammatory based therapies. Biomed. Res. Int. 2015, 628192 (2015).

60. C. P. Webster, E. F. Smith, C. S. Bauer, A. Moller, G. M. Hautbergue, L. Ferraiuolo, M. A. Myszczynska, A. Higginbottom, M. J. Walsh, A. J. Whitworth, B. K. Kaspar, K. Meyer, P. J. Shaw, A. J. Grierson, K. J. De Vos, The C9orf72 protein interacts with Rab1a and the ULK1 complex to regulate initiation of autophagy. EMBO J. 35, 1656–1676 (2016).

61. S. Xiao, L. MacNair, J. McLean, P. McGoldrick, P. McKeever, S. Soleimani, J. Keith, L. Zinman, E. Rogaeva, J. Robertson, C9orf72 isoforms in amyotrophic lateral sclerosis and frontotemporal lobar degeneration. Brain Res. 10.1016/j.brainres.2016.04.062 (2016).

62. S. Xiao, L. MacNair, P. McGoldrick, P. M. McKeever, J. R. McLean, M. Zhang, J. Keith, L. Zinman, E. Rogaeva, J. Robertson, Isoform-specific antibodies reveal distinct

subcellular localizations of C9orf72 in amyotrophic lateral sclerosis. Ann. Neurol. 78, 568–583 (2015).

63. J.-F. Chen, Y. Zhang, J. Wilde, K. C. Hansen, F. Lai, L. Niswander, Microcephaly disease gene Wdr62 regulates mitotic progression of embryonic neural stem cells and brain size. Nat. Commun. 5, 3885 (2014).

CHAPTER 3

Smcr8 deficiency disrupts axonal transport-dependent lysosomal function and promotes axonal swellings and gain of toxicity in C9ALS/FTD mouse models

Chen Liang, Qiang Shao, Wei Zhang, Mei Yang, Qing Chang, Rong Chen and Jian-Fu Chen.
Human Molecular Genetics, Volume 28, Issue 23, 1 December 2019, Pages 3940-3953
Reprinted here with permission of Oxford University Press.
URL: https://academic.oup.com/hmg/article-abstract/28/23/3940/5589185

Abstract

G4C2 repeat expansions in an intron of C9ORF72 cause the most common familial amyotrophic lateral sclerosis and frontotemporal dementia (collectively, C9ALS/FTD). Mechanisms and mediators of C9ALS/FTD pathogenesis remain poorly understood. C9orf72 and Smcr8 form a protein complex. Here, we show that expression of Smcr8, like C9orf72, is reduced in C9ALS/FTD mouse models and patient tissues. Since Smcr8 is highly conserved between human and mouse, we evaluated the effects of Smcr8 downregulation in mice. Smcr8 knockout (KO) mice exhibited motor behavior deficits, which resemble those of C9ALS/FTD mouse models, and displayed axonal swellings in their spinal cords and neuromuscular junctions. These deficits are caused by impaired autophagy-lysosomal functions due to disrupted axonal transport in mutant motor neurons. Consistent with its interaction with C9orf72 and their downregulation in patient tissues, Smcr8 deficiency exacerbated autophagy-lysosomal impairment in C9orf72 KO mice. The disease relevance of Smcr8 downregulation was reflected by exacerbated axonal swellings and gain of toxicity pathology arising from Smcr8 haploinsufficiency in a mouse model of C9ALS/FTD. Thus, our in vivo studies suggested that Smcr8 deficiency impairs axonal transport dependent autophagy-lysosomal function and exacerbates axonal degeneration and gain of toxicity in C9ALS/FTD mouse models.

Introduction

Frontotemporal dementia (FTD) and amyotrophic lateral sclerosis (ALS) are neurodegenerative disorders that occur simultaneously in certain populations of patients (1, 2). G4C2 hexanucleotide repeat expansion in a noncoding region of the gene chromosome 9 open reading frame 72 (C9ORF72) is the most common cause of familial ALS and FTD (C9ALS/FTD) (3–6). C9ORF72-associated ALS accounts for around 40% of familial ALS and about 5–10% of sporadic ALS cases (4, 5). Haploinsufficiency of C9ORF72 protein is a key proposed disease mechanism, which may act in parallel with gain of toxicity from toxic RNAs of repeat transcription and dipeptide repeat proteins (DPRs) from repeat-associated non-AUG (RAN) translation (1, 2). Consistent with this loss-of-function notion, C9ORF72 expression is reduced in C9ALS/FTD patient tissues (3, 5, 7, 8); haploinsufficiency of C9ORF72 is considered to contribute to the degeneration of motor neurons (MNs) derived from induced pluripotent stem cells of ALS patients (9); C9orf72 deficiency exacerbates motor behavior deficits of a C9ALS/FTD mouse model in vivo (10). Therefore, studying C9orf72 biology may provide new insights into pathogenesis of C9ALS/FTD from the perspective of loss-of-function.

C9orf72 forms a protein complex with Smcr8 (11–17). They are both DENN domain-containing proteins (18, 19) and regulate autophagy, a lysosome-dependent degradation process (20, 21). Enlarged lysosomal sizes and impaired lysosomal degradation have been observed in cells deficient in C9orf72 or Smcr8 (22, 23). These

results suggest the possibility that autophagy-lysosomal function may be impaired in C9ALS/FTD. Interestingly, neither heterozygous nor homozygous knockout (KO) of C9orf72 in neurons leads to MN degeneration or motor deficits in mice at advanced ages (24). This raises the question whether and to what extent C9orf72's functions are dysregulated in C9ALS/FTD in vivo. Consequently, the potential autophagy-lysosomal deficiency in C9ALS/FTD in vivo is unclear, and the mediators and underlying mechanisms remain poorly understood.

Using a C9ORF72 bacterial artificial chromosome (BAC) transgenic mouse model (*C9-BAC*) (25), we recently generated a genetic mouse model (*C9orf72*$^{+/-}$*;C9-BAC*) of C9ALS/FTD with both loss- and gain-of-function features. We found that C9orf72 deficiency and haploinsufficiency exacerbate motor behavior deficits of C9-BAC mice in a dose-dependent manner, and this occurs early in the course of pathogenesis (10). To investigate the mechanisms underlying these motor deficits, we examined Smcr8 and found that it, like C9orf72, is reduced in C9ALS/FTD mouse models and patient tissues. Smcr8 mutant mice developed motor behavior deficits, suggesting that Smcr8 downregulation could be a mediator of motor deficits in *C9orf72*$^{+/-}$*;C9-BAC* mice. Mechanistic studies revealed that Smcr8 deficiency disrupted axonal transport in MNs, impaired autophagy-lysosomal function, and led to abnormal axonal swellings in spinal cords and neuromuscular junctions (NMJs) in mice. These deficits were more severe in the background of C9orf72 KO. Smcr8 deficiency also exacerbated the accumulation of DPRs in C9-BAC mouse models, suggesting the interaction between loss- and gain-of-function in the pathogenesis of C9ALS/FTD.

Materials and Methods

Mice

To generate *Smcr8*$^{\beta geo/\beta geo}$ mutant mice, *Smcr8*$^{tm1(KOMP)vlcg}$ embryonic stem (ES) cells were obtained from the KO mouse project repository at the University of California, Davis. The majority of Smcr8 exon 1 was replaced by a cassette containing lacZ-polyA followed by a loxP-flanked hUbCpro-neo-polyA sequence. The Mouse Genetics Core Facility at National Jewish Health in Denver performed the ES cell injections into C57BK/6N blastocysts. The chimeric offsprings were mated to 129S1/SvImJ mice for germline transmission. Germline-transmitted heterozygous females were crossed with CMV-Cre males to remove the Neo cassette. Smcr8$^{-/-}$ mice were backcrossed into C57BL/6J for four generations. *C9-BAC* mice (Cat#: 029099) were ordered from Jackson laboratory, and were backcrossed into C57BL/6J for four generations. All animal studies were conducted under protocols approved by the Institutional Animal Care and Use Committee at the University of Georgia or University of Southern California.

Mutant characterization, immunofluorescence staining and western blot analysis

Histological processing and immunohistochemical labeling of sections were performed as described previously (48, 49). Mice were anesthetized with CO2 and perfusion-fixed with 4% paraformaldehyde (PFA). Spinal cords were harvested and post-fixed in 4% PFA, washed with PBS and immersed in 25% sucrose overnight at 4°C followed by standard OCT embedding and coronal sectioning. The following primary

antibodies were used: anti-Lamp1 (1D4B, DSHB), anti-p62 (610 832, BD Biosciences), anti-160 kD NF Medium (ab65845, Abcam), anti-NF H, Nonphosphorylated (SMI 32, Biolegend), anti-beta Galactosidase (CGAL-45A-Z, Immune Systems), anti-GFAP (MAB3402, EMD Millipore), anti-Iba1 (019-19 741, Wako), anti-LC3 (5F10, NanoTools), Tuj1 (T3952, Sigma), ChAT (AB144P, EMP Millipore), GA (MABN889, Millipore) and poly GP (24494-1-AP, Proteintech). The secondary antibodies used were Alexa 488, Alexa 555 and Alexa 647 conjugated to specific IgG types (Invitrogen Molecular Probes). Axonal staining was performed by Bielschowsky staining with Hito Bielschowsky OptimStain™ Kit (Hito Biotec) according to the manufacturer's protocol. X-gal activity was assessed by incubating sections with LacZ staining solution (1 mg/ml of X-gal, 5 mM potassium ferrocyanide, 5 mM potassium ferricyanide and 2 mM MgCl2 in PBS) overnight at 37°C.

TEM

Spinal cords were fixed in 2% PFA plus 2.5% glutaraldehyde in 0.1 M Sodium Cacodylate buffer (PH = 7.4) for 24 h at 4°C. Tissues were embedded and sectioned for TEM by the Department of Pathology, EM Division at the University of Georgia.

Mouse MN isolation, transfection and live imaging

Isolation and culture of spinal cord motoneurons from E 13.5 mice were performed as previously described (50). Spinal cords were isolated and dorsal root ganglia were removed carefully. MNs were enriched by lectin-based purification. Isolated cells were plated onto poly-DL-ornithine hydrobromide/laminin (Sigma) coated 35 mm glass

bottom culture dishes (MatTek). Cells were cultured in Neurobasal medium (Invitrogen) with 1 × B27 supplement (Invitrogen), 5% inactivated horse serum (Invitrogen), 1% Glutamax (Invitrogen) and 10 ng/ml CNTF at 37°C in a 5% CO2 incubator. Half the volume of culture medium was exchanged every 2 days. At 4 days in vitro (DIV4), neurons were transfected using NeuroMag transfection reagent (Oz Biosciences) as previously described (51). Briefly, 1 h before magnetofection, complete medium was replaced with serum-free Neurobasal/B27/Glutamax medium. Plasmid DNA (1.5 µg) was incubated with 4 µl Neuromag in 300 µl OptiMEM for 15 minutes, and then added drop-wise to the cultures. Cells were incubated on top of a magnetic plate (Oz Biosciences) for 15 minute and complete medium was restored after 1 h. For live cell imaging, 35 mm glass bottom dishes containing normal growth medium were mounted in a temperature-controlled stage and maintained at 37°C and 5% CO2 conditions. Cells were visualized at DIV6-9 on a Zeiss LSM 710 confocal microscope using a 100 × oil-immersion lens. Digital images were acquired with a camera using ZEN software. Laser lines at 488 nm were used. Time-lapse sequences of 1024 × 1024 pixels were collected at 7.8 second intervals for 15 minutes.

Transport analysis

Kymographs were generated using the Image J plugin Kymograph (https://www.embl.de//eamnet/html/kymograph.html). Net run speeds and lengths of vesicle movement were calculated by drawing a slope from the beginning to the end of the run on the kymograph. The transport direction was manually determined: vesicles were classified as retrograde (moved ≥ 1.5 µm in the retrograde direction), anterograde

(moved ≥ 1.5 μm in the anterograde direction) or stationary (moved < 1.5 μm during the duration of the 15-minute video). The percentage motility of vesicles along the axon (retrograde, anterograde or stationary) was calculated as a percentage of the total number of imaged vesicles per neuron. The instantaneous velocities were quantified by Image J's TrackMate v3.4.2 plugin (52), and stalls were defined as a vesicle with velocity < 0.1 μm/s for ≥8 s. The numbers of stalls per trace were calculated with a custom Python script.

NMJ analysis

Muscles were fixed for 10 minutes in freshly prepared PBS containing 4% (w/v) PFA. After washing with PBS, further connective tissues were detached from the muscles, and individual fibers were carefully teased apart to facilitate antibody penetration. Muscles were permeabilized with 2% Triton X-100 in PBS for 30 minute and then blocked in 4% BSA and 1% Triton X-100 in PBS for 30 minutes. Samples were incubated overnight at 4°C in blocking solution with α-Bungarotoxin, Alexa Fluor™ 488 conjugate (1:500 dilution), and primary antibodies against NF (2H3, 1: 70 dilution) and Lamp-1 (1D4B, 1:70 dilution) to visualize the AChRs, axons and lysosomes. The following day, muscles were washed three times for 10 minute each in PBS before incubation for 2 h with AlexaFluor 555 and 647 secondary antibodies and α-Bungarotoxin, Alexa Fluor™ 488 conjugate in PBS in the dark. Last, muscles were washed three times for 10 minute each in PBS and mounted on slides with coverslips. A Leica TCS SP8 microscope was used to image the NMJs with Z-stacks at 3 μm intervals.

Behavioral testing

The experimenter was blind to the animal's genotype during all tests. Open filed test was performed using an overhead SMART video tracking system (Panlab), which measures distance traveled, time spent in each zone, and speed. The apparatus consisted of a gray open top plastic box (w × d × h: 45 × 45 × 40 cm) divided into four equal arenas. After a 2 h acclimatization to the behavioral testing room, each animal was placed in the center of the open field and left undisturbed for 30 minutes. The apparatus was wiped between trials with a 70% ethanol solution. For rotarod test, an accelerating rotarod (Panlab) was used to analyze motor coordination and balance. Mice were trained three times on the rotarod with 4 rpm/minute speed 1 day before testing. During test conditions, we measured the latency (time) to the mouse falling from the rotating beam while ramping up the speed from 4 to 40 rpm over a 5-minute trial period. Mice were given four trials per day, with an intertrial interval of 20 minutes. The average of the three trials was used to evaluate latency to fall. For grip strength, the grip strength of front paws was measured using a grip strength meter (Bioseb). Each mouse was held by the tail and lowered toward the apparatus. Front paws were allowed to grasp the assembly. The mouse was then pulled backward in the horizontal plane until the pull-bar was released. The trial was repeated four times, and the force generated by pulling the animal away from the wire mesh was recorded.

Results

Smcr8 is downregulated in C9ALS/FTD mouse models and patient tissues

C9orf72 dose reduction exacerbates motor deficits of *C9-BAC* mice at an early stage (10), when C9-BAC mice display no behavior deficits (25). To investigate mechanisms underlying these motor deficits, we focused on Smcr8. Smcr8 and C9orf72 form a protein complex that regulates autophagy-lysosomal functions (11–17). They stabilize each other; Smcr8 protein level is reduced in C9orf72-deficient cells (13, 15, 26). However, it remains unknown whether the Smcr8 protein level changes under pathological conditions in which C9orf72 protein is partially lost. Therefore, we examined Smcr8 expression in spinal cords from C9-BAC mice with different C9orf72 dose reductions. Western blot analyses confirmed C9orf72 protein dose reduction with or without the presence of *C9-BAC* (Fig. 3.1A and B). Interestingly, Smcr8 protein levels were reduced accordingly in response to C9orf72 dose reduction. In contrast, the level of Atg101, another complex-associated protein, did not change (Fig. 3.1A and B) (12), suggesting the specificity of Smcr8 downregulation.

To investigate whether Smcr8 downregulation exists at the mRNA level, we performed RT-PCR analyses and found that there were no significant changes of Smcr8 mRNA levels (Fig. 3.1C). These results suggest that Smcr8 downregulation may occur post-transcriptionally. To determine whether SMCR8 downregulation occurs in patient tissues, we performed western blot analyses using postmortem patient brain tissues. As reported in published data (3, 4, 7), C9ORF72 protein levels were reduced in patient brain lysates (Fig. 3.1D). Consistent with Smcr8 downregulation from mouse models, SMCR8 protein expression was also decreased in patient brain tissues (Fig. 3.1D).

Figure 3.1. Smcr8 downregulation in C9ALS/FTD and mutant mouse generation.

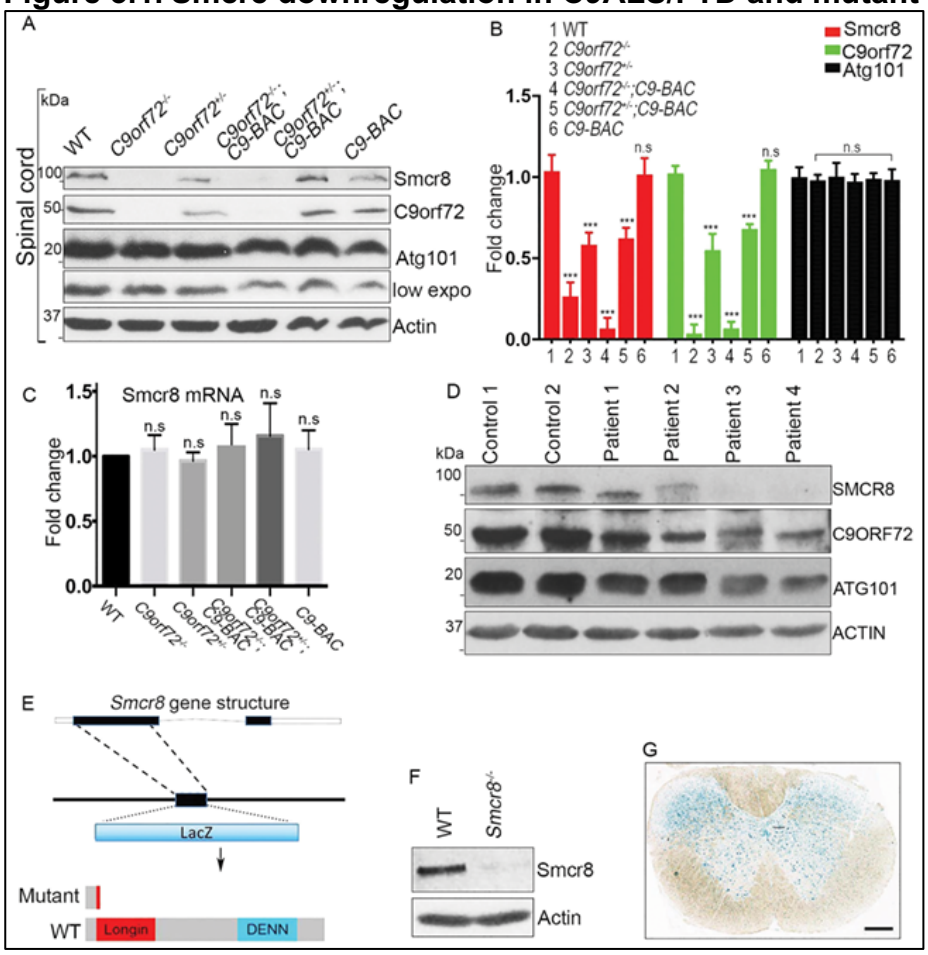

(A) Western blot analysis of protein expression in spinal cords. β-Actin serves as the loading control. (B) Quantification of protein levels of Smcr8 and other proteins in spinal cords. (C) RT-PCR analysis of Smcr8 mRNA expression. (D) Western blot analysis of the protein expression of Smcr8, C9orf72 and Atg101 in C9ALS/FTD patient brain tissues. β-Actin serves as the loading control. (E) Diagram of the generation of Smcr8−/− mutant mice. (F) Western blot analysis confirmed the absence of Smcr8 protein in mutant mice. β-actin serves as the loading control. (G) LacZ staining of coronal sections from 2-month-old heterozygous mice shows Smcr8 expression in spinal cord. Scale bars: 100 μm. Data are presented as mean ± SEM from three independent experiments containing one WT and one mutant mice in each experiment (n = 3). Statistical analyses were performed with one-way ANOVA with Bonferroni's post hoc test (***P < 0.001, n.s. represents no significant difference detected).

Together, our studies revealed a Smcr8 protein reduction in C9ALS/FTD mouse models and patient brain tissues.

Smcr8 deficient mice exhibit motor behavior deficits

To investigate the importance of Smcr8 downregulation, we generated Smcr8 null mice in which the majority of Smcr8 exon 1 was replaced by a LacZ cassette (Fig. 3.1E). Western blot analyses confirmed the absence of Smcr8 proteins in the homozygous mutant mice (Fig. 3.1F); therefore, we refer to these mice as *Smcr8*$^{-/-}$. To guide our functional studies, we examined Smcr8's expression pattern by performing X-gal staining. We found that Smcr8 was ubiquitously expressed in the spinal cords and in different brain regions including the cerebral cortex, hippocampus and cerebellum (Fig. 3.1G, Fig. 3.S1A). Immunohistochemical (IHC) staining revealed that Smcr8 was expressed in the cytoplasm of NeuN-positive neurons (Fig. 3.S1B), including SMI32-labeled MNs (Fig. 3.S1C).

Smcr8$^{-/-}$ mice were fertile, viable and displayed no visiable developmental defects. Offspring from heterozygous matings were born in the expected Mendelian ratios. To assess motor behaviors, we examined motor strength by measuring forelimb grip strength. *Smcr8*$^{-/-}$ mice exhibited a decrease in motor strength compared to WT controls, in both males and females, at 9 months of age (Fig. 3.2A). Grip strength deficits could be detected at 3, 9 and 12 months of age (Fig. 3.2B). After detecting grip strength deficits in both sexes, we focused on female mice because C9-BAC female mice exhibited more consistent behavior deficits than male mice (25). To measure motor coordination and motor learning, we performed an accelerating rotarod test. *Smcr8*$^{+/-}$ and *Smcr8*$^{-/-}$ mice had a significant reduction in latency to fall compared to

Figure 3.2. Smcr8 KO mice exhibit motor behavior deficits.

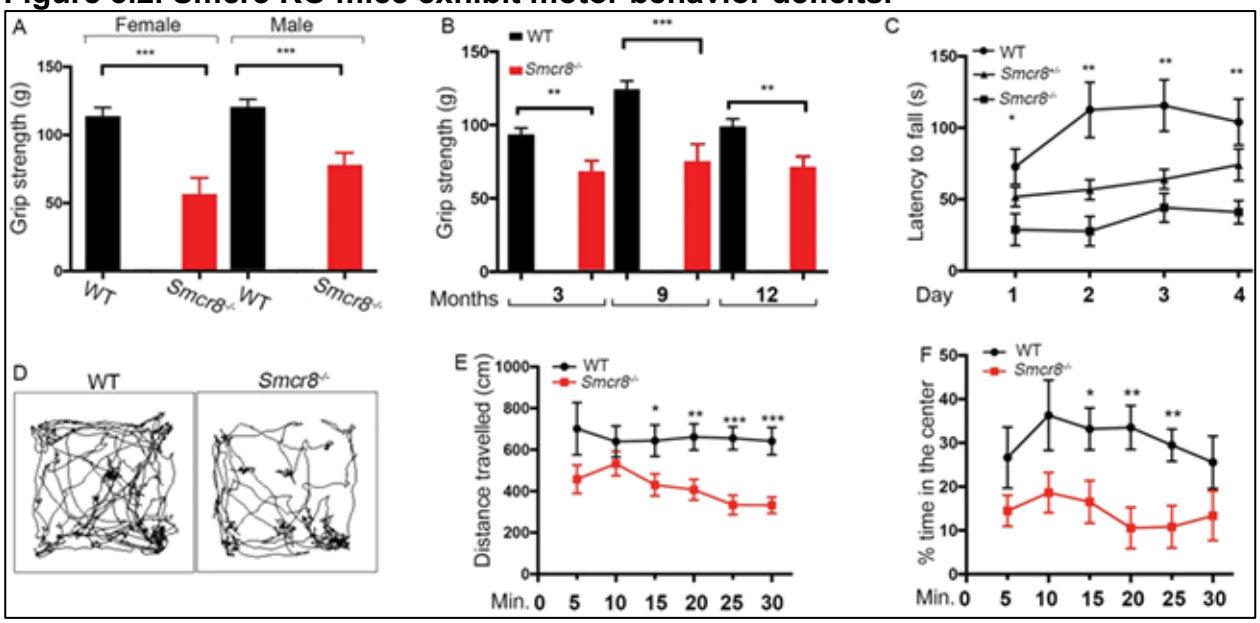

(A) Forelimb grip strength assay on 9-month-old WT (n = 9 females, 13 males) and *Smcr8*$^{-/-}$ (n = 8 females, 12 males) mice. (B) Forelimb grip strength is reduced in *Smcr8*$^{-/-}$ (n = 11) female mice compared to WT *Smcr8*$^{+/+}$ (n = 10) mice at 3, 9 and 12 months of age. (C) Rotarod assay reveals the decreased latency to fall in *Smcr8*$^{-/-}$ (n = 11) female mice compared to WT *Smcr8*$^{+/+}$ (n = 10). *Smcr8*$^{-/-}$mice exhibited a decreased rate of motor learning in the rotarod test over a 4-day test period compared to WT controls. (D) Representative traces showing the paths of mice in the open field chambers (snapshots taken at 5-minute intervals). (E) *Smcr8*$^{-/-}$ (n = 12) mutant mice traveled less distance (5-minute interval) compared to *Smcr8*$^{+/+}$ (n = 10) control mice. (F) *Smcr8*$^{-/-}$ (n = 12) mutant mice spent less time in the center of the open field chambers in every 5-minute trial compared to *Smcr8*$^{+/+}$ (n = 10) control mice. Statistical analysis was performed by one-way ANOVA analysis with Bonferroni correction; n.s. represents no significant difference detected (*P < 0.05, **P < 0.01 and ***P < 0.001).

age-matched WT controls (Fig. 3.2C). WT mice exhibited an increased trend of latency to fall in the rotarod test over a 4-day test period, indicating an active learning process during this period of time (Fig. 3.2C). In contrast, *Smcr8*$^{-/-}$ mice failed to display an increase in latency to fall, suggesting motor learning deficits. Open field analyses revealed that *Smcr8*$^{-/-}$ mice had a decrease in the total distance traveled and the percentage of time spent in the center (Fig. 3.2D–F). Together, these results suggest that Smcr8 deficiency developed motor behavior deficits in mice.

Smcr8 deletion disrupts autophagy-lysosomal degradation and leads to axonal swellings

To identify the cellular basis of motor deficits in *Smcr8*$^{-/-}$ mutant mice, we first examined the central nervous system in 7-month-old mice. H&E staining did not reveal obvious loss or disorganization of major brain or spinal cord regions; NeuN-positive neurons were not lost in the cortex or spinal cord of *Smcr8*$^{-/-}$ mice. Next, we assessed nerve fibers in spinal cords using Bielschowsky silver impregnation analysis, which is used for the visualization of neuronal processes including axons. Although swollen neuronal processes were seldom detected in WT controls, there was a robust increase in swollen neuronal processes in mutant spinal cords (Fig. 3.3A and B). We used antibodies against neurofilament (NF) to label axons. *Smcr8*$^{-/-}$ spinal cords exhibited mainly NF-positive swellings (white arrowheads in Fig. 3.3C). These results suggest that these neuronal processes were of axonal origin; therefore, we refer to them as axonal swellings. Statistical analysis revealed that axonal swellings increased as age advanced in *Smcr8*$^{-/-}$ spinal cords (Fig. 3.3D).

Figure 3.3. Impaired autophagy-lysosomal degradation leads to axonal swellings in *Smcr8*$^{-/-}$ mice.

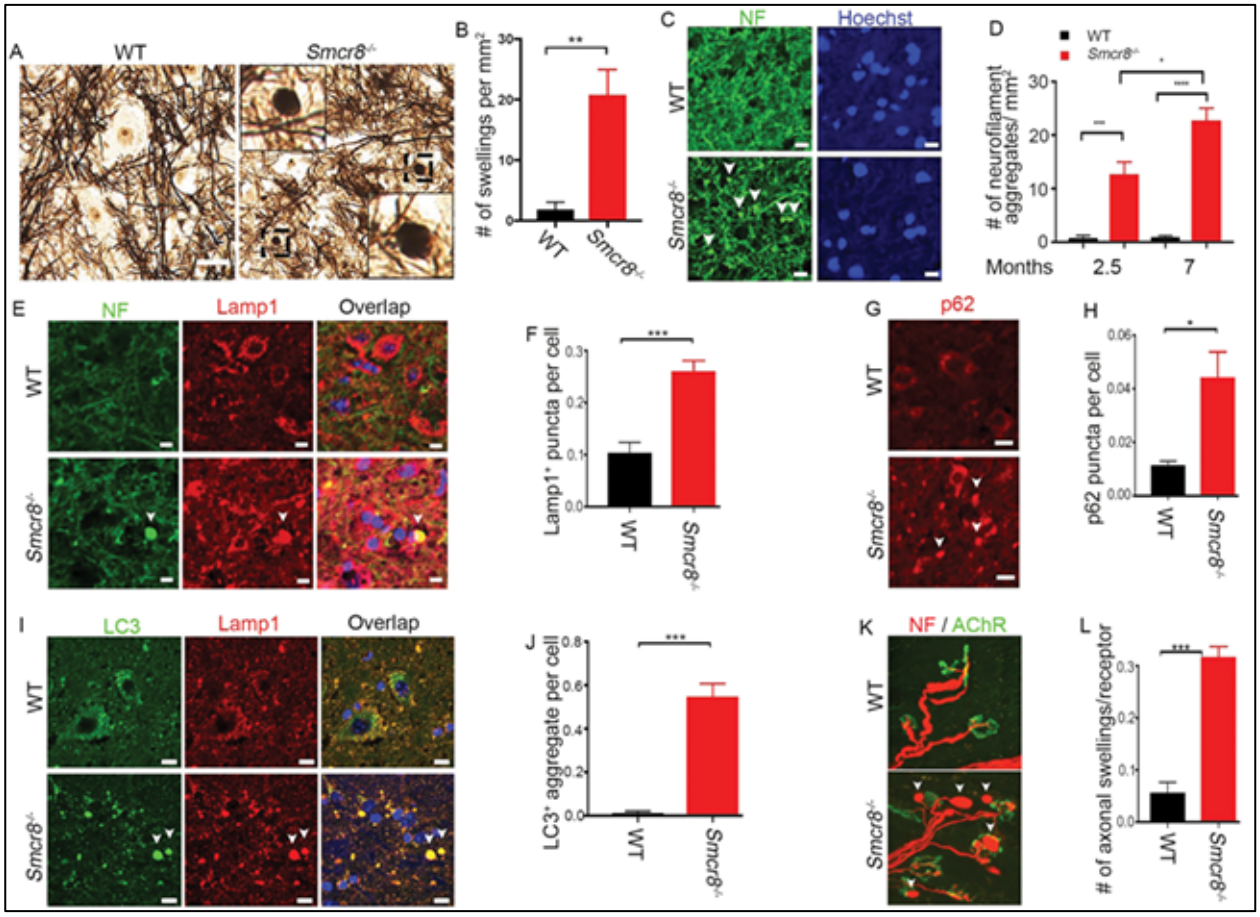

(A) Bielschowsky silver impregnation analyses revealed swelling neuronal processes in 7-month-old mutant spinal cords. Individual spheroid structures are enlargements of black boxed areas. Scale bars: 20 μm. (B) Quantification of numbers of swollen neuronal processes in spinal cord sections. (C) Representative imaging of spinal cords stained with antibodies against NF (NF, green). White arrowheads represent axonal swellings. Hoechst stains nuclei. Scale bars: 10 μm. (D) Quantification of NF-positive axonal swellings per mm2 in the spinal cords. Two-way ANOVA analysis with Bonferroni correction detected a significant difference between 2.5 and 7 months. (E, G, I) Confocal imaging of spinal cord sections stained with antibodies against NF (NF, green), LC3 (green), Lamp1 (red) and p62 (red). White arrowheads indicate axonal swellings, LC3-positive aggregates, or p62 puncta. Scale bars: 10 μm. (F, H, J) Quantification of Lamp1-positive puncta outside of perinuclear areas per cell (F), the number of p62 puncta per cell (H), and the number of LC3+ aggregate per cell (J). (K) *Smcr8*$^{-/-}$ mice display NMJ swellings stained with antibodies against NF (NF, red) and AChR (green). White arrowheads indicate swelling NMJs. (L) Quantification of numbers of NMJ swellings in *Smcr8*$^{-/-}$ mice. For all the experiments, error bars represent SEM using measurements averaged from ≥3 sections of each mutant mice (n = 3). Statistical analyses were performed with non-parametric Mann-Whitney test (*P < 0.05, **P < 0.01 and ***P < 0.001).

Smcr8 is a lysosome-associated protein and regulates autophagy-lysosomal functions (12, 13). Massive accumulation of Lamp1-positive axonal lysosomes has been reported in patients with neurodegenerative conditions (27). Therefore, we examined Lamp1 and found that it mainly co-localized with NF in the axonal swellings (Fig. 3.3E), and was barely detected in GFAP-labeled astrocytes and Iba1-labeled microglia (Fig. 3.S2A and B). Lamp1-positive aggregate numbers were significantly increased in mutants (Fig. 3.3F). Lamp1-positive aggregates in mutant spinal cords were scattered in the cytoplasm without the perinuclear concentration seen in WT (Fig. 3.3E), suggestive of immature lysosome precursors with deficient degradation capacity. In support of this notion, *Smcr8*$^{-/-}$ spinal cords displayed abnormal accumulation of p62, a substrate and receptor of autophagy degradation (Fig. 3.3G and H). Mutant spinal cords also exhibited an increase in the numbers of LC3-positive aggregates, which co-localize with Lamp1 (Fig. 3.3I and J). These results suggested impaired autophagy-lysosomal degradation coupled with axonal swellings in *Smcr8*$^{-/-}$ spinal cords. To determine whether these deficts occur at the axonal terminals of MNs, we examined the NMJs. The presynaptic terminals of mutant MNs exhibited swellings with NF accumulation (white arrowheads, Fig. 3.3K). Quantification confirmed that the numbers of axonal swellings were significantly increased in mutant NMJs (Fig. 3.3L).

To further investigate autophagy-lysosomal deficits, we examined axons using transmission electron microscopy (TEM) for the presence of autophagic vacuoles (AVs). Multiple criteria have been used to define AVs, including size, the presence of a double membrane, and the existence of multiple membrane-derived structures within a single vacuole (28). WT spinal cords had axonal structures that appeared typical, with no

Figure 3.4. Transmission electronic microscopy (TEM) study reveals swollen axons with organelle accumulation in mutant spinal cords.

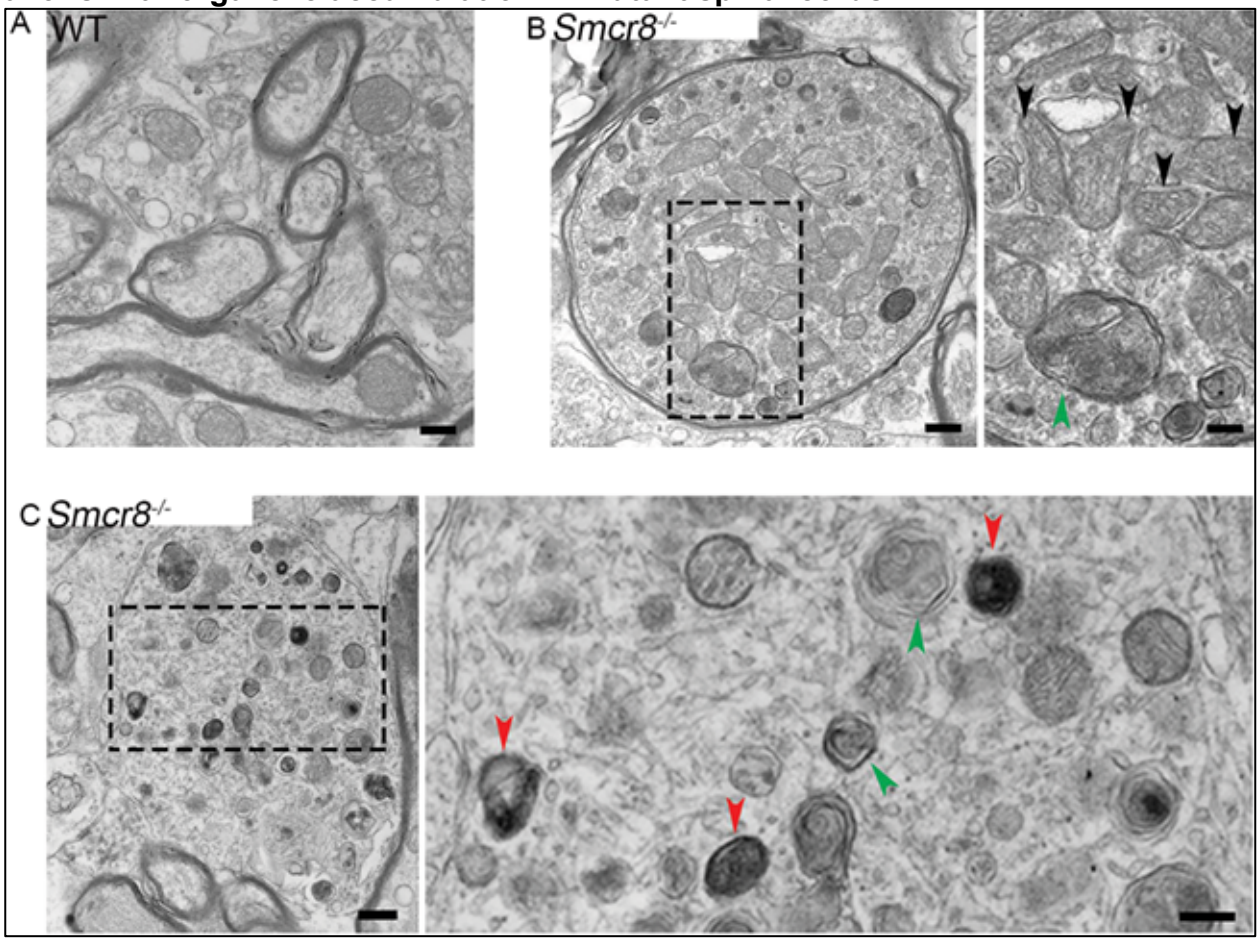

(A) Representative TEM imaging of axons in WT spinal cords. Scale bar: 400 nM. (B) TEM images of mutant spinal cords showing an axonal swelling filled with double-membrane autophagosomes (green arrowhead) and multiple mitochondria (black arrowheads) in mutants. Scale bars: 400 (left panel), and 200 nM (right panel). (C) A typical axonal swelling filled with large numbers of lysosome-like organelles at different maturation stages. Red arrowheads represent late stage-autolysosomes containing degraded organelles; green arrowheads represent autophagosomes in the early stage of autophagy. Scale bars: 400 (left panel) and 200 nM (right panel).

abnormal accumulation of organelles or vesicles (Fig. 3.4A). In contrast, *Smcr8*$^{-/-}$ spinal cords displayed swollen axons accompanied by large numbers of accumulated organelles and vesicles, including mitochondria (black arrows in Fig. 3.4B), double-membrane AVs containing engulfed organelles in the early stages of autophagy (green arrowheads in Fig. 3.4B and C), and late-stage autolysosomes containing degraded organelles (red arrowheads in Fig. 3.4C). Together, these results suggest that Smcr8 deletion disrupted autophagy-lysosomal degradation and led to axonal degeneration characterized by dystrophic neurites.

Axonal transport is disrupted in *Smcr8*$^{-/-}$ MNs

Our previous mass spectrometry studies revealed that the C9orf72/Smcr8 complex associates with Dynein (12). Dynein is the major motor that drives retrograde transport of autophagosomes from the distal axons to somas of neurons (29, 30). Disruption of dynein-mediated axonal transport leads to autophagic stress and axonal terminal enlargement (31, 32), which were observed in *Smcr8*$^{-/-}$ mice. Therefore, we hypothesized that Smcr8 promotes axonal transport, disruption of which leads to impaired autophagy-lysosomal functions and axonal swellings. To test this hypothesis, we examined axonal transport of GFP-LC3-labeled autophagosomes in mouse spinal MNs using time-lapse imaging approaches. In WT MNs, autophagosomes appeared as smooth vesicular structures distributed evenly along neuronal processes. In contrast, they were clustered in *Smcr8*$^{-/-}$ MNs (Fig. 3.5A and B). Time-lapse imaging revealed that autophagosomes in WT MNs exhibited robust motility along the processes, with a predominant retrograde direction. However, the net run speed and run length of autophagosomes were significantly reduced in *Smcr8*$^{-/-}$ MNs (Fig. 3.5C and D). The

Figure 3.5. Axonal transport is disrupted in *Smcr8*$^{-/-}$ MNs.

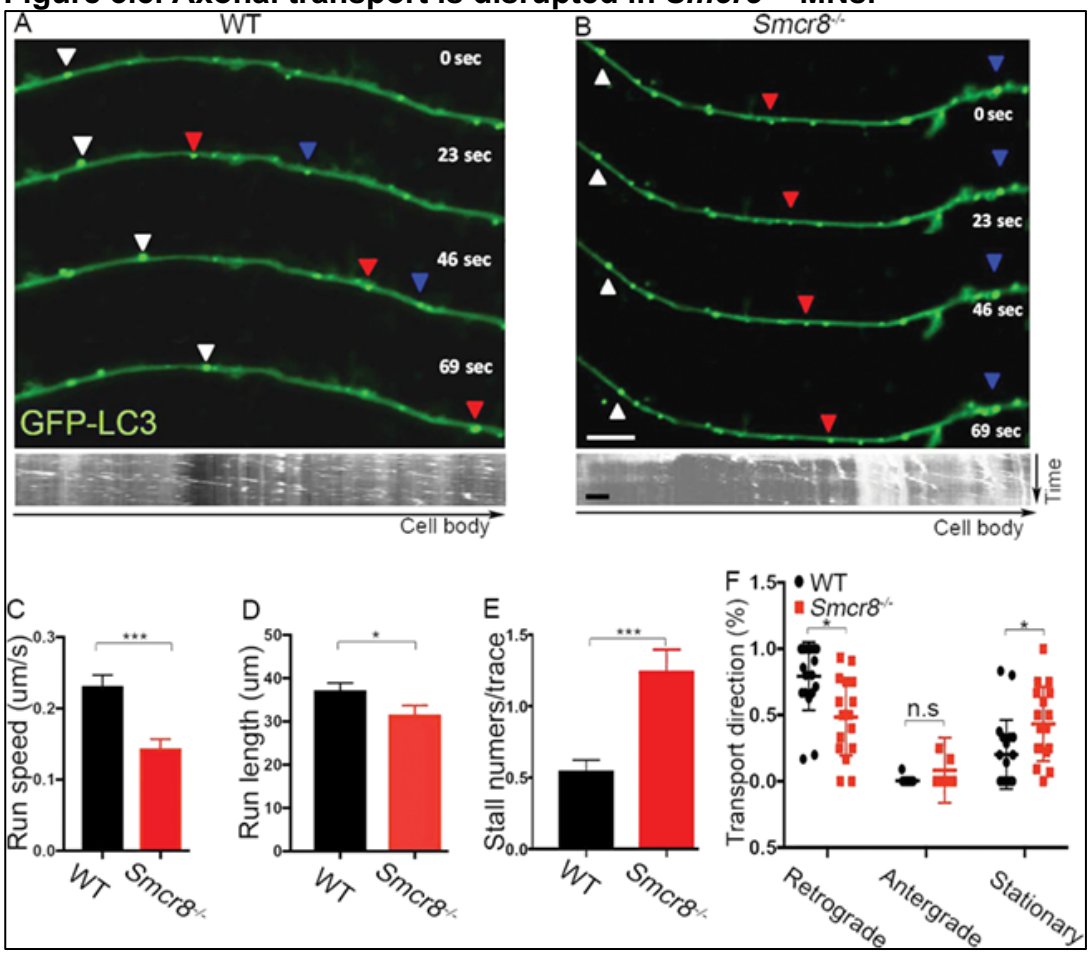

(A, B) Representative time-lapse images and corresponding kymographs of GFP-LC3-labeled autophagosome transport in spinal MNs isolated from E13.5 spinal cords. Individual autophagosomes marked by white triangles show robust retrograde transport in WT and diminished motility in mutant MNs. Scale bars: 2 μm. (C) Quantification of net run speed in WT (n = 126) and *Smcr8*$^{-/-}$ (n = 120) MNs. (D) Quantification of total run length in WT (n = 145) and *Smcr8*$^{-/-}$ (n = 87) MNs. (E) Quantification of stall numbers per trace in WT (n = 109) and *Smcr8*$^{-/-}$ (n = 125) MNs. (F) Quantification of the percentages of retrograde, anterograde, and stationary transport in WT (n = 20) and *Smcr8*$^{-/-}$ (n = 18) MNs. Error bars represent SEM of ≥5 independent experiments with more than five mice per group (n > 5). Statistical analyses were performed with non-parametric Mann-Whitney test (*P < 0.05, ***P < 0.001, n.s. represents no significant difference detected).

stall numbers per trace were increased in mutant MNs (Fig. 3.5E). *Smcr8*$^{-/-}$ MNs had a significantly reduced percentage of retrograde transport accompanied by an increased percentage of stationary autophagosomes (Fig. 3.5F). Thus, Smcr8 deletion disrupted axonal transport in MNs, which could result in autophagy-lysosomal impairment and axonal swellings in mutant mice.

C9orf72 loss of function exacerbates autophagy-lysosomal deficits in Smcr8 mutant mice

C9orf72 depletion in neurons failed to generate neurodegeneration or motor deficits (24); C9orf72's neuronal functions remain unknown. C9orf72 and Smcr8 form a protein complex and belong to the same DENN (differentially expressed in neoplastic versus normal cells) domain family (18, 33). Therefore, we hypothesized that Smcr8, which has robust neuronal function as described above, may compensate for the loss of C9orf72 in *C9orf72*$^{-/-}$ neurons. To test this hypothesis, we deleted C9orf72 in the background of *Smcr8*$^{-/-}$ mice. We examined axonal integrity and autophagy-lysosomal functions by performing side-by-side comparisons of spinal cords from WT, *C9orf72*$^{-/-}$, *Smcr8*$^{-/-}$ and *C9orf72*$^{-/-}$*;Smcr8*$^{-/-}$ double knockout (dKO) mice. In contrast to *Smcr8*$^{-/-}$ mice, *C9orf72*$^{-/-}$ mutant spinal cords displayed no significant changes in the numbers of Lamp1-positive organelles (Fig. 3.6A and B), NF aggregates (Fig. 6C and D), or p62 puncta (Fig. 3.6E and F). However, in the background of *Smcr8*$^{-/-}$, C9orf72 deletion promoted deficits in the numbers of Lamp1- and p62-positive puncta as well as NF aggregates (Fig. 3.6B, D, and F). Together, these results suggest that C9orf72 deficiency exacerbates autophagy-lysosomal deficits and axonal swellings in *Smcr8*$^{-/-}$ spinal cords.

Figure 3.6. Smcr8 deficiency exacerbates autophagy-lysosomal impairment in *C9orf72*$^{-/-}$ spinal cords.

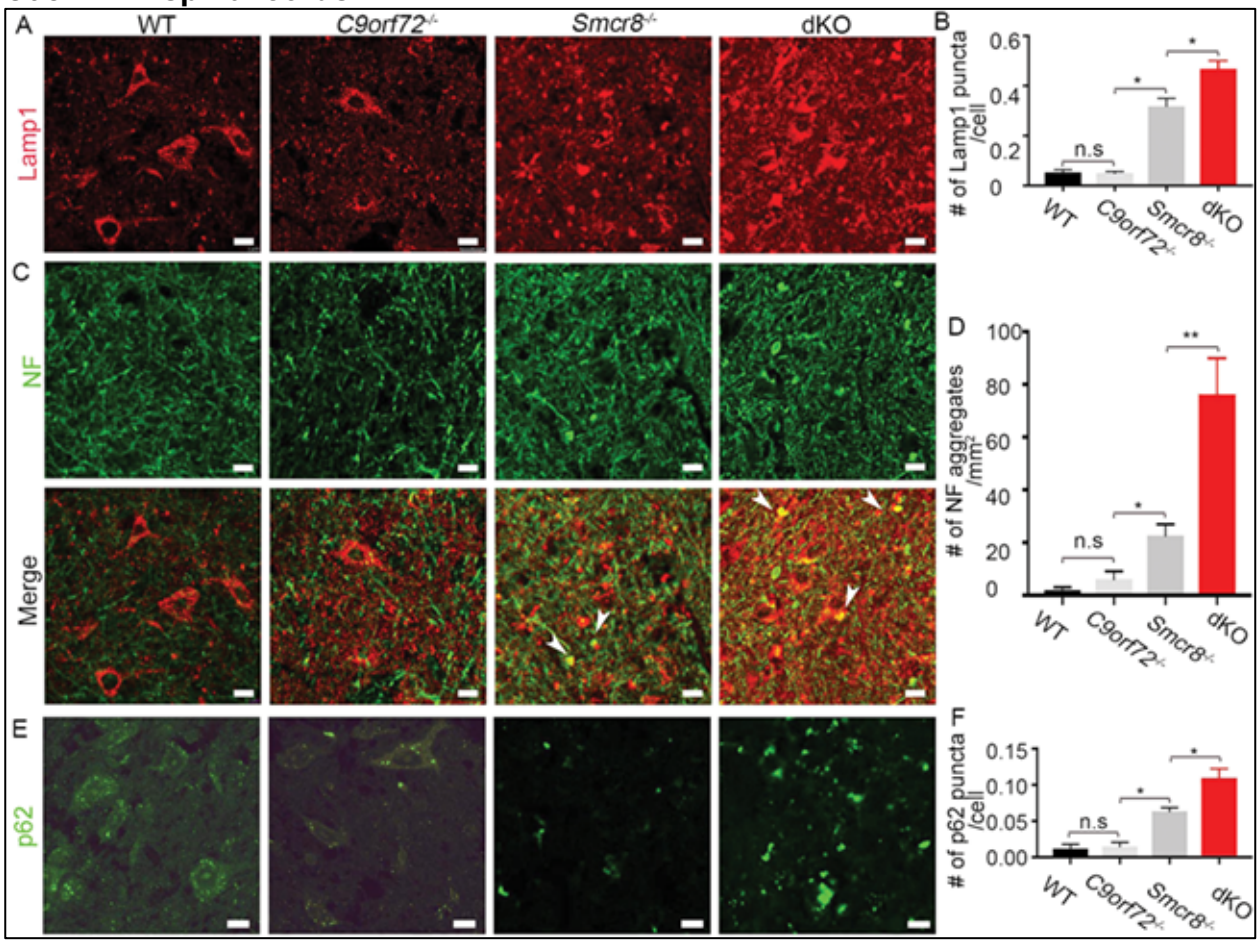

(A, C, E) Representative confocal imaging of spinal cords from wild type (WT), *C9orf72*$^{-/-}$, *Smcr8*$^{-/-}$ and *C9orf72*$^{-/-}$;*Smcr8*$^{-/-}$ dKO mice at 7 months of age. Coronal sections were stained with antibodies against Lamp1 (red), NF (green), or p62 (green). Hoechst stains nuclei. White arrowheads represent axonal swellings with the co-localization of Lamp1 and NF. Scale bars: 20 μm. (B, D, F) Quantification of Lamp1-positive puncta per cell, numbers of NF aggregates per mm2 area, or numbers of p62-positive puncta per cell (F). All data are presented as mean ± SEM using measurements averaged from ≥3 sections of each mutant mice (n = 3). Statistical analyses were performed with one-way ANOVA with Bonferroni correction's post hoc test (*P < 0.05, **P < 0.01); n.s. represents no significant difference detected.

Next, we extended our studies to the axonal terminals of MNs by focusing on diaphragm NMJs in 7-month-old mice. Similar to WT animals, *C9orf72*$^{-/-}$ diaphragms presented with normal NMJ morphology. NF-labeled presynaptic terminals were able to form synapses appropriately with AChR-positive postsynaptic terminals without Lamp1-positive organelle accumulation (Fig. 3.7A–C), while the size of NMJ axonal terminal was slightly increased in *C9orf72*$^{-/-}$ mice (Fig. 3.7E). *Smcr8*$^{-/-}$ mice exhibited multiple NMJ abnormalities, including an increase in the numbers and sizes of axonal terminals (Fig. 3.7D and E). In comparison to *Smcr8*$^{-/-}$ single mutants, dKO mice displayed a significant increase in the number of axonal swellings per NMJ receptor as well as an increase in the axonal terminal sizes (Fig. 3.7D and E). Together, these results suggest that C9orf72 has neuronal functions in promoting autophagy-lysosomal degradation, which are similar to and dominated by Smcr8 under physiological conditions.

Smcr8 deficiency promotes axonal swellings of NMJs in C9-BAC mouse models

C9orf72 deficiency promotes motor behavior deficits in a gain-of-function mouse model of C9ALS/FTD (10), but the underlying mechanisms remain unknown. C9orf72 stabilizes its interaction protein Smcr8 (13, 15); Smcr8 expression is reduced in mouse models and patient tissues of C9ALS/FTD. Smcr8 deficiency is sufficient to disrupt autophagy-lysosomal functions and lead to axonal swellings and motor deficits, which resemble phenotypes in *C9orf72*$^{+/-}$*;C9-BAC* mice. Therefore, we hypothesized that Smcr8 deficiency promotes autophagy-lysosomal impairment and leads to axonal swellings in *C9-ABC* mice. To test this hypothesis, we crossed Smcr8 deficient mice with *C9-BAC* mice, and focused our analyses on age-matched WT, *Smcr8*$^{+/-}$, *C9-BAC*, and *Smcr8*$^{+/-}$*;C9-BAC* mice. Impaired autophagy-lysosomal function led to axonal

Figure 3.7. C9orf72 deficiency promotes terminal axon degeneration of *Smcr8*$^{-/-}$ NMJs.

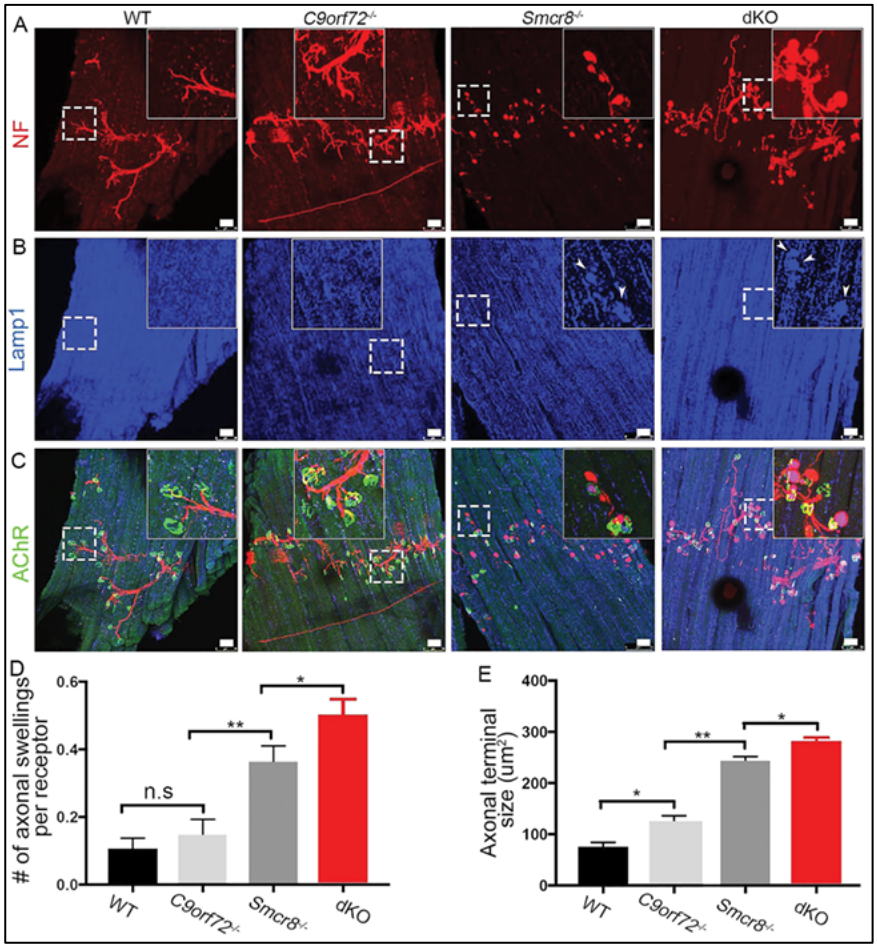

(A–C) Representative confocal imaging of diaphragms from wild type (WT), *C9orf72*$^{-/-}$, *Smcr8*$^{-/-}$ and *C9orf72*$^{-/-}$*; Smcr8*$^{-/-}$ dKO mice. Diaphragms from 7-month-old mice were stained with antibodies against NF (red), Lamp1 (blue), and acetylcholine receptor AChR (green). Hoechst stains nuclei. Inserts in top panels are enlargements of white boxed areas in individual panels. Scale bars: 50 μm. (D, E) Quantification of the numbers of axonal swellings associated with each AChR receptor, and sizes of axonal swellings. All data are presented as mean ± SEM using measurements averaged from ≥3 muscle bundles of each mutant mice (n = 3). Statistical analyses were performed with one-way ANOVA with Bonferroni's post hoc test; n.s. represents no significant difference detected (*P < 0.05, **P < 0.01).

Figure 3.8. Smcr8 deficiency promotes axonal swellings in *C9-BAC* mice.

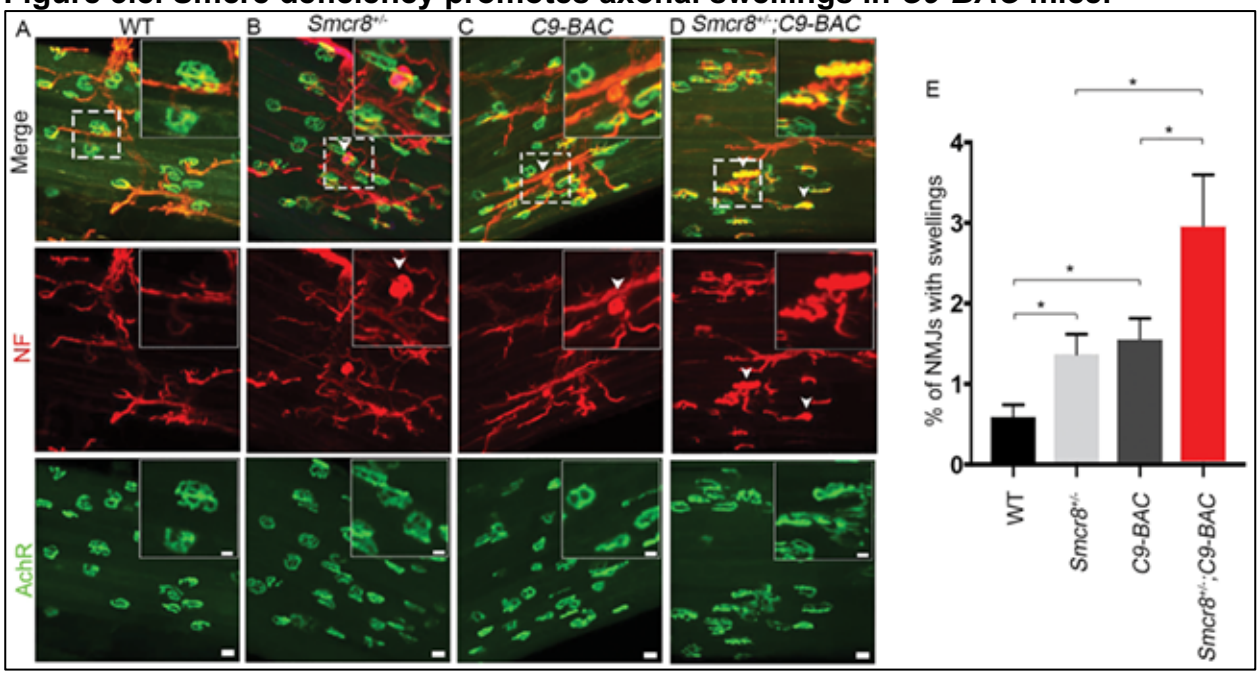

(A–D) Representative confocal imaging of 9-month-old mouse diaphragms stained with antibodies against NF (NF, red), and acetylcholine receptor AChR (green). White arrowheads represent NF-positive axonal swellings or Lamp1-positive puncta, which are rarely detected in WT controls. Upper right panels are enlargements of white boxed areas in merged panels. Scale bars: 10 (upper panels) and 20 μm (bottom panels). (E) Quantification of NMJs with swellings. All data are presented as mean ± SEM using measurements averaged from ≥3 muscle bundles of each mutant mouse ($n > 3$). Statistical analysis was performed by one-way ANOVA analysis with Bonferroni correction (*$P < 0.05$).

swellings. In comparison to WT, *C9-BAC* and *Smcr8*$^{+/-}$ mice exhibited an increase in the percentage of NMJs with axonal swellings (Fig. 3.8A–D), which was further exacerbated in *Smcr8*$^{+/-}$*;C9-BAC* mice (Fig. 3.8E). Together, these results suggest that Smcr8 deficiency promotes axonal swellings of NMJs in *C9-BAC* mouse models.

Smcr8 deficiency exacerbates dipeptide repeat (DPR) abundance in C9-BAC mice

Gain of toxicity is attributed by DPRs from RAN translation in C9ALS/FTD (34, 35). Transgenic mice containing C9ORF72 BAC from patient DNA have been generated to model gain-of-toxicity (25, 36–38). In addition to axonal swellings, we attempted to test whether Smcr8 deficiency promotes the accumulation of DPRs, which are toxic to neurons. It has been documented that the amount of inclusions for poly (PR) and poly (PA) are relatively rare in postmortem C9ALS/FTD patient brains (39, 40). Whereas the poly (GP) is considered to be benign, both poly (GR) and poly (GA) have been shown to be particularly toxic in various cell types and animal models (41–43). We focused our studies on poly (GA) and poly (GP). We barely detected poly (GA) staining in 7-month-old WT mouse tissues. In contrast, age matched *C9-BAC* mouse spinal cords exhibited robust poly (GA) signals (Fig. 3.9A). The percentage of poly (GA)-positive cells was significantly increased in *Smcr8*$^{+/-}$*;C9-BAC* mice compared to *C9-BAC* mice (Fig. 3.9B). Next, we examined poly (GP), and barely found poly (GP) staining in spinal cord tissues of 7-month-old WT mice (Fig. 3.9C). Age matched *C9-BAC* mice displayed an increase in the percentage of poly (GP)-positive cells, which was further increased by the Smcr8 heterozygosity (Fig. 3.9D). Together, these results suggest that Smcr8 deficiency exacerbates the DPR gain of toxicity in *C9-BAC* mice.

Figure 3.9. Smcr8 deficiency exacerbates gain of toxicity in *C9-BAC* mice.

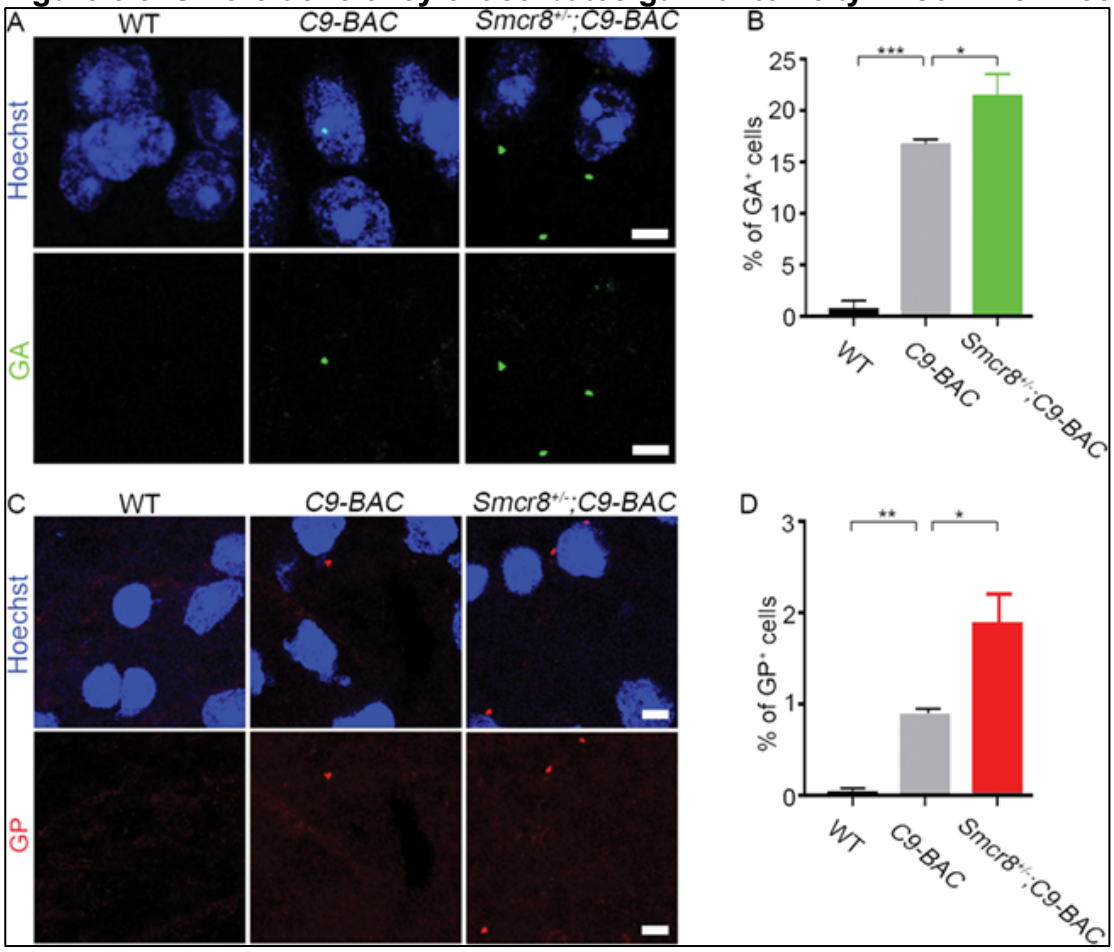

(A) Representative imaging of coronal sections stained with antibodies against poly (GA) (green). Age-matched 7-month-old mice were used to prepare sections in the area of spinal cords. Scale bars: 5 μm. (B) Quantification of the percentage of cells with poly (GA) puncta out of total cells from 3 WT, 4 *C9-BAC* and 4 *Smcr8*$^{+/-}$*;C9-BAC* mice. (C) Representative imaging of coronal sections stained with antibodies against poly (GP) (red). Age-matched 7-month-old mice were used to prepare sections in the area of spinal cords. Scale bars: 5 μm. (D) Quantification of the percentage of cells with poly (GP) puncta out of total cells from 4 WT, 4 *C9-BAC* and 3 *Smcr8*$^{+/-}$*; C9-BAC* mice. Error bars represent SEM of four independent experiments. Statistical analyses were performed with one-way ANOVA with Bonferroni's post hoc test (*$P < 0.05$, **$P < 0.01$ and ***$P < 0.001$).

Discussion

Here, we discovered that Smcr8 deficiency disrupts MN axonal transport and lysosomal functions, leading to axonal swellings, which in turn contributes to motor behavior deficits in mice. The expression of Smcr8, like that of C9orf72, is reduced in mouse models and patient tissues. Smcr8 deficiency exacerbates axonal swellings and DPR gain of toxicity in C9-BAC mouse models, providing new insights into the pathogenesis of C9ALS/FTD.

Using genetic KO mouse models, for the first time, our studies discovered Smcr8's neuronal and behavioral functions in vivo. Specifically, Smcr8 promotes autophagy-lysosomal functions in MNs. It has been reported that local homeostasis of axon terminals, in comparison to dendrites or spines, is particularly vulnerable to autophagy impairment (45, 46). Indeed, progressive axonal dystrophic swellings were identified as early and pronounced deficits in Smcr8 mutant mice. Although Smcr8 is widely expressed, these axonal swellings were mostly detected in spinal cords and NMJs, not in different brain regions of mutant mice. These observations are consistent with the notion that MNs, with their unique long axons, are particularly vulnerable to the disruption of autophagy-lysosomal pathway (47). With progressive age, axonal swellings in *Smcr8*$^{-/-}$ mice become more severe, which correlates with motor behavior deficits in mutant mice. Multiple evidences suggest that NF-positive swellings are axon-derived, including TEM studies and NMJs. Recent studies suggest that Lamp1-labeled lysosomal precursors, including endosomes and autophagosomes, are initiated at the distal tips of axons and mature via axonal transport toward proximal regions where luminal proteases can be effectively obtained (27, 29–31). We found that Smcr8 mutant

MNs exhibited disrupted axonal transport of autophagosomes, including reduced net run speed, run length and retrograde transport. Future studies should determine the mechanisms underlying the impaired axonal transport in *Smcr8*$^{-/-}$ MNs, such as potential deficits in motor activities, cargo loading, or cargo releasing. It is also important to investigate to what extent restoring axonal transport can rescue autophagy-lysosomal degradation and axonal swelling deficits in *Smcr8*$^{-/-}$ MNs. Overall, Smcr8 deletion impaired axonal transport and autophagy-lysosomal functions, which resulted in axonal swellings contributing to motor deficits in mutant mice.

Our Smcr8 studies provided new mechanistic insights into C9ALS/FTD pathogenesis from the loss-of-function perspective. We and others previously reported that C9orf72 and Smcr8 form a protein complex and regulate autophagy (11–17). Although these studies linked C9orf72 with autophagy, neuronal deletion of C9orf72 failed to produce neurodegeneration and motor deficits in mice (24). Whether and how autophagy-lysosomal functions are impaired in C9ALS/FTD in vivo remain unknown. We found that expression of Smcr8, like C9orf72, is reduced in C9ALS/FTD mouse models and patient tissues; Smcr8 heterozygous or homozygous mice displayed motor deficits; Smcr8 heterozygosity exacerbated axonal swellings in *C9-BAC* mouse models. Therefore, these results provide the in vivo evidences that Smcr8 downregulation impaires the autophagy-lysosomal function, which in turn promotes axonal degeneration in C9ALS/FTD. In addition to axonal swellings, Smcr8 deficiency also exacerbated poly (GA) and poly (GP) gain of toxicity, highlighting the cross talk between loss- and gain-of-function in the pathogenesis of C9ALS/FTD. It is possible that Smcr8 downregulation impaires the autophagy-lysosomal degradation of poly (GA)/(GP). Alternatively, Smcr8

deficiency may promote cellular stress and result in the increased DPR biogenesis. Future studies should identify mechanisms by which Smcr8 deficiency-mediated loss-of-function interacts with gain of toxicity in C9ALS/FTD.

We uncovered C9orf72's neuronal functions in promoting autophagy-lysosomal degradation. Whereas C9orf72 deletion alone produced no neurodegeneration or MN deficits, its absence in the background of Smcr8 KO exacerbated Lamp1-positive organelle accumulation, p62 elevation and axonal swellings in spinal cords as well as NMJ swellings, all of which were more severe in dKO than single *Smcr8*$^{-/-}$ mutant mice. These results suggest that C9orf72, like Smcr8, promotes autophagy-lysosomal functions and prevents axonal degeneration. C9orf72's neuronal functions were manifested in the absence of Smcr8, suggesting that these neuronal functions are dominated by the presence of Smcr8 under physiological conditions. We speculate that Smcr8 has similar but more potent neuronal functions than C9orf72 in regulating autophagy-lysosomal degradation; they act in parallel, not in a single linear pathway, such that Smcr8 can compensate for the loss of C9orf72 but not vice versa. Overall, our studies provided the first comprehensive functional studies of Smcr8 in neurons in vivo, and uncovered C9orf72's neuronal functions in autophagy-lysosomal pathway. Furthermore, Smcr8 deficiency exacerbates axonal swellings and gain of toxicity in *C9-BAC* mice, suggesting of the interaction between loss- and gain-of-function in the pathogenesis of C9ALS/FTD.

Acknowledgements

We thank Chen laboratory colleagues for stimulating discussions. We are grateful for Bridget Samuels's critical reading of the manuscript. The authors wish to thank Dr. Nikolay Filipov for help with behavioral experiments, and Ms. Mary Ard for help with electron microscopy.

Supplemental Figure 3.S1. *Smcr8* expression pattern.

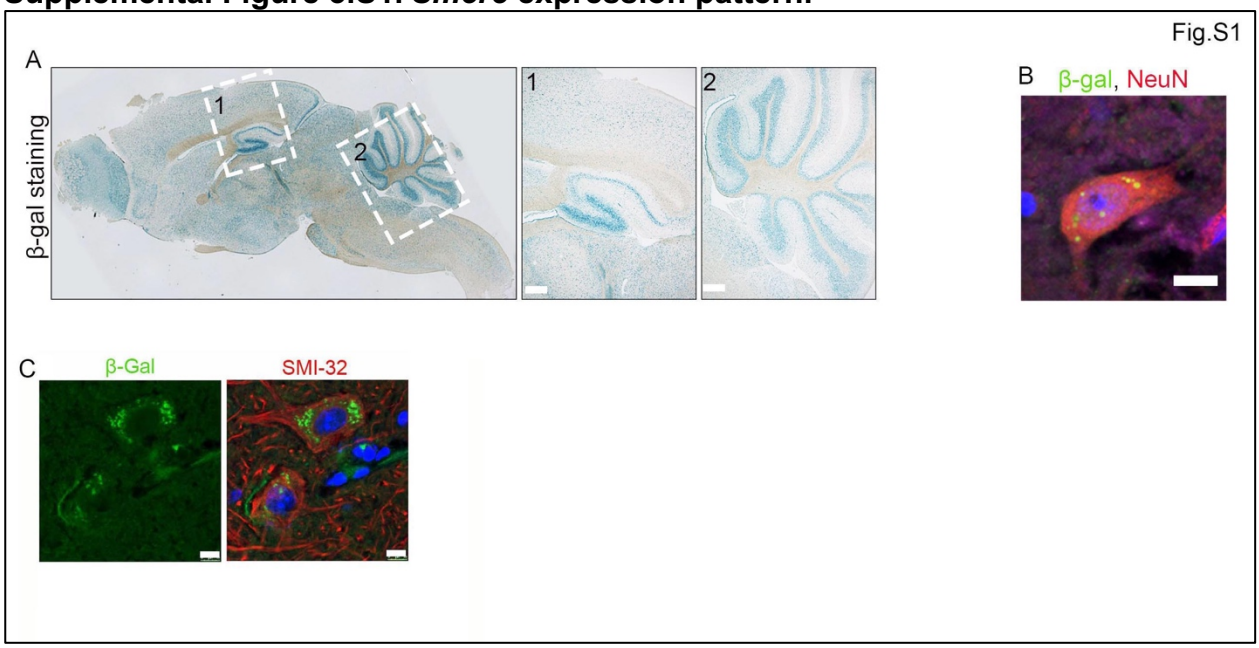

(A) LacZ staining of coronal sections from 2-month-old heterozygous mice shows Smcr8 expression in cortex and hippocampus (white rectangle 1), cerebellum (white rectangle 2). Scale bars: 200 μm. (B) Confocal imaging of spinal cord sections from 2-month-old heterozygous mice stained with antibodies against beta-galactosidase (β-gal, green) and NeuN (red). Hoechst stains nuclei (blue). Scale bar: 10 μm. (C) Smcr8 expression in motor neurons revealed by confocal imaging of spinal cord sections stained with antibodies against β-gal (green) and SMI-32 (red). Hoechst stains nuclei (blue). Scale bars: 10 μm.

Supplemental Figure 3.S2. Lysosomal accumulations are barely co-localized with astrocytes and microglia.

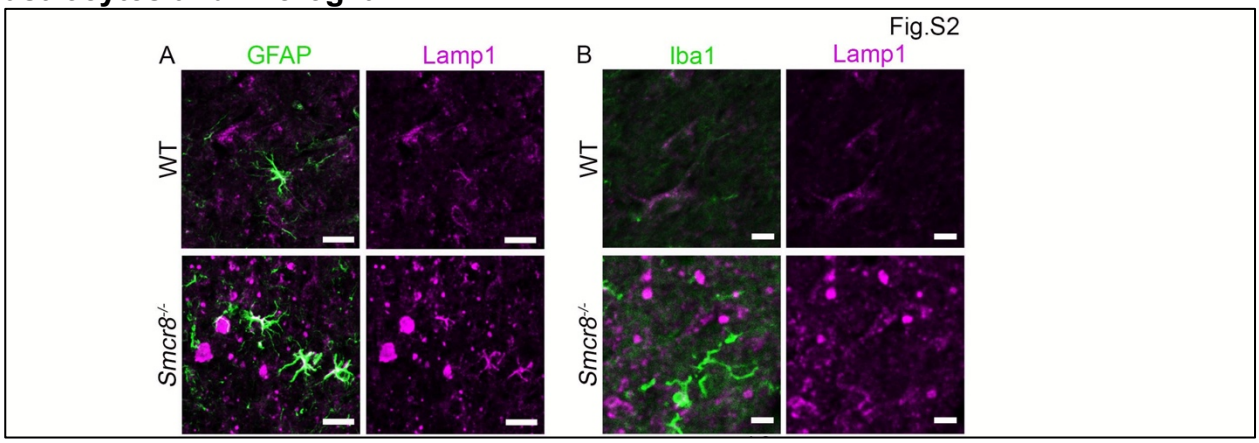

(A, B) Confocal imaging of 7-month-old spinal cord sections stained with antibodies against GFAP and Lamp1 (A), or Iba1 and Lamp1 (B). Scale bars: 10 μm.

References

1. Ling, S.-C., Polymenidou, M. and Cleveland, D.W. (2013) Converging mechanisms in ALS and FTD: disrupted RNA and protein homeostasis. Neuron, 79, 416–438.

2. Gao, F.-B., Almeida, S. and Lopez-Gonzalez, R. (2017) Dysregulated molecular pathways in amyotrophic lateral sclerosis-frontotemporal dementia spectrum disorder. EMBO J., 36, 2931–2950.

3. Gijselinck, I., Van Langenhove, T., van der Zee, J., Sleegers, K., Philtjens, S., Kleinberger, G., Janssens, J., Bettens, K., Van Cauwenberghe, C., Pereson, S. et al. (2012) A C9orf72 promoter repeat expansion in a Flanders-Belgian cohort with disorders of the frontotemporal lobar degeneration-amyotrophic lateral sclerosis spectrum: a gene identification study. Lancet Neurol., 11, 54–65.

4. Renton, A.E., Majounie, E., Waite, A., Simón-Sánchez, J., Rollinson, S., Gibbs, J.R., Schymick, J.C., Laaksovirta, H., van Swieten, J.C., Myllykangas, L. et al. (2011) A hexanucleotide repeat expansion in C9ORF72 is the cause of chromosome 9p21-linked ALS-FTD. Neuron, 72, 257–268.

5. DeJesus-Hernandez, M., Mackenzie, I.R., Boeve, B.F., Boxer, A.L., Baker, M., Rutherford, N.J., Nicholson, A.M., Finch, N.A., Flynn, H., Adamson, J. et al. (2011) Expanded GGGGCC hexanucleotide repeat in noncoding region of C9ORF72 causes chromosome 9p-linked FTD and ALS. Neuron, 72, 245–256.

6. Majounie, E., Renton, A.E., Mok, K., Dopper, E.G.P., Waite, A., Rollinson, S., Chiò, A., Restagno, G., Nicolaou, N., Simón-Sánchez, J. et al. (2012) Frequency of the

C9orf72 hexanucleotide repeat expansion in patients with amyotrophic lateral sclerosis and frontotemporal dementia: a cross-sectional study. Lancet Neurol., 11, 323–330.
7. Waite, A.J., Bäumer, D., East, S., Neal, J., Morris, H.R., Ansorge, O. and Blake, D.J. (2014) Reduced C9orf72 protein levels in frontal cortex of amyotrophic lateral sclerosis and frontotemporal degeneration brain with the C9ORF72 hexanucleotide repeat expansion. Neurobiol. Aging, 35, 1779.e5–e1779.e13.
8. Mizielinska, S., Lashley, T., Norona, F.E., Clayton, E.L., Ridler, C.E., Fratta, P. and Isaacs, A.M. (2013) C9orf72 frontotemporal lobar degeneration is characterised by frequent neuronal sense and antisense RNA foci. Acta Neuropathol., 126, 845–857.
9. Shi, Y., Lin, S., Staats, K.A., Li, Y., Chang, W.-H., Hung, S.-T., Hendricks, E., Linares, G.R., Wang, Y., Son, E.Y. et al. (2018) Haploinsufficiency leads to neurodegeneration in C9ORF72 ALS/FTD human induced motor neurons. Nat. Med., 24, 313–325.
10. Shao, Q., Liang, C., Chang, Q., Zhang, W., Yang, M. and Chen, J.-F. (2019) C9orf72 deficiency promotes motor deficits of a C9ALS/FTD mouse model in a dose-dependent manner. Acta Neuropathol. Commun., 7, 32.
11. Jung, J., Nayak, A., Schaeffer, V., Starzetz, T., Kirsch, A.K., Müller, S., Dikic, I., Mittelbronn, M. and Behrends, C. (2017) Multiplex image-based autophagy RNAi screening identifies SMCR8 as ULK1 kinase activity and gene expression regulator. elife, 6, 2.
12. Yang, M., Liang, C., Swaminathan, K., Herrlinger, S., Lai, F., Shiekhattar, R. and Chen, J.-F. (2016) A C9ORF72/SMCR8-containing complex regulates ULK1 and plays a dual role in autophagy. Sci. Adv., 2, e1601167–e1601167.

13. Amick, J., Roczniak-Ferguson, A. and Ferguson, S.M. (2016) C9orf72 binds SMCR8, localizes to lysosomes, and regulates mTORC1 signaling. Mol. Biol. Cell, 27, 3040–3051.

14. Sullivan, P.M., Zhou, X., Robins, A.M., Paushter, D.H., Kim, D., Smolka, M.B. and Hu, F. (2016) The ALS/FTLD associated protein C9orf72 associates with SMCR8 and WDR41 to regulate the autophagy-lysosome pathway. Acta Neuropathol. Commun., 4, 51.

15. Ugolino, J., Ji, Y.J., Conchina, K., Chu, J., Nirujogi, R.S., Pandey, A., Brady, N.R., Hamacher-Brady, A. and Wang, J. (2016) Loss of C9orf72 enhances autophagic activity via deregulated mTOR and TFEB signaling. PLoS Genet., 12, e1006443.

16. Sellier, C., Campanari, M.-L., Julie Corbier, C., Gaucherot, A., Kolb-Cheynel, I., Oulad-Abdelghani, M., Ruffenach, F., Page, A., Ciura, S., Kabashi, E. et al. (2016) Loss of C9ORF72 impairs autophagy and synergizes with poly Q Ataxin-2 to induce motor neuron dysfunction and cell death. EMBO J, 35, 1276–97.

17. Webster, C.P., Smith, E.F., Bauer, C.S., Moller, A., Hautbergue, G.M., Ferraiuolo, L., Myszczynska, M.A., Higginbottom, A., Walsh, M.J., Whitworth, A.J. et al. (2016) The C9orf72 protein interacts with Rab 1a and the ULK1 complex to regulate initiation of autophagy. EMBO J., 35, 1656–1676.

18. Zhang, D., Iyer, L.M., He, F. and Aravind, L. (2012) Discovery of novel DENN proteins: implications for the evolution of eukaryotic intracellular membrane structures and human disease. Front. Genet., 3, 283.

19. Levine, T.P., Daniels, R.D., Gatta, A.T., Wong, L.H. and Hayes, M.J. (2013) The product of C9orf72, a gene strongly implicated in neurodegeneration, is structurally related to DENN Rab-GEFs. Bioinformatics, 29, 499–503.

20. Mizushima, N. and Komatsu, M. (2011) Autophagy: renovation of cells and tissues. Cell, 147, 728–741.

21. Mizushima, N., Levine, B., Cuervo, A.M. and Klionsky, D.J. (2008) Autophagy fights disease through cellular self-digestion. Nature, 451, 1069–1075.

22. O'Rourke, J.G., Bogdanik, L., Yáñez, A., Lall, D., Wolf, A.J., Muhammad, A.K.M.G., Ho, R., Carmona, S., Vit, J.P., Zarrow, J. et al. (2016) C9orf72 is required for proper macrophage and microglial function in mice. Science, 351, 1324–1329.

23. Corrionero, A. and Horvitz, H.R. (2018) A C9orf72 ALS/FTD ortholog acts in endolysosomal degradation and lysosomal homeostasis. Curr. Biol., 28, 1522–1535.e5.

24. Koppers, M., Blokhuis, A.M., Westeneng, H.-J., Terpstra, M.L., Zundel, C.A.C., Vieira de Sá, R., Schellevis, R.D., Waite, A.J., Blake, D.J., Veldink, J.H. et al. (2015) C9orf72 ablation in mice does not cause motor neuron degeneration or motor deficits. Ann. Neurol., 78, 426–438.

25. Liu, Y., Pattamatta, A., Zu, T., Reid, T., Bardhi, O., Borchelt, D.R., Yachnis, A.T. and Ranum, L.P.W. (2016) C9orf72 BAC mouse model with motor deficits and neurodegenerative features of ALS/FTD. Neuron, 90, 521–534.

26. Zhang, Y., Burberry, A., Wang, J.-Y., Sandoe, J., Ghosh, S., Udeshi, N.D., Svinkina, T., Mordes, D.A., Mok, J., Charlton, M. et al. (2018) The C9orf72-interacting protein Smcr 8 is a negative regulator of autoimmunity and lysosomal exocytosis. Genes Dev., 32, 929–943.

27. Gowrishankar, S., Yuan, P., Wu, Y., Schrag, M., Paradise, S., Grutzendler, J., De Camilli, P. and Ferguson, S.M. (2015) Massive accumulation of luminal protease-deficient axonal lysosomes at Alzheimer's disease amyloid plaques. Proc. Natl. Acad. Sci. U. S. A., 112, E3699–E3708.

28. Glaumann, H., Ericsson, J.L. and Marzella, L. (1981) Mechanisms of intralysosomal degradation with special reference to autophagocytosis and heterophagocytosis of cell organelles. Int. Rev. Cytol., 73, 149–182.

29. Maday, S., Wallace, K.E. and Holzbaur, E.L.F. (2012) Autophagosomes initiate distally and mature during transport toward the cell soma in primary neurons. J. Cell Biol., 196, 407–417.

30. Cheng, X.-T., Zhou, B., Lin, M.-Y., Cai, Q. and Sheng, Z.-H. (2015) Axonal autophagosomes recruit dynein for retrograde transport through fusion with late endosomes. J. Cell Biol., 209, 377–386.

31. Tammineni, P., Ye, X., Feng, T., Aikal, D. and Cai, Q. (2017) Impaired retrograde transport of axonal autophagosomes contributes to autophagic stress in Alzheimer's disease neurons. elife, 6, 343.

32. Xie, Y., Zhou, B., Lin, M.-Y., Wang, S., Foust, K.D. and Sheng, Z.-H. (2015) Endolysosomal deficits augment mitochondria pathology in spinal motor neurons of asymptomatic fALS mice. Neuron, 87, 355–370.

33. Marat, A.L., Dokainish, H. and McPherson, P.S. (2011) DENN domain proteins: regulators of Rab GTPases. J. Biol. Chem., 286, 13791–13800.

34. Gendron, T.F. and Petrucelli, L. (2018) Disease mechanisms of C9ORF72 repeat expansions. Cold Spring Harbor Perspect. Med., 8, a024224.

35. Zu, T., Pattamatta, A. and Ranum, L.P.W. (2018) Repeat-associated non-ATG translation in neurological diseases. Cold Spring Harbor Perspect. Biol., 10, a033019.
36. O'Rourke, J.G., Bogdanik, L., Muhammad, A.K.M.G., Gendron, T.F., Kim, K.J., Austin, A., Cady, J., Liu, E.Y., Zarrow, J., Grant, S. et al. (2015) C9orf72 BAC transgenic mice display typical pathologic features of ALS/FTD. Neuron, 88, 892–901.
37. Peters, O.M., Cabrera, G.T., Tran, H., Gendron, T.F., McKeon, J.E., Metterville, J., Weiss, A., Wightman, N., Salameh, J., Kim, J. et al. (2015) Human C9ORF72 hexanucleotide expansion reproduces RNA foci and dipeptide repeat proteins but not neurodegeneration in BAC transgenic mice. Neuron, 88, 902–909.
38. Jiang, J., Zhu, Q., Gendron, T.F., Saberi, S., McAlonis-Downes, M., Seelman, A., Stauffer, J.E., Jafar-Nejad, P., Drenner, K., Schulte, D. et al. (2016) Gain of toxicity from ALS/FTD-linked repeat expansions in C9ORF72 is alleviated by antisense oligonucleotides targeting GGGGCC-containing RNAs. Neuron, 90, 535–550.
39. Mackenzie, I.R.A., Frick, P., Grässer, F.A., Gendron, T.F., Petrucelli, L., Cashman, N.R., Edbauer, D., Kremmer, E., Prudlo, J., Troost, D. et al. (2015) Quantitative analysis and clinico-pathological correlations of different dipeptide repeat protein pathologies in C9ORF72 mutation carriers. Acta Neuropathol., 130, 845–861.
40. Mackenzie, I.R.A., Frick, P. and Neumann, M. (2014) The neuropathology associated with repeat expansions in the C9ORF72 gene. Acta Neuropathol., 127, 347–357.
41. May, S., Hornburg, D., Schludi, M.H., Arzberger, T., Rentzsch, K., Schwenk, B.M., Grässer, F.A., Mori, K., Kremmer, E., Banzhaf-Strathmann, J. et al. (2014) C9orf72

FTLD/ALS-associated Gly-Ala dipeptide repeat proteins cause neuronal toxicity and Unc 119 sequestration. Acta Neuropathol., 128, 485–503.

42. Zhang, Y.-J., Gendron, T.F., Grima, J.C., Sasaguri, H., Jansen-West, K., Xu, Y.-F., Katzman, R.B., Gass, J., Murray, M.E., Shinohara, M. et al. (2016) C9ORF72 poly (GA) aggregates sequester and impair HR23 and nucleocytoplasmic transport proteins. Nat. Neurosci., 19, 668–677.

43. Mizielinska, S., Grönke, S., Niccoli, T., Ridler, C.E., Clayton, E.L., Devoy, A., Moens, T., Norona, F.E., Woollacott, I.O.C., Pietrzyk, J. et al. (2014) C9orf72 repeat expansions cause neurodegeneration in drosophila through arginine-rich proteins. Science, 345, 1192–1194.

44. Saberi, S., Stauffer, J.E., Jiang, J., Garcia, S.D., Taylor, A.E., Schulte, D., Ohkubo, T., Schloffman, C.L., Maldonado, M., Baughn, M. et al. (2018) Sense-encoded poly-GR dipeptide repeat proteins correlate to neurodegeneration and uniquely co-localize with TDP-43 in dendrites of repeat-expanded C9orf72 amyotrophic lateral sclerosis. Acta Neuropathol., 135, 459–474.

45. Yue, Z., Horton, A., Bravin, M., DeJager, P.L., Selimi, F. and Heintz, N. (2002) A novel protein complex linking the delta 2 glutamate receptor and autophagy: implications for neurodegeneration in lurcher mice. Neuron, 35, 921–933.

46. Komatsu, M., Wang, Q.J., Holstein, G.R., Friedrich, V.L., Iwata, J.-I., Kominami, E., Chait, B.T., Tanaka, K. and Yue, Z. (2007) Essential role for autophagy protein Atg 7 in the maintenance of axonal homeostasis and the prevention of axonal degeneration. Proc. Natl. Acad. Sci. U. S. A., 104, 14489–14494.

47. Kulkarni, V.V. and Maday, S. (2018) Compartment-specific dynamics and functions of autophagy in neurons. Dev. Neurobiol., 78, 298–310.

48. Yang, M., Yang, S.-L., Herrlinger, S., Liang, C., Dzieciatkowska, M., Hansen, K.C., Desai, R., Nagy, A., Niswander, L., Moss, E.G. et al. (2015) Lin 28 promotes the proliferative capacity of neural progenitor cells in brain development. Development, 142, 1616–1627.

49. Shao, Q., Herrlinger, S., Yang, S.-L., Lai, F., Moore, J.M., Brindley, M.A. and Chen, J.-F. (2016) Zika virus infection disrupts neurovascular development and results in postnatal microcephaly with brain damage. Development, 143, 4127–4136.

50. Conrad, R., Jablonka, S., Sczepan, T., Sendtner, M., Wiese, S. and Klausmeyer, A. (2011) Lectin-based isolation and culture of mouse embryonic motoneurons. J. Vis. Exp. Sep 15;(55).

51. Fallini, C., Bassell, G.J. and Rossoll, W. (2010) High-efficiency transfection of cultured primary motor neurons to study protein localization, trafficking, and function. Mol. Neurodegener., 5, 17.

52. Tinevez, J.-Y., Perry, N., Schindelin, J., Hoopes, G.M., Reynolds, G.D., Laplantine, E., Bednarek, S.Y., Shorte, S.L. and Eliceiri, K.W. (2017) TrackMate: an open and extensible platform for single-particle tracking. Methods, 115, 80–90.

CHAPTER 4

C9orf72 deficiency promotes motor deficits of a C9ALS/FTD mouse model in a dose-dependent manner

Qiang Shao*, Chen Liang*, Qing Chang, Wei Zhang, Mei Yang and Jian-Fu Chen. Acta Neuropathological Communications 2019 7:32 (*Co-first author)
Reprinted here with permission of the publisher with slight modification.
URL: https://actaneurocomms.biomedcentral.com/articles/10.1186/s40478-019-0685-7

Introduction

G4C2 hexanucleotide repeat expansions in the first intron of C9ORF72 are the most common cause of familial amyotrophic lateral sclerosis (ALS) and frontotemporal dementia (FTD) (collectively, C9ALS/FTD) [4, 6, 11, 14]. Haploinsufficiency (loss-of-function) of C9ORF72 protein is a key proposed disease mechanism which may act in parallel with gain-of-function mechanisms, including toxic RNAs from repeat transcription and dipeptide repeat proteins (DPRs) from repeat-associated non-AUG (RAN) translation [5, 9, 17]. However, the effect of C9orf72 deficiency in the background of gain-of-function has not been examined in vivo. Neither heterozygous nor homozygous knockout (KO) of C9orf72 in neurons leads to motor deficits in mice [8]. Recently, gain-of-function mouse models were generated using a C9ORF72 bacterial artificial chromosome (BAC) from C9ALS/FTD patient DNA under the control of the endogenous regulatory elements. Interestingly, three out of four of these C9-BAC transgenic mice did not develop motor behavior deficits, even at advanced ages [7, 12, 13]. Since these C9-BAC mouse models contain elevated C9orf72 proteins from the endogenous mouse gene, we hypothesized that C9orf72 provides neuroprotective effects against motor deficits in C9-BAC mice.

Results

To test the hypothesis that C9orf72 provides a protective role in C9-BAC mice and investigate the in vivo significance of C9orf72 haploinsufficiency, we crossed *C9orf72*$^{+/-}$ mice with *C9-BAC* mice and examined the consequences of C9orf72 protein dose reduction (loss-of-function) in the background of *C9-BAC* (gain-of-function). We found that C9orf72 loss and haploinsufficiency exacerbate motor behavior deficits in a dose-dependent manner, and this occurs early in the course of pathogenesis (4 months of age). Among the four published *C9-BAC* mouse models, we selected the one with motor deficits (we refer to this *C9orf72 BAC*$^{Tg/+}$ model as the *C9-BAC* line here) [10]. To reduce C9orf72 protein levels at different doses, we crossed *C9orf72*$^{+/-}$ and *C9-BAC* mice for two generations. We isolated proteins from brain tissues and confirmed the expected C9orf72 protein dose reduction (Fig. 4.1a, Supplemental Figure 4.S1A). The unchanged protein level of Atg101, which is associated with the C9orf72/Smcr8 complex based on our previous study [16], suggests the specificity of C9orf72 reduction (Fig. 4.1a, Supplemental Figure 4.S1A).

To study effects of C9orf72 deficiency on the motor behaviors of *C9-BAC* mice, we monitored a cohort of mice [20 WT (10 females + 10 males), 18 *C9-BAC* (11 females + 7 males), 26 *C9orf72*$^{+/-}$*;C9-BAC* (14 females + 12 males), and 19 *C9orf72*$^{-/-}$*;C9-BAC* (10 females + 9 males)]. We excluded *C9orf72*$^{+/-}$ and *C9orf72*$^{-/-}$ mice for the following reasons: C9orf72 heterozygous and homozygous KO mice exhibited no neurodegeneration and motor deficits based on previous studies [8]; complete deletion of C9orf72, which does not occur in C9ALS/FTD patients, led to autoimmune disorders and reduced survival in mice [1], which may complicate large-scale behavior and

Figure. 4.1. C9orf72 dose is critical for motor deficits in C9ALS/FTD mouse models.

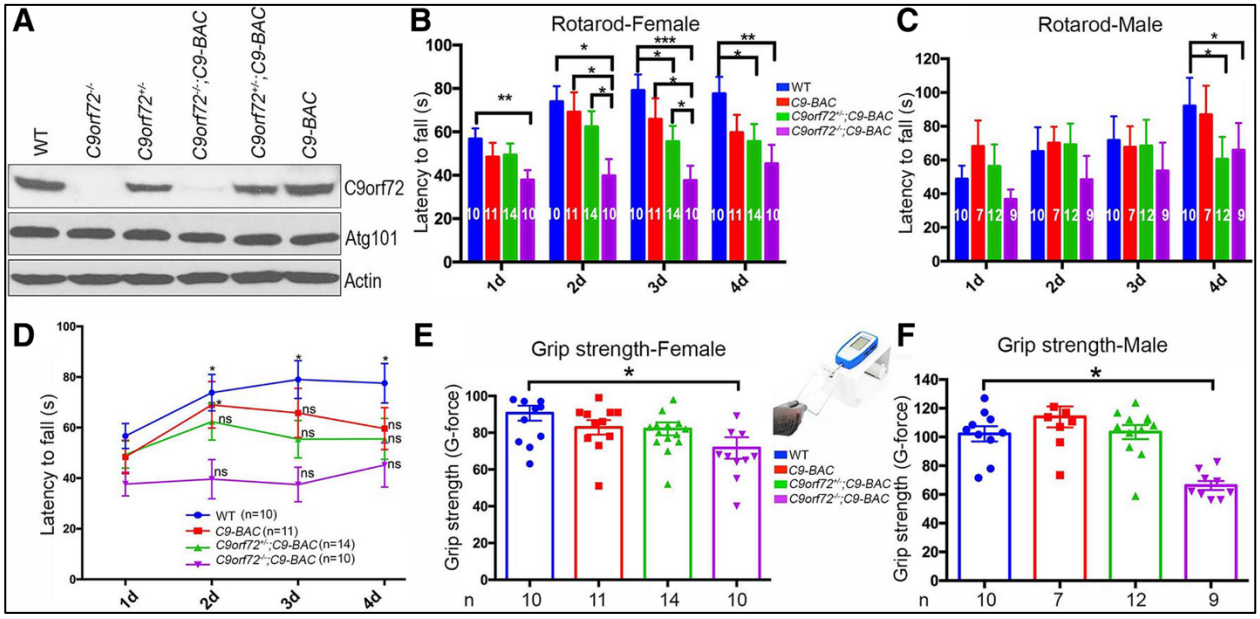

(a) Western blot analysis of C9orf72 and Atg101 protein levels in 2-month-old mouse cortex. β-Actin serves as the loading control. (b, c) Accelerating rotarod test was performed on 4-month-old mice to examine the latency to fall of females (b) and males (c). C9orf72 deficiency decreases the latency to fall of C9-BAC female mice in a dose-dependent manner. d A 4-consecutive-day rotarod assay reveals defective motor learning in *C9orf72*$^{+/-}$*;C9-BAC* and *C9orf72*$^{-/-}$*;C9-BAC* female mice in comparison to WT. e, f Grip strength test was performed to measure front paw strength in 4-month-old females (e) and males (f). All data are presented as mean ± SEM using numbers (n) of mice as indicated. Statistical analyses were performed with one-way ANOVA with Bonferroni's post hoc test (*$p < 0.05$, **$p < 0.01$, ***$p < 0.001$, N.s represents no significant difference detected in measurement of 2d, 3d, or 4d in comparison to that of 1d)

survival studies. We found that there were no significant differences among the four tested groups in their survival around 4 months, when behaviors were assessed. They also exhibited similar body weights, taking the sex of the mice into account (Supplemental Figure 4.S1B-1C). To examine their general anxiety levels, we performed an open field test [3]. *C9-BAC* mice with different C9orf72 levels behaved similarly in total distance traveled, distance traveled in the center, and time spent in the center (Supplemental Figure 4.S1E-1G).

We next examined their motor coordination and balance using an accelerating (4–40 rpm in 5 min) rotarod test. Mice were given five trials per day, with an inter-trial interval of 20 min, for 4 consecutive days. A C9orf72 dose-dependent decrease in latency to fall was detected in *C9-BAC* female mice (Fig. 4.1b), and in *C9-BAC* male mice on day 4 of the rotarod assay (Fig. 4.1c). These results suggest that motor coordination is sensitive to C9orf72 protein levels in *C9-BAC* mice. We further analyzed motor learning in female mice. WT mice exhibited an increase in latency to fall over the course of 4 consecutive days, indicating active motor learning (Fig. 4.1d). Latency to fall of *C9-BAC* mice was increased on day 2 but dropped on days 3 and 4 (Fig. 4.1d). Importantly, there was no increase in latency to fall from day 1 to day 4 in *C9orf72*$^{+/-}$*;C9-BAC* and *C9orf72*$^{-/-}$*;C9-BAC* animals (Fig. 4.1d). These results suggest that C9orf72 deficiency impaired motor coordination and motor learning of C9-BAC mice in a dose-dependent manner.

To examine motor strength, we measured forearm grip strength and found that it was significantly reduced in both male and female *C9orf72*$^{-/-}$*;C9-BAC* animals compared to other genotypes (Fig. 4.1e, f). Lastly, we measured the maximal speed at

which each animal fell from the rotarod device. Results showed that C9orf72 deficiency, in a dose-dependent manner, decreased the maximum speed at which *C9-BAC* mice fell (Supplemental Figure 4.S1H, S1I), which is consistent with the data on their latency to fall.

Discussion

The rotarod assay revealed more evident motor impairment in female mice than in male mice. This could be due to toxic gain-of-function since *C9-BAC* female mice exhibited earlier and more pronounced abnormalities than male mice [10]. It will be important to examine using similar cohorts of mice whether motor neurons (MNs) degenerate or reduce in number in a C9orf72 dose-dependent manner and whether these deficits correlate with the observed motor behavior deficits. Future studies should also investigate whether C9orf72 exhibits dose-dependent effects in the three other *C9-BAC* mouse models [7, 12, 13]. It will be informative to examine the effects of C9orf72 deficiency in the background of adeno-associated virus (AAV)-mediated G4C2 repeat expression [2]. Our study indicates that C9orf72 haploinsufficiency contributes to disease onset in a mouse model by exacerbating the pathogenic effects of RNA/DPR-mediated neurotoxicity. Together with a recent report on patient iPSC-derived MNs [15], this study suggests indeed that we should focus more on the combination of loss- and toxic gain-of-function. Together, for the first time, our mouse genetic studies showed that C9orf72 loss or haploinsufficiency in a gain-of-function mouse model of C9ALS/FTD exacerbate motor behavior deficits in a dose-dependent manner, demonstrating the importance of C9orf72 haploinsufficiency in vivo.

Supplemental Figure 4.S1. C9orf72 deficiency promotes motor deficits of a C9ALS/FTD mouse model in a dose-dependent manner.

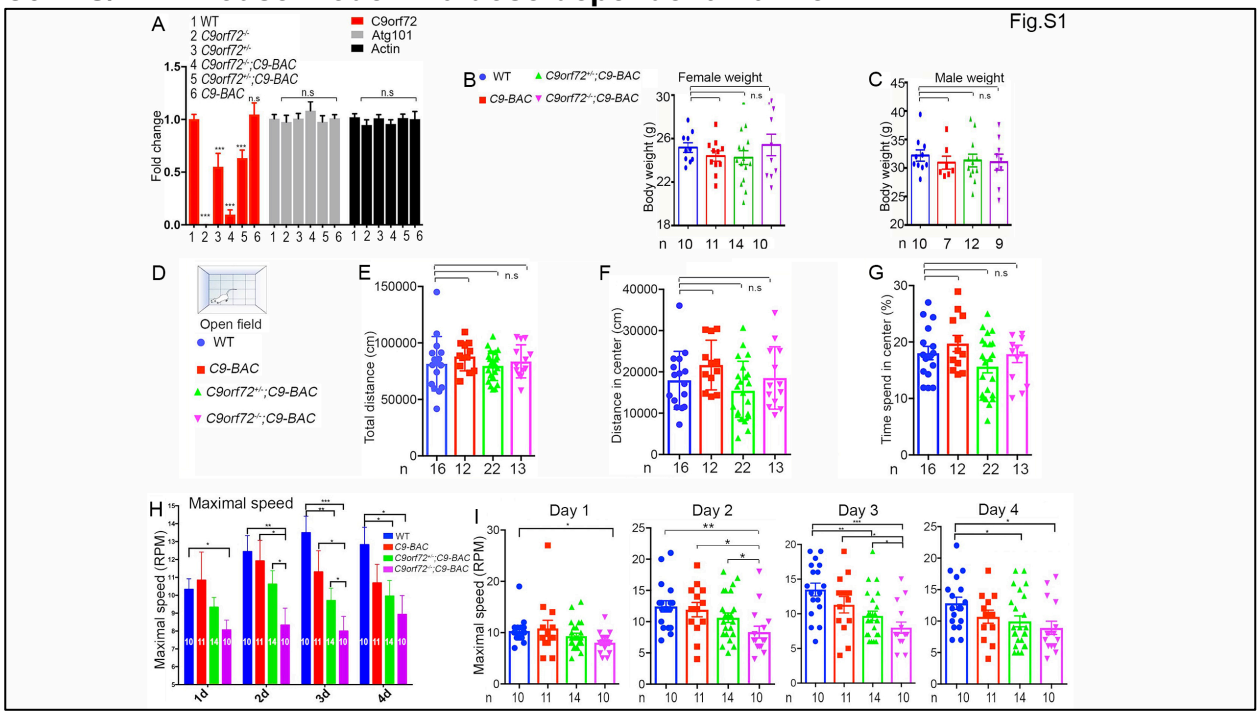

(A) Quantification of C9orf72/Atg101 protein levels. Data are presented as mean ± SEM from three independent experiments. (B, C) Body weight of female (B) and male (C) mice at 4 months of age. (D-G) Open field test was performed on 4-month-old mice to examine the total distance traveled (E), distance traveled in the center (F), and percentage of time spent in the center (G). (H, I) Quantification of the maximal g force from five trials of rotarod assay. C9orf72 deficiency decreases the maximal g force of *C9-BAC* female mice in a dose-dependent manner. All data are presented as mean ± SEM using numbers (n) of mice as indicated. Statistical analyses were performed with one-way ANOVA with Bonferroni's post hoc test (*$p < 0.05$, **$p < 0.01$, ***$p < 0.001$, n.s represents no significant difference detected).

References

1. Burberry A, Suzuki N, Wang J-Y, Moccia R, Mordes DA, Stewart MH et al (2016) Loss-of-function mutations in the C9ORF72 mouse ortholog cause fatal autoimmune disease. Sci Transl Med 8:347ra93–347ra93

2. Chew J, Gendron TF, Prudencio M, Sasaguri H, Zhang Y-J, Castanedes-Casey M et al (2015) Neurodegeneration. C9ORF72 repeat expansions in mice cause TDP-43 pathology, neuronal loss, and behavioral deficits. Science. 348:1151–1154

3. Crawley JN (1999) Behavioral phenotyping of transgenic and knockout mice: experimental design and evaluation of general health, sensory functions, motor abilities, and specific behavioral tests. Brain Res 835:18–26

4. DeJesus-Hernandez M, Mackenzie IR, Boeve BF, Boxer AL, Baker M, Rutherford NJ et al (2011) Expanded GGGGCC hexanucleotide repeat in noncoding region of C9ORF72 causes chromosome 9p-linked FTD and ALS. Neuron. 72:245–256

5. Gao F-B, Almeida S, Lopez-Gonzalez R (2017) Dysregulated molecular pathways in amyotrophic lateral sclerosis-frontotemporal dementia spectrum disorder. EMBO J EMBO Press 36:2931–2950

6. Gijselinck I, Van Langenhove T, van der Zee J, Sleegers K, Philtjens S, Kleinberger G et al (2012) A C9orf72 promoter repeat expansion in a Flanders-Belgian cohort with disorders of the frontotemporal lobar degeneration-amyotrophic lateral sclerosis spectrum: a gene identification study. Lancet Neurol 11:54–65

7. Jiang J, Zhu Q, Gendron TF, Saberi S, McAlonis-Downes M, Seelman A et al (2016) Gain of toxicity from ALS/FTD-linked repeat expansions in C9ORF72 is alleviated by antisense oligonucleotides targeting GGGGCC-containing RNAs. Neuron. 90:535–550

8. Koppers M, Blokhuis AM, Westeneng H-J, Terpstra ML, Zundel CAC, Vieira de Sá R et al (2015) C9orf72 ablation in mice does not cause motor neuron degeneration or motor deficits. Ann Neurol 78:426–438
9. Ling S-C, Polymenidou M, Cleveland DW (2013) Converging mechanisms in ALS and FTD: disrupted RNA and protein homeostasis. Neuron. 79:416–438
10. Liu Y, Pattamatta A, Zu T, Reid T, Bardhi O, Borchelt DR et al (2016) C9orf72 BAC mouse model with motor deficits and neurodegenerative features of ALS/FTD. Neuron. 90:521–534
11. Majounie E, Renton AE, Mok K, Dopper EGP, Waite A, Rollinson S et al (2012) Frequency of the C9orf72 hexanucleotide repeat expansion in patients with amyotrophic lateral sclerosis and frontotemporal dementia: a cross-sectional study. Lancet Neurol
12. O'Rourke JG, Bogdanik L, Muhammad AKMG, Gendron TF, Kim KJ, Austin A et al (2015) C9orf72 BAC transgenic mice display typical pathologic features of ALS/FTD. Neuron. 88:892–901
13. Peters OM, Cabrera GT, Tran H, Gendron TF, McKeon JE, Metterville J et al (2015) Human C9ORF72 Hexanucleotide expansion reproduces RNA foci and dipeptide repeat proteins but not neurodegeneration in BAC transgenic mice. Neuron. 88:902–909
14. Renton AE, Majounie E, Waite A, Simón-Sánchez J, Rollinson S, Gibbs JR et al (2011) A hexanucleotide repeat expansion in C9ORF72 is the cause of chromosome 9p21-linked ALS-FTD. Neuron. 72:257–268
15. Shi Y, Lin S, Staats KA, Li Y, Chang W-H, Hung S-T et al (2018) Haploinsufficiency leads to neurodegeneration in C9ORF72 ALS/FTD human induced motor neurons. Nat Med Nature Publishing Group 24:313–325

16. Yang M, Liang C, Swaminathan K, Herrlinger S, Lai F, Shiekhattar R et al (2016) A C9ORF72/SMCR8-containing complex regulates ULK1 and plays a dual role in autophagy. Sci Adv American Association for the Advancement of Science 2:e1601167–e1601167

17. Zu T, Pattamatta A, LPW R (2018) Repeat-Associated Non-ATG Translation in Neurological Diseases. Cold Spring Harb Perspect Biol. Cold Spring Harbor Lab 10:a033019

CHAPTER 5

C9orf72 promotes axonal transport and has dose-dependent neuroprotective roles against axonal degeneration and behavioral deficits in a mouse model of C9FTD/ALS

Chen Liang, Li Ma, Jianhui Bai, Qiang Shao, Qing Chang, Wei Zhang, Mei Yang, Zhipeng Lu and Jian-Fu Chen.
To be submitted to Human Molecular Genetics

Abstract

Hexanucleotide repeat expansion in C9ORF72 is the most common cause of familial frontotemporal dementia and amyotrophic lateral sclerosis (collectively, C9FTD/ALS). Despite its implication in C9FTD/ALS, the pathophysiological roles of C9ORF72 in vivo in neurons remain to be identified. Moreover, C9orf72 homozygous knockout mice surprisingly exhibit no phenotype in motor neurons. Here we discovered that C9orf72 attenuates dipeptide repeat protein accumulations and axonal degeneration in C9FTD/ALS mouse models. Importantly, C9orf72 haploinsufficiency in C9FTD/ALS mouse models exacerbates social and cognitive behavior deficits. Mechanistic studies using C9orf72 mutant mice reveal disruption of axonal transport in motor neurons (MNs), which is further validated in MNs derived from patient's induced pluripotent stem cells (iPSCs). Our studies suggest dose-dependent neuroprotective effects of C9orf72 against gain of toxicity, axonal degeneration and behavioral deficits possibly through promoting axonal transport and autophagy-lysosome functions, providing insights into the pathological mechanisms of C9FTD/ALS.

Introduction

Frontotemporal dementia (FTD) and amyotrophic lateral sclerosis (ALS) are neurodegenerative disorders leading to dementia and loss of motor functions (Ling et al., 2013; Gao et al., 2017). G4C2 hexanucleotide repeat (GGGGCC) expansion in a noncoding region of the gene chromosome 9 open reading frame 72 (C9ORF72) is the most common cause of familial ALS and FTD (C9ALS/FTD) (Gijselinck et al, 2012; Renton et al., 2011; DeJesus-Hernandez et al., 2011; Majounie et al, 2012). C9ORF72-associated ALS accounts for about 40% of familial ALS and about 5-10% of sporadic ALS cases (Renton et al., 2011; DeJesus-Hernandez et al., 2011). Haploinsufficiency of C9ORF72 protein is a key proposed disease mechanism, which may act in parallel with additional pathological mechanisms including toxic RNAs from repeat transcription and dipeptide protein from repeat-associated non-AUG (RAN) translation (Ling et al., 2013; Gao et al., 2017). This is supported by the fact that C9ORF72 expression levels are decreased in C9ALS/FTD patient tissues (Gijselinck et al, 2012; DeJesus-Hernandez et al., 2011; Waite et al., 2014; Mizielinska et al., 2013). In the presence of elevated glutamate levels, haploinsufficiency of C9ORF72 leads to the degeneration of motor neurons derived from induced pluripotent stem cells (iPSCs) of ALS patients (Shi et al, 2018). However, neither heterozygous nor homozygous knockout (KO) of C9orf72 in neurons leads to motor neuron degeneration or motor deficits in mice (Koppers et al., 2015). Therefore, the in vivo significance of C9orf72 haploinsufficiency in C9ALS/FTD remains unknown. Recently, four gain-of-function mouse models were generated from independent laboratories using C9orf72 bacterial artificial chromosome (BAC) from

C9ALS/FTD patient DNA that is under control of the endogenous regulatory elements. Although these C9-BAC transgenic mice exhibited RNA foci and dipeptides, three of them failed to develop motor behavior deficits at advanced ages (O'Rourke et al., 2015; Peters et al., 2015; Jiang et al., 2016). Since these C9-BAC mouse models contain the endogenous mouse C9orf72 gene, it is important to reduce C9orf72 protein dose (loss-of-function) in the background of C9-BAC (gain-of-function) in order to assess the in vivo importance of C9orf72 haploinsufficiency in C9ALS/FTD.

To investigate the in vivo significance of C9orf72 haploinsufficiency, we crossed *C9orf72*$^{+/-}$ mice with *C9-BAC* mice (Liu et al., 2016) and examined the consequences of C9orf72 protein dose reduction (loss-of-function) in the background of gain-of-function. We found that C9orf72 haploinsufficiency exacerbates motor deficits, social deficits and cognitive dysfunction at advanced age possibly through disruption of axonal transport in motor neurons (MNs) or impairment of di-peptide clearance. Furthermore, C9orf72 haploinsufficiency leads to abnormal axonal swellings in neuromuscular junctions (NMJs) in *C9-BAC* mice. Abnormal axonal transport and swellings are also found in MNs derived from patient iPSCs.

Materials and Methods

Mutant characterization, immunofluorescence staining

Histological processing and immunohistochemical labeling of sections were performed as described previously (Yang et al., 2015; Shao et al., 2016). Mice were anesthesized with CO2 and perfusion-fixed with 4% paraformaldehyde (PFA). Spinal cords and brains were harvested and post-fixed in 4% PFA, washed with PBS, and immersed in 25% sucrose overnight at 4°C followed by standard OCT embedding and coronal sectioning. The following primary antibodies were used: GA (MABN889, Millipore) and poly GP (24494-1-AP, Proteintech).

Motor neuron generation from patient iPSCs and transfection

Motor neuron (MN) induction of iPSCs was performed as previously described with minor modifications (Du et al., 2015). The control and patient iPSCs were cultured in mTeSR1 medium (Stem cell technologies) on a Matrigel-coated plate, dissociated with ReLeSR (Stem cell technologies), and split 1:6 on Matrigel-coated plates. To generate MN progenitor cells, the mTeSR1 medium was replaced with a defined neural induction medium, including DMEM/F12, Neurobasal medium at 1:1, 0.5 × N2, 0.5 × B27, 0.1 mM ascorbic acid, 1 × Glutamax and 1 × penicillin/streptomycin. CHIR99021 (3 μM), 2 μM DMH1 and 2 μM SB431542 (Selleckchem) were added to the medium. The culture medium was changed every other day. After 6 days, cells were dissociated with ReLeSR and split at 1:6 with the same medium described above. RA (0.1 μM, Sigma) and 0.5 μM Purmorphamine (Selleckchem) were added in combination with

2 μM DMH1,1 μM CHIR99021 and 2 μM SB431542. The medium was changed every other day. Cells maintained under these conditions for 6 days were induced to become motor neuron progenitor cells (MNPs). To induce MN differentiation, MNPs were dissociated with ReLeSR and cultured in suspension in the neural induction medium above with 0.5 μM RA and 0.1 μM Purmorphamine. The medium was changed every other day. MNPs under these conditions for 6 days were differentiated into primary MNs. The MNs were then dissociated with Accutase (Millipore) into single cells and plated on Matrigel-coated plates. The MNs were cultured with 0.5 μM RA, 0.1 μM Purmorphamine, 10 ng/ml BDNF (PeproTech) and 10 μM DAPT (Selleckchem) for 4 weeks.

iMNs were transfected using NeuroMag transfection reagent (Oz Biosciences). Plasmid DNA (1.5 μg) was incubated with 4.5 μl Neuromag in 300 μl OptiMEM for 15 minutes, and then added drop-wise to the cultures. Cells were incubated on top of a magnetic plate (Oz Biosciences) for 15 minutes and fresh medium was replaced after 1 hour. Images were acquired 3 days later on a Leica TCS SP8 confocal microscope using a 63 X 1.4 numerical aperture oil-immersion objective.

Mouse motor neuron isolation, transfection, and live imaging

Isolation and culture of spinal cord motoneurons from E 13.5 mice were performed as previously described (Conrad et al., 2011). Spinal cords were isolated and dorsal root ganglia were removed carefully. MNs were enriched by lectin-based purification. Isolated cells were plated onto poly-DL-ornithine hydrobromide/laminin (Sigma) coated 35 mm glass bottom culture dishes (MatTek). Cells were cultured in

Neurobasal medium (Invitrogen) with 1× B27 supplement (Invitrogen), 5% inactivated horse serum (Invitrogen), 1% Glutamax (Invitrogen) and 10 ng/ml CNTF at 37°C in a 5% CO2 incubator. Half the volume of culture medium was exchanged every 2 days. At 4 days in vitro (DIV4), neurons were transfected using NeuroMag transfection reagent (Oz Biosciences) as previously described (Fallini et al., 2010). Briefly, 1 hour before magnetofection, complete medium was replaced with serum-free Neurobasal/B27/Glutamax medium. Plasmid DNA (1.5 µg) was incubated with 4 µl Neuromag in 300 µl OptiMEM for 15 minutes, and then added drop-wise to the cultures. Cells were incubated on top of a magnetic plate (Oz Biosciences) for 15 minutes and complete medium was restored after 1 hour. For live cell imaging, 35 mm glass bottom dishes containing normal growth medium were mounted in a temperature-controlled stage and maintained at 37°C and 5% CO2 conditions. Cells were visualized at DIV6-9 on a Zeiss LSM 710 confocal microscope using a 100 x oil-immersion lens or Leica TCS SP8 microscope using a 63X 1.4 numerical aperture oil-immersion objective. Digital images were acquired with a camera using LAS software. Laser lines at 488 nm were used. Time-lapse sequences of 1024 x 1024 pixels were collected at 8 sec intervals for 15 min.

Transport analysis

Kymographs were generated using the Image J plugin Kymograph (https://www.embl.de//eamnet/html/kymograph.html). Net run speeds and lengths of vesicle movement were calculated by drawing a slope from the beginning to the end of the run on the kymograph.

Neuromuscular junction (NJM) analysis

Muscles were fixed for 10 min in freshly prepared PBS containing 4% (w/v) PFA. After washing with PBS, further connective tissues were detached from the muscles, and individual fibers were carefully teased apart to facilitate antibody penetration. Muscles were permeabilized with 2% Triton X-100 in PBS for 30 min then blocked in 4% BSA and 1% Triton X-100 in PBS for 30 min. Samples were incubated overnight at 4 °C in blocking solution with α-Bungarotoxin, Alexa Fluor™ 488 conjugate (1:500 dilution), and primary antibodies against neurofilament (2H3, 1: 70 dilution) to visualize the AChRs and axons. The following day, muscles were washed three times for 10 min each in PBS before incubation for 2 h with AlexaFluor 555 and 647 secondary antibodies and α-Bungarotoxin, Alexa Fluor™ 488 conjugate in PBS in the dark. Lastly, muscles were washed three times for 10 min each in PBS and mounted on slides with coverslips. A Leica TCS SP8 microscope was used to image the NMJs with Z-stacks at 3 μm intervals.

Behavioral testing

The experimenter was blind to the animal's genotype during all tests. A cohort of mice was analyzed using the following behavior assays. 1) **Open field analysis**. Open field test was performed using an overhead SMART video tracking system (Panlab), which measures distance traveled, time spent in each zone, and speed. The apparatus consisted of a grey, open-top plastic box (90 x 90 x 40 cm). After a 1- or 2-hour period of acclimation to the behavioral testing room, each animal was placed in the center of the open field and left undisturbed for 30 min. The apparatus was wiped between trials

with a 70% ethanol solution. The trace path, total distance, center time were analyzed with smart video software (Harvard Apparatus). 2) **Three-chamber social task**. Sociability and social novelty were evaluated with the three-chamber (Harvard Apparatus) task. Briefly, the subject mouse was placed in the middle chamber for adaptation for 10 min. followed by a sociability test session: one of the control mice (Stranger 1) was placed inside a wire containment cup located in the left side chamber. An empty wire containment cup was placed in the right side of the chamber. The subject mouse was allowed to explore all three chambers for 10 min. This was followed by a social novelty test: instead of the empty cup, a second control mouse (Stranger 2) was placed inside an identical wire containment cup in the right chamber. The subject mouse was allowed to freely explore all chambers for 10 min. Time spent in each chamber during the sociability session and social novelty session were analyzed with smart video software. 3) **Novel object recognition task**. Subject mice were transported to the behavioral room for at least 1 hour of habituation. Training session: the subject mouse was placed into a home cage with two identical plastic dice (Object 1 and Object 2), each placed 5 cm from one of the walls and 10 cm apart. The mice were allowed to explore the cage for 10 min. Testing session: the subject mouse was removed from the cage for 5 min, and Object 2 was replaced with a novel marble of similar size to Object 2. The mice were allowed to explore the cage for 5 min. The duration of time in which the head of the mouse was < 2 cm from each object was recorded for each session.

Results

C9orf72 haploinsufficiency in C9FTD/ALS mouse models exacerbates motor, social and cognitive deficits

We hypothesized that C9orf72 deficiency exacerbates cognitive and social deficits in C9ALS/FTD. Among the four published *C9-BAC* mouse models, we selected the one with motor deficits and neurodegenerative features of FTD/ALS (we refer to this *C9orf72 BAC*$^{Tg/+}$ model as the *C9-BAC* line here) (Liu et al., 2016). To reduce C9orf72 protein levels at different doses, we crossed *C9orf72*$^{+/-}$ and *C9-BAC* mice for more than two generations, and examined social behaviors, cognitive functions as well as motor behaviors using 18-months WT, *C9-BAC* and *C9orf72*$^{+/-}$*;C9BAC* littermates.

To study effects of C9orf72 haploinsufficiency on the cognitive functions of *C9-BAC* mice, we performed novel object recognition test. A mouse is presented with two identical objects during the first session, and then one of the objects is replaced by a different object during a second session (Fig. 5.1A). We found that WT and *C9-BAC* mice showed more preference for the novel object, however *C9orf72*$^{+/-}$*;C9BAC* mice showed less preference than wild-type mice for the novel object compared to the familiar object (Fig. 5.1B), suggesting an impairment in discriminating between familiar and novel objects.

To examine social behaviors, we used three-chamber sociability and social novelty test. The subject mouse first encounters a mouse under a cup and an empty cup in the "sociability" session. In the "social novelty" session, the subject encounters the first familiar mouse as well as a novel mouse (Fig. 5.1C). Mice normally prefer to spend more time with another mouse, which is called sociability and they will investigate a

Figure 5.1. C9orf72 dose is critical for cognitive, social and motor deficits in C9FTD/ALS mouse models.

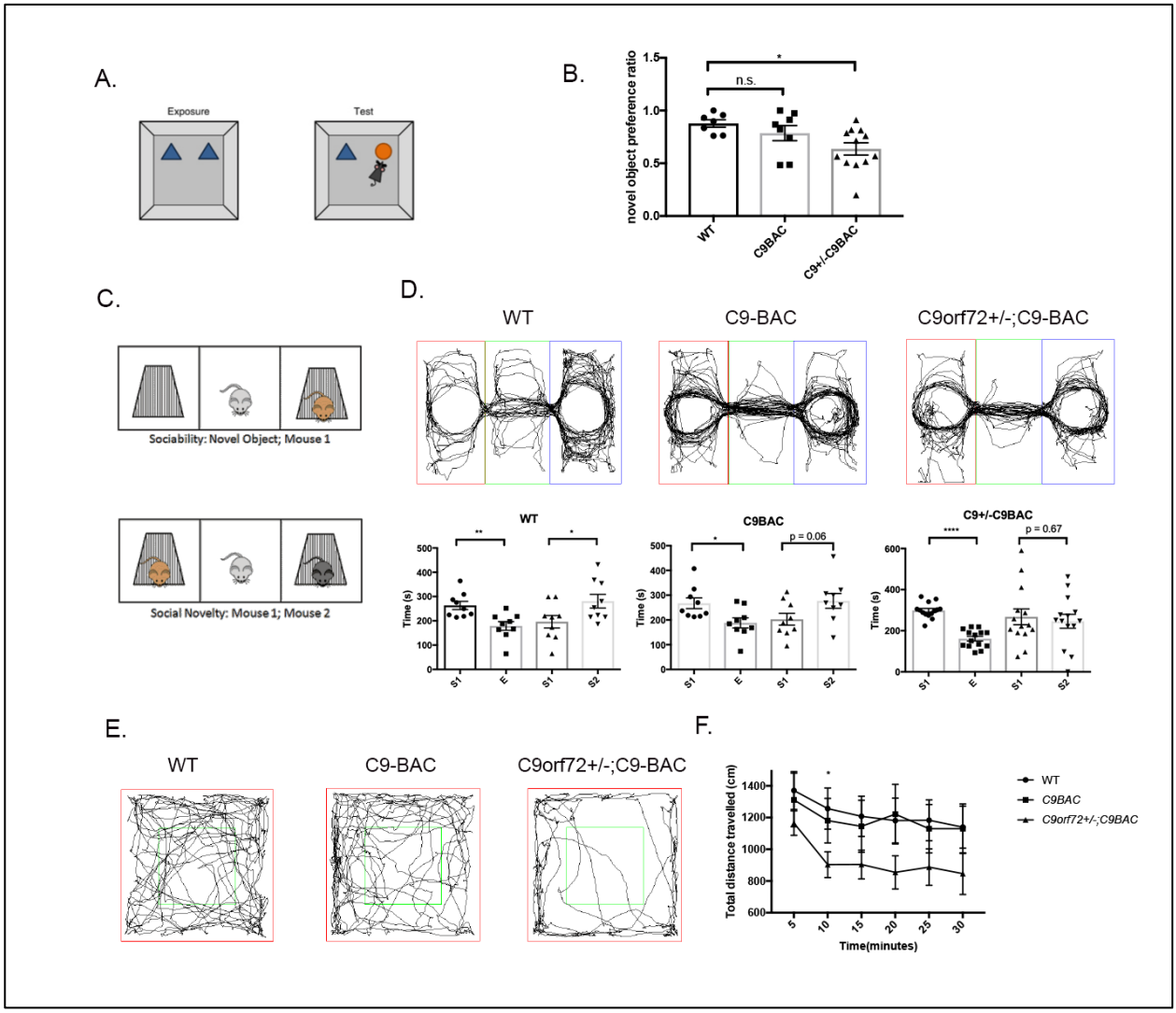

(A-B) Novel object recognition task was performed to measure cognitive functions using WT, *C9-BAC* and *C9orf72*$^{+/-}$*;C9-BAC* (N = 7-14) at 18 months of age. *C9orf72*$^{+/-}$*;C9-BAC* mice showed less preference for the novel object compared to the familiar object than WT mice. (C-D) Three-chamber task was performed to measure sociability and preference for social novelty at 18 months of age. All genotypes preferred to interact with Stranger 1 (S1) over an empty (E) chamber. WT mice preferred to interact with Stranger 2 (S2) over S1. *C9-BAC* mice showed less preference and *C9orf72*$^{+/-}$*;C9-BAC* mice showed no preference to interact with S2 as shown in the upper panel. (E-F) Open field test was performed on 18-month-old mice to examine the total distance traveled. All data are presented as mean ± SEM. Statistical analyses were performed with one-way ANOVA with Bonferroni's post hoc test (*p<0.05, **p<0.01, ***p<0.001, n.s represents no significant difference detected). A modified from Barkus et al. 2014, C modified from https://med.stanford.edu/sbfnl/services/bm/si/three-chamber.html

stranger mouse more than a familiar one, which is called social novelty. We found that *C9-BAC* mice are normal in sociability session, but they show no significant preference for the novel mouse in the social novelty session, and C9orf72 haploinsufficiency exacerbates the social novelty defect (Fig. 5.1D).

Because *C9orf72*$^{+/-}$*;C9BAC* mice showed no general locomotor deficits in the open field at 4-months old **(Chapter 4)**, we performed open field test at 18-months old of age to examine if C9orf72 haploinsufficiency promotes motor behavioral deficits in an age-dependent manner. We found that *C9orf72*$^{+/-}$*;C9BAC* mice showed a decreased trend of total distance travelled compared with WT at all time bins during a 30-minute test period at 18-months old (Fig. 5.1E-F), indicating age-dependent motor behavioral deficits.

Axonal transport defects and axonal swellings in C9orf72 haploinsufficient *C9-BAC* mouse models and patient iMNs

To study the mechanisms underlying dose-dependent motor behavioral deficits in *C9orf72*$^{+/-}$*;C9BAC* mice, we examined the neuromuscular junctions (NMJs). WT animals exhibited normal NMJs, as reflected by normal postsynaptic acetylcholine receptor (AChR) staining and Neurofilament-labeled presynaptic compartments. In contrast, the presynaptic terminals of *C9orf72*$^{+/-}$*;C9BAC* mice exhibited swellings with neurofilament accumulation (white arrowheads, Fig. 5.2A). Together, these results suggest that C9orf72 deficiency promotes axonal swellings of NMJs in *C9-BAC* mouse models.

These axonal swelling may be caused by impaired axonal transport and autophagy-lysosomal function. To test this hypothesis, we examined axonal transport of GFP-LC3 labeled autophagosomes in isolated spinal MNs using time-lapse imaging

Figure 5.2. C9orf72 deficiency promotes axonal swellings in *C9-BAC* mice.

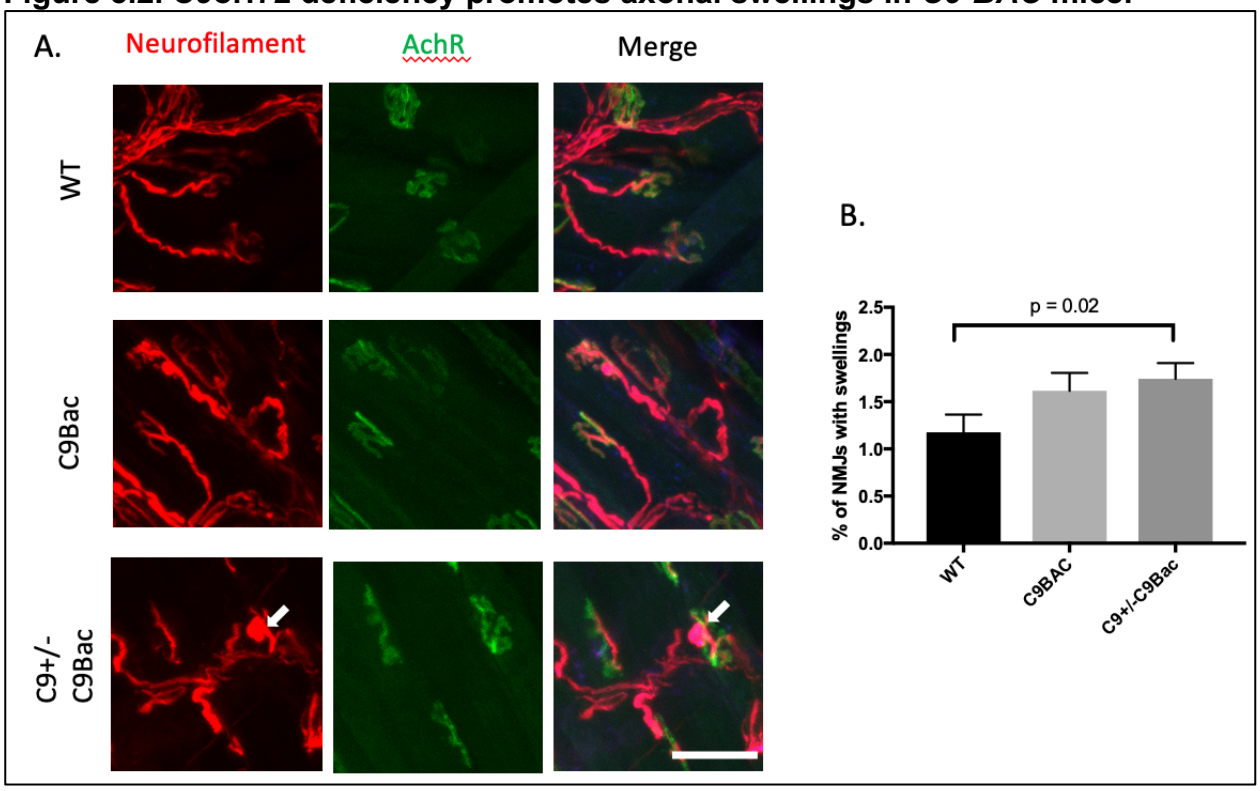

(A) Representative confocal imaging of 9-month-old mouse diaphragms stained with antibodies against NF (NF, red), and acetylcholine receptor AchR (green). White arrows represent NF-positive axonal swellings, which are rarely detected in WT controls. Scale bars: 50 μm. (B) Quantification of NMJs with swellings. All data are presented as mean ± SEM using measurements averaged from ⩾3 muscle bundles of each mutant mouse ($n > 3$). Statistical analysis was performed by one-way ANOVA analysis with Bonferroni correction.

approaches. Autophagosomes in WT MNs exhibited robust motility along the processes, with a predominant retrograde direction. Their net run speeds and run lengths were significantly reduced in *C9orf72*$^{-/-}$ MNs (Fig. 5.3A-D). Thus, C9orf72 might promote axonal transport in MNs under physiological conditions. To determine whether C9orf72 plays roles in axonal transport in MNs under pathological conditions, we isolated MNs from WT, *C9-BAC*, *C9orf72*$^{+/-}$*;C9BAC*, and *C9orf72*$^{-/-}$*;C9-BAC* embryonic spinal cords and conducted time-lapse imaging of GFP-LC3 labeled autophagosomes. We did not detect significant differences in net run speed between WT and *C9-BAC* MNs. In contrast, C9orf72 deletion resulted in a decrease in net run speed in the *C9-BAC* background (Fig. 5.3E).

To determine whether the axonal transport defects and neurodegeneration observed in animal models occur in human C9FTD/ALS diseased cells, we turned to MNs derived from patient iPSCs. We obtained three controls and three C9ORF72-associated human pluripotent stem cell (hPSC) lines from the NINDS Human Cell and Data Repository housed at Rutgers University. MNs were generated from these hPSCs using standard protocols (Fig. 5.4A) (Du et al., 2015). As reported in published studies, we used a combination of small molecules and guided both control and patient hPSCs to differentiate into nearly pure MN progenitors, labeled by Isl1/TuJ1 (Fig. 5.4B). We were able to generate > 50% ChAT-positive MNs in both control and patient cells, with no significant differences between the patient and control groups (Fig. 5.4C-E), indicative of their normal differentiation.

Figure 5.3. C9orf72 deficiency disrupts axonal transport in mouse MNs.

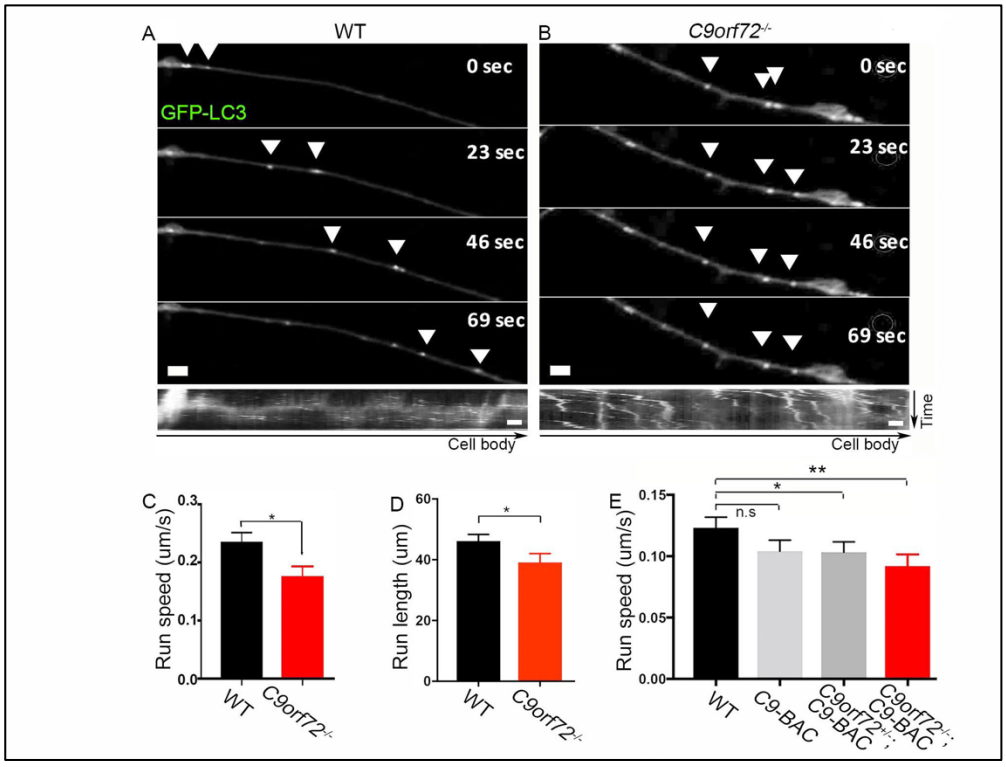

(A, B) Representative time-lapse images and corresponding kymographs of GFP-LC3-labeled autophagosome transport in spinal motor neurons isolated from E13.5 mouse spinal cords. Individual autophagosomes marked by white triangles show robust retrograde transport in WT and diminished motility in mutant MNs. Scale bars: 2 μm. (C) Quantification of net run speed in WT (n=126) and *C9orf72*$^{-/-}$ (n=117) MNs. (D) Quantification of total run length in WT (n=127) and *C9orf72*$^{-/-}$ (n=107) MNs. (E) Quantification of net run speed in WT (n=150), *C9-BAC* (n=162), *C9orf72*$^{+/-}$*;C9-BAC* (n=162), and *C9orf72*$^{-/-}$*;C9-BAC* (n=123) MNs. Student's t-test in C and D; one-way ANOVA with Bonferroni's post hoc test in E (**p<0.01, *p<0.05, n.s represents no significant difference detected).

Figure 5.4. Axonal transport disruption and autophagic stress coupled with axonal swellings in MNs from patient iPSCs.

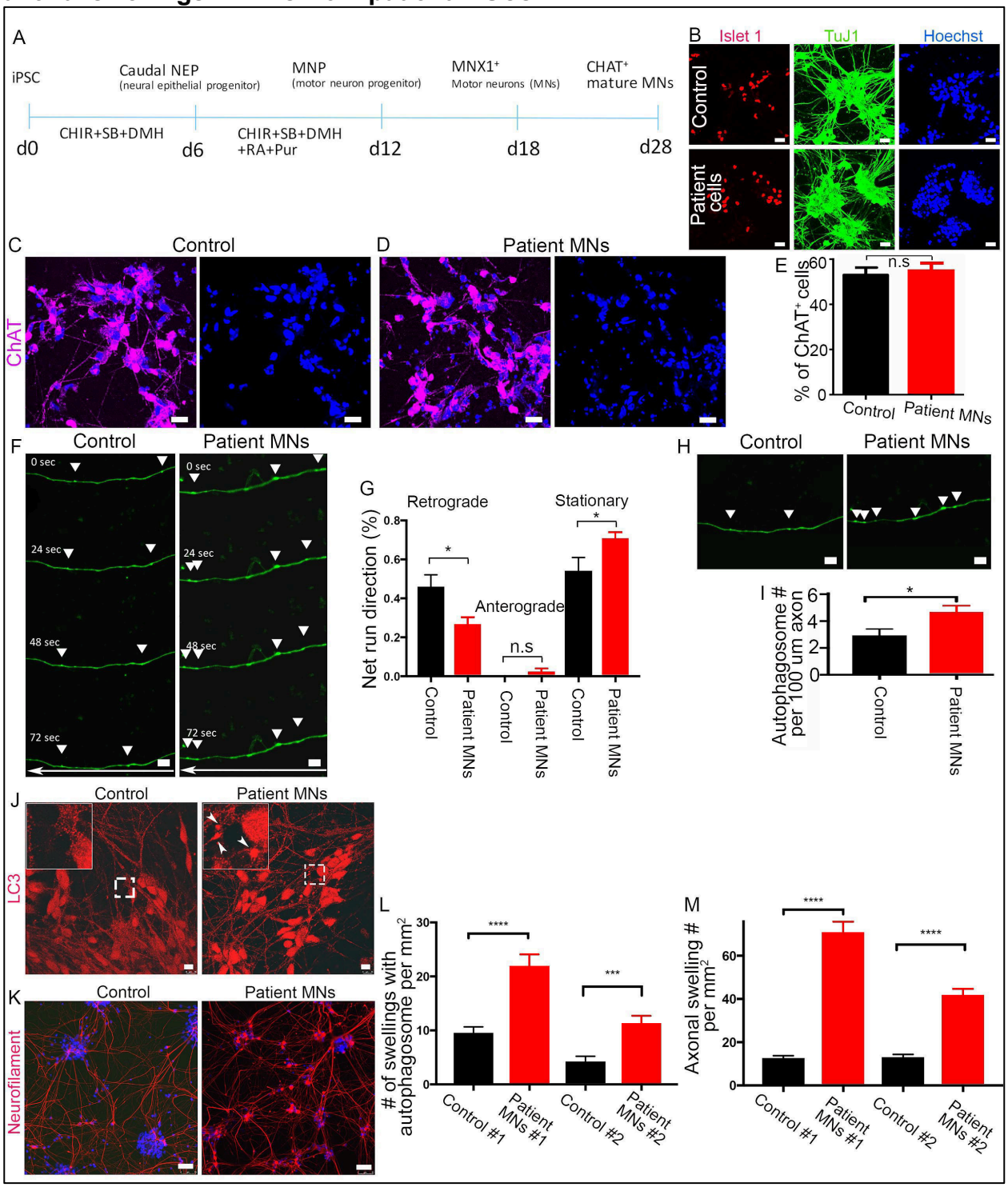

(A) Diagram of the procedure of MN generation from patient iPSCs. (B) Representative imaging of the iPSC-derived neurons stained with antibodies against Islet1 (red) and Tuj1 (green). Hoechst stains nuclei (blue). Scale bars: 25 μm. (C, D) Representative

imaging of iPSC-derived MNs stained with antibodies against ChAT (purple). Hoechst stains nuclei (blue). Scale bars: 25 μm. (E) Quantification of the percentage of ChAT-positive cells out of total cells. Error bars represent SEM of three independent experiments; n.s represents no significant difference detected (Student's t-test). (F) Representative time-lapse images and corresponding kymographs of GFP-LC3-labeled autophagosome transport in motor neurons (MNs) derived from control and patient iPSCs. Individual autophagosomes marked by white triangles. Scale bars: 5 μm. (G) Quantification of the percentages of retrograde, anterograde, and stationary transport in control (n=8) and patient iPSC-derived (n=16) motor neurons (MNs). (H) Representative imaging of GFP-LC3-positive autophagosomes. (I) Quantification of GFP-LC3-positive autophagosomes per 100 μm axon in control (n=7) and patient iPSC-derived MNs (n=14). (J-K) Representative imaging of MNs stained with antibodies against LC3 (red in J), or neurofilament (red in K). Inserts at top left are enlargements of white boxed areas. White arrowheads represent LC3-positive puncta. Hoechst stains nuclei (blue). Scale bars: 10 μm in J; 50 μm in K. (L, M) Quantification of the numbers of swellings with autophagosomes (J) and axonal swellings (K) per mm^2. Error bars represent SEM of three independent experiments, ***$p < 0.001$ (Student's t-test).

We performed time-lapse imaging studies and examined axonal transport of autophagosomes labeled by GFP-LC3. In comparison to control MNs, patient MNs exhibited a decrease in the percentage of retrograde transport of autophagosomes, alongside a significant increase in stationary autophagosomes (Fig. 5.4F-G). These results are consistent with the impaired axonal transport observed in *C9orf72*$^{-/-}$ mouse MNs and in MNs from mice with C9orf72 deficiency in the background of *C9-BAC* (Fig.5.3). Impaired axonal transport leads to autophagic stress (Tammineni et al., 2017). We next assessed autophagosome retention and observed an enhanced density of axonal puncta in patient MNs compared to controls (Fig. 5.4H-I), suggesting increased autophagic stress in patient MNs. To further validate these autophagy defects, we examined endogenous LC3-positive puncta and found that there was a significant increase in autophagosome accumulations in patient MNs relative to controls (Fig. 5.4J, 5.4L). Moreover, the number of neurofilament-labeled axonal swellings was significantly increased in patient MNs compared to control MNs (Fig. 5.4K, M), suggesting autophagic stress is coupled with axonal degeneration in patient MNs. Thus, our studies from C9FTD/ALS mouse models and patient MNs suggest that C9orf72 has a neuroprotective role against axonal degeneration possibly by promoting axonal transport and autophagy-lysosome functions.

C9orf72 haploinsufficiency exacerbates dipeptide repeat (DPR) abundance in *C9-BAC* mice

To test whether C9orf72 deficiency promotes the accumulation of DPRs, which are toxic to neurons, we examined poly (GA) and poly (GP) in motor cortex and spinal cord of 16-months old WT, *C9-BAC*, *C9orf72*$^{+/-}$*;C9-BAC* and *C9orf72*$^{-/-}$*;C9-BAC* mice. We

Figure 5.5. C9orf72 deficiency exacerbates gain of toxicity in *C9-BAC* mice.

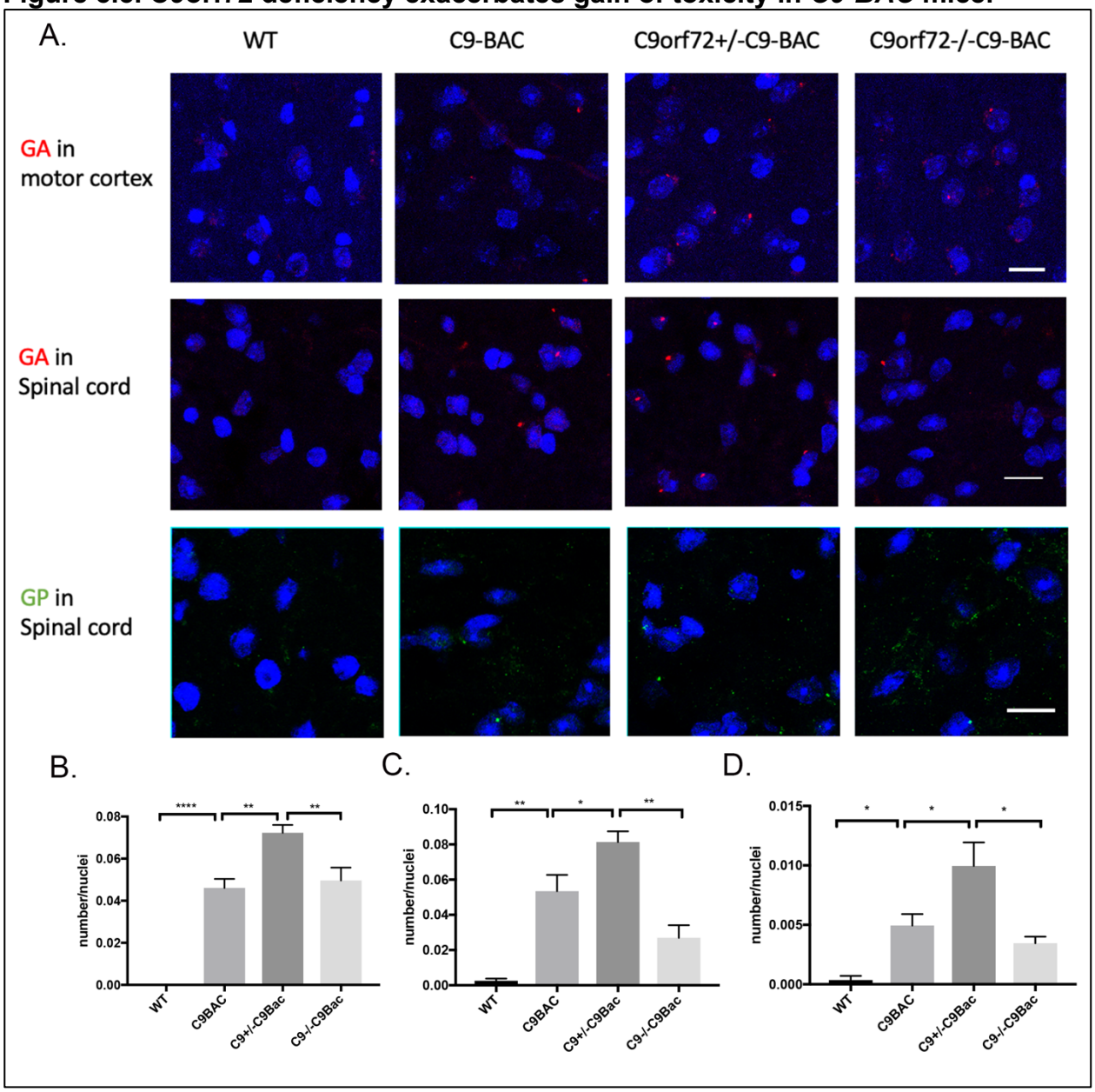

(A) Representative imaging of coronal sections stained with antibodies against poly (GA) (red) or poly (GP) (green). Age-matched 16-month-old mice were used to prepare sections in the area of motor cortex or spinal cord. Scale bars: 12 μm. (B) Quantification of the percentage of cells with poly (GA) puncta out of total cells from motor cortex of WT, *C9-BAC*, *C9orf72*$^{+/-}$*;C9-BAC* and *C9orf72*$^{-/-}$*;C9-BAC* mice. N = 3 – 5. (C) Quantification of the percentage of cells with poly (GA) puncta out of total cells from spinal cords of WT, *C9-BAC*, *C9orf72*$^{+/-}$*;C9-BAC* and *C9orf72*$^{-/-}$*;C9-BAC* mice. (D) Quantification of the percentage of cells with poly (GP) puncta out of total cells from spinal cords of WT, *C9-BAC*, *C9orf72*$^{+/-}$*;C9-BAC* and *C9orf72*$^{-/-}$*;C9-BAC* mice. Error bars represent SEM of four independent experiments. Statistical analyses were performed with one-way ANOVA with Bonferroni's post hoc test (*P < 0.05, **P < 0.01 and ***P < 0.001).

barely detected poly (GA) and poly (GP) staining in WT mouse tissues (Fig. 5.5A). In contrast, age matched *C9-BAC* mice exhibited robust poly (GA) and poly (GP) signals in brain and spinal cord, which was further exacerbated by C9orf72 heterozygosity (Fig. 5.5). Surprisingly, the percentage of poly (GA) or poly (GP) positive cells in *C9orf72*$^{-/-}$*;C9-BAC* mice were comparable to that in *C9-BAC* mice, possibly through compensating mechanisms from immune system activation.

Discussion

Here we discovered C9orf72's physiological roles in promoting axonal transport, autophagy-lysosome degradation, and the maintenance of axonal integrity of spinal motor neurons in vivo. Our efforts to investigate C9orf72's pathological functions revealed that C9orf72 haploinsufficiency in C9FTD/ALS mouse models exacerbates gain of function and behavioral deficits. C9orf72 deficiency-mediated cellular defects in axonal transport and autophagic stress were recapitulated in patient iPSC-derived motor neurons. These data collectively provide novel insights into the pathological mechanisms of C9FTD/ALS diseases.

C9orf72's cellular functions in patient iPSC-derived MNs

Two promising compounds, olesoxime and dexpramipexole, failed in Phase III clinical trials in ALS patients, although both of them have shown beneficial effects in ALS mouse models (Cudkowicz et al., 2011; Sunyach et al., 2012). These results suggest the importance of incorporating alternative approaches, such as using patient iPSC-derived MNs, into mechanistic and translational research on ALS and related diseases. On the other hand, modeling ALS using iPSCs is challenging due to the wide range of variation in individual genetic background and the heterogeneity of target cells,

as well as the immaturity of the resulting differentiated cells, which are not fully functional adult MNs (Sances et al., 2016). Thus, it is necessary to combine work on patient-derived cells with a complementary system, such as a mouse model, to increase the robustness and rigor of the research. This strategy led to the combined mouse/iPSC approach we took in the present study. Previous studies reported that C9orf72 haploinsufficiency led to neurodegeneration in patient iPSC-derived MNs in the presence of elevated glutamate levels (Shi et al., 2018). Our mechanistic studies further revealed that those cellular phenotypes identified in C9orf72-/- and C9FTD/ALS mouse models were recapitulated in patient iPSC-derived MNs, including defects in axonal transport, autophagic stress, and axonal degeneration characterized by swollen axons.

Dose-dependent pathological functions of C9orf72 in C9FTD/ALS in vivo

One of the discoveries of this study is that C9orf72 haploinsufficiency in C9FTD/ALS mouse models exacerbated motor behavior deficits in an age-dependent manner. *C9orf72*$^{+/-}$*;C9-BAC* mice travelled similar distances in the open field compared to WT at 4-month-old, but haploinsufficiency of C9orf72 exacerbated defects of *C9-BAC* mice in locomotor ability at 18-month-old. Compelling evidences suggest that axonal degeneration precedes clinical symptoms and cell body loss in both normal aging and a variety of neurodegenerative diseases, including Alzheimer's disease, ALS, and Parkinson's disease (Salvadores et al., 2017). Impaired proteostasis including autophagy is a major cause of axonal degeneration (Salvadores et al., 2017). Recent studies suggest the local autophagy of synaptic vesicles as a pathogenic mechanism in MN diseases (Lüningschrör et al., 2017). In addition to its association with lysosomes, C9orf72 protein also localizes to the presynaptic terminals of MNs (Frick et al., 2018).

Our results showed that C9orf72 haploinsufficiency led to axonal degeneration characterized by abnormal swelling of NMJs in the background of *C9-BAC* mice. In addition to lower motor neuron function, higher level motor functions in motor cortex and/or cerebellum might also be influenced by C9orf72 protein levels. C9orf72 dosage affects the di-peptide aggregates in the motor cortex. Future studies should further determine whether and how C9orf72 depletion affects neurodegeneration and TDP-pathology in the motor units, including upper MNs in Layer V of the motor cortex. C9orf72 KO mice exhibited pronounced immune dysfunctions (O'Rourke et al., 2016; Burberry et al., 2016; Atanasio et al., 2016; Jiang et al., 2016), consistent with the increased prevalence of autoimmune disease and neuroinflammation in C9FTD/ALS patients (Miller et al., 2016; Ismail et al., 2013). It would also be important to investigate how the interaction between the immune system and the nervous system contributes to the behavioral and pathological changes.

C9orf72 haploinsufficiency affected C9-BAC mice in multiple FTD-like behaviors, including social novelty and cognitive functions. Our preliminary data revealed altered synaptic protein levels of GluA2 in the cortex of *C9orf72*$^{+/-;}$*C9-BAC* mice without changes in protein levels of GluA1. Future studies should examine how changes in composition or function of AMPAR affect postsynaptic responsiveness.

Clinical trials using antisense oligonucleotides (ASOs) to treat C9FTD/ALS disease have been launched. To fully assess the potential side effects and optimal timing of these therapeutic strategies to inactivate the C9orf72 locus, it is necessary to study the consequences of removing C9orf72 before and after phenotype manifestation in C9FTD/ALS mouse models. Importantly, identification of C9orf72's dose-dependent

pathological roles suggests that C9FTD/ALS disease progression is sensitive to alterations of C9orf72 protein levels. Therefore, future studies might be able to harness the neuroprotective functions of C9orf72 against C9FTD/ALS by modulating its expression level.

References

S.-C. Ling, M. Polymenidou, D. W. Cleveland, Converging mechanisms in ALS and FTD: disrupted RNA and protein homeostasis. Neuron. 79, 416–438 (2013).

F.-B. Gao, S. Almeida, R. Lopez-Gonzalez, Dysregulated molecular pathways in amyotrophic lateral sclerosis-frontotemporal dementia spectrum disorder. EMBO J. 36, 2931–2950 (2017).

I. Gijselinck et al., A C9orf72 promoter repeat expansion in a Flanders-Belgian cohort with disorders of the frontotemporal lobar degeneration-amyotrophic lateral sclerosis spectrum: a gene identification study. Lancet Neurol. 11, 54–65 (2012).

A. E. Renton et al., A hexanucleotide repeat expansion in C9ORF72 is the cause of chromosome 9p21- linked ALS-FTD. Neuron. 72, 257–268 (2011).

M. DeJesus-Hernandez et al., Expanded GGGGCC hexanucleotide repeat in noncoding region of C9ORF72 causes chromosome 9p-linked FTD and ALS. Neuron. 72, 245–256 (2011).

E. Majounie et al., Frequency of the C9orf72 hexanucleotide repeat expansion in patients with amyotrophic lateral sclerosis and frontotemporal dementia: a cross-sectional study. Lancet Neurol. 11, 323–330 (2012).

A. J. Waite et al., Reduced C9orf72 protein levels in frontal cortex of amyotrophic lateral sclerosis and frontotemporal degeneration brain with the C9ORF72 hexanucleotide repeat expansion. Neurobiol. Aging. 35, 1779.e5–1779.e13 (2014).

S. Mizielinska et al., C9orf72 frontotemporal lobar degeneration is characterised by frequent neuronal sense and antisense RNA foci. Acta Neuropathol. 126, 845–857 (2013).

Y. Shi et al., Haploinsufficiency leads to neurodegeneration in C9ORF72 ALS/FTD human induced motor neurons. Nat. Med. 24, 313–325 (2018).

M. Koppers et al., C9orf72 ablation in mice does not cause motor neuron degeneration or motor deficits. Ann. Neurol. 78, 426–438 (2015).

J. G. O'Rourke et al., C9orf72 BAC Transgenic Mice Display Typical Pathologic Features of ALS/FTD. Neuron. 88, 892–901 (2015).

O. M. Peters et al., Human C9ORF72 Hexanucleotide Expansion Reproduces RNA Foci and Dipeptide Repeat Proteins but Not Neurodegeneration in BAC Transgenic Mice. Neuron. 88, 902–909 (2015).

Y. Liu et al., C9orf72 BAC Mouse Model with Motor Deficits and Neurodegenerative Features of ALS/FTD. Neuron. 90, 521–534 (2016).

Yang, M. et al. Lin28 promotes the proliferative capacity of neural progenitor cells in brain development. Development 142, 1616–1627 (2015).

Shao, Q. et al. Zika virus infection disrupts neurovascular development and results in postnatal microcephaly with brain damage. Development 143, 4127–4136 (2016).

Du, Z.-W. et al. Generation and expansion of highly pure motor neuron progenitors from human pluripotent stem cells. Nat Commun 6, 6626 (2015).

Conrad, R. et al. Lectin-based isolation and culture of mouse embryonic motoneurons. J Vis Exp e3200–e3200 (2011). doi:10.3791/3200

Fallini, C., Bassell, G. J. & Rossoll, W. High-efficiency transfection of cultured primary motor neurons to study protein localization, trafficking, and function. Mol Neurodegener 5, 17 (2010).

Cudkowicz, M. et al. The effects of dexpramipexole (KNS-760704) in individuals with amyotrophic lateral sclerosis. Nat. Med. 17, 1652–1656 (2011).

Sunyach, C. et al. Olesoxime delays muscle denervation, astrogliosis, microglial activation and motoneuron death in an ALS mouse model. Neuropharmacology 62, 2346–2352 (2012).

Sances, S. et al. Modeling ALS with motor neurons derived from human induced pluripotent stem cells. Nature Neuroscience 19, 542–553 (2016).

Shi, Y. et al. Haploinsufficiency leads to neurodegeneration in C9ORF72 ALS/FTD human induced motor neurons. Nat. Med. 24, 313–325 (2018).

Salvadores, N., Sanhueza, M., Manque, P. & Court, F. A. Axonal Degeneration during Aging and Its Functional Role in Neurodegenerative Disorders. Front Neurosci 11, 451 (2017).

Lüningschrör, P. et al. Plekhg5-regulated autophagy of synaptic vesicles reveals a pathogenic mechanism in motoneuron disease. Nat Commun 8, 678 (2017).

Frick, P. et al. Novel antibodies reveal presynaptic localization of C9orf72 protein and reduced protein levels in C9orf72 mutation carriers. Acta Neuropathol Commun 6, 72 (2018).

O'Rourke, J. G. et al. C9orf72 is required for proper macrophage and microglial function in mice. Science 351, 1324–1329 (2016).

Burberry, A. et al. Loss-of-function mutations in the C9ORF72 mouse ortholog cause fatal autoimmune disease. Sci Transl Med 8, 347ra93–347ra93 (2016).

Miller, Z. A. et al. Increased prevalence of autoimmune disease within C9 and FTD/MND cohorts: Completing the picture. Neurol Neuroimmunol Neuroinflamm 3, e301 (2016).

Ismail, A. et al. Concurrence of multiple sclerosis and amyotrophic lateral sclerosis in patients with hexanucleotide repeat expansions of C9ORF72. J. Neurol. Neurosurg. Psychiatr. 84, 79–87 (2013).

Jiang, J., Zhu, Q., Gendron, T.F., Saberi, S., McAlonis-Downes, M., Seelman, A., Stauffer, J.E., Jafar-Nejad, P., Drenner, K., Schulte, D. et al. (2016) Gain of toxicity from ALS/FTD-linked repeat expansions in C9ORF72 is alleviated by antisense oligonucleotides targeting GGGGCC-containing RNAs. Neuron, 90, 535–550.

Atanasio, A., Decman, V., White, D. et al. C9orf72 ablation causes immune dysregulation characterized by leukocyte expansion, autoantibody production and glomerulonephropathy in mice. Sci Rep 6, 23204 (2016). https://doi.org/10.1038/srep23204

CHAPTER 6

DISCUSSION AND FUTURE DIRECTIONS

6.1 Cellular functions of C9orf72 and Smcr8

6.1.1 Summary of findings

The data presented in **Chapter 2** and **Chapter 3** have outlined several major functions of the C9orf72/Smcr8 complex in autophagy and axonal transport. Previous studies showed that C9orf72 colocalized with Rab proteins implicated in autophagy and endocytic transport (Farg et al., 2014). In this dissertation work, I have shown that C9ORF72 forms a protein complex with SMCR8, WDR41, and ATG101 (Fig. 2.1). The C9ORF72 complex exhibits a GTPase activity and acts as a GEF for RAB39B (Fig. 2.2). C9ORF72 interacts with both SMCR8 and WDR41 in a DENN domain-dependent manner, but the interaction between SMCR8 and WDR41 is not dependent on DENN domain (Fig. 2.3). Using shRNAs and knockout cell lines, we found that the magnitude of increase in LC3-II and GFP-LC3 puncta number is less in *C9orf72* and/or *Smcr8* knockdown/knockout cell lines under amino starvation/Rapamycin treatment conditions compared to WT cells (Fig. 2.4-5), suggesting that autophagy induction is compromised in *C9orf72* and/or *Smcr8* deficient cells. In contrast, the modulation of autophagic flux is opposite in *Smcr8*-deficient and *C9orf72*-deficient cells: autophagic flux is suppressed in *Smcr8*-deficient cells (Fig. 2.7) and is enhanced in *C9orf72*-deficient cells (Fig. 2.8). The mechanisms of autophagy induction modulation likely involve the regulation of the ULK1 complex, because the interaction between C9ORF72/SMCR8 complex with ULK1 is

enhanced under starvation conditions, and ULK1 protein level and activity are regulated by C9ORF72 and SMCR8 (Fig. 2.6). The expression and processing of lysosome proteases Cathepsin D and Cathepsin L are altered in C9orf72-deficient cells (Fig. 2.8) and Smcr8-deficient cells (Fig. 2.7), suggesting lysosomal functions are disrupted, which may explain the changed autophagic flux. We also showed that in primary motor neurons, C9ORF72 and SMCR8 play a potential role in regulating retrograde axonal transport of autophagosomes (Fig. 3.5, Fig. 5.3).

Overall, these studies implicated important functions of C9ORF72 and its associated protein SMCR8 in different steps of autophagic flow and axonal transport, which are particularly critical for motor neurons. These results support that C9ORF72 itself has functions in maintaining neuronal health and loss of its normal function may contribute to the disease mechanisms.

6.1.2 Remaining questions and considerations

Our studies showed that C9ORF72 and SMCR8 regulate ULK1 expression and activity (Fig. 2.6). The mechanisms of the regulation remain to be further studied. Our immunoprecipitation results show that C9ORF72 or SMCR8 can pull down endogenous ULK1 and this co-IP is drastically enhanced when C9orf72 is overexpressed together with Smcr8, which was also observed by Sullivan et al. (2016). This result suggests these two proteins might play synergistic effects in the interaction with the ULK1 complex. Overexpressing both proteins might also stabilize themselves, considering that C9ORF72 and SMCR8 form a cognate complex that protects each other from degradation (Ugolino et al., 2016), and further enhance their interaction with ULK1. We also found that the interaction between the C9ORF72 complex and the ULK1 complex

is enhanced under amino acid starvation conditions, suggesting that the C9ORF72 complex preferentially regulates ULK1 during autophagy induction. Indeed, Webster et al. (2016) found that C9ORF72 functions as a Rab1a effector and modulates initiation of autophagy by regulating ULK1 translocation. It would be interesting to use live cell imaging to track the dynamic localization of ULK1 and DFCP1, which is a PtdIns3*P* effector and an omegasome marker (Karanasios et al., 2013), in WT and *C9orf72*$^{-/-}$ neurons.

It is intriguing that C9ORF72 and SMCR8 modulate ULK1 activity towards opposite directions (Fig. 2.6), suggesting they may play distinct roles in regulating ULK1. Indeed, SMCR8 regulates the protein levels of ULK1 and ATG13 (Fig. 2.6) by enhancing ULK1 transcription, while ULK1 protein level is not altered in *C9orf72* deficient cells (Jung et al., 2017).

Alternative ways of modulating autophagy by the C9ORF72/SMCR8 complex have been identified by other groups. Sellier et al. (2016) found that the C9ORF72/SMCR8 complex is phosphorylated by TBK1 and ULK1 kinases and functions as a GEF for RAB39b, which regulates autophagy induction by interacting with P62. Amick et al. (2016) found that C9orf72 localizes to lysosomes and regulates the response of mTORC1 to changes in amino acid availability. Ugolino et al. (2016) found that C9orf72 regulates autophagy by modulating the protein levels of TFEB, which is a master regulator of lysosomal and autophagy genes.

These findings are complementary to each other and it is possible that dysfunction of multiple pathways contributes to neurodegeneration (Balendra et al., 2018). C9orf72 may also have different functions in different cell types. C9orf72 has

been shown to regulate microglia (O'Rourke et al., 2016) and macrophage (Shao et al., 2018) function by modulating lysosomal degradation. Xiao et al. (2019) found that C9orf72 localizes to pre- and post- synapses and regulates post-synaptic glutamate receptor 1 levels in the hippocampus. These results suggest that multiple cellular pathways involving both cell-autonomous and non-cell-autonomous effects contribute to disease progression.

Our discovery that C9orf72 and Smcr8 regulate autophagosome axonal transport in motor neurons (Fig. 3.5, Fig. 5.3) provides additional support for the specialized functions in differentiated post-mitotic cell types. Axonal transport defect was observed in both mouse model of C9ALS/FTD (Fig. 5.3) and patient iPSC-derived MNs (Fig. 5.4). Our mass spectrometry studies revealed that the C9orf72/Smcr8 complex associates with Dynein, suggesting this complex might regulate axonal transport by modulating the motor protein. Alternatively, this complex might regulate the association between cargo and motor or motor and microtubule. Additional biochemical assays with fragmented proteins combined with Subpixel colocalization assays (Szpankowski et al., 2012) should help clarify these possibilities. Our electron microscopy results show that mitochondria and lysosomes are accumulated within the axonal swellings of *Smcr8*$^{-/-}$ spinal cord, suggesting C9orf72 and Smcr8 might also regulate transport of other proteins and organelles, such as Neurofilament, lysosomes or mitochondria, and it will be interesting to test if mis-trafficking of these proteins/organelles in patient iPSNs contributes to the pathological mechanisms.

6.2 Dose dependent role of C9orf72 in behaviors and gain of toxicity

6.2.1 Summary of Findings

Our data showed that like C9orf72, Smcr8 is also downregulated in patient tissues (Fig. 3.1). Therefore, we studied the neuronal function of Smcr8 using Smcr8 deficient mice **(Chapter 3)**. These Smcr8 deficient mice exhibited motor behavior deficits, including decreased grip strength, endurance on the rotarod and total distance travelled in the open field (Fig. 3.2). They also showed increased anxiety-like behaviors (Fig. 3.2). Going into the cellular mechanisms, we found that Smcr8 depletion disrupted autophagy-lysosomal degradation and led to axonal swellings, shown by accumulations of autophagosome and lysosome markers, LC3, P62 and Lamp1, which co-localized with axon marker Neurofilament (Fig. 3.3), as well as transmission electronic microscopy images (Fig. 3.4). In addition, Smcr8 deficient mice also showed swellings in the neuromuscular junctions (NMJs), which are the axonal terminals of motor neurons (Fig. 3.3). *C9orf72* deficiency can exacerbate these cellular deficits. *C9orf72*$^{-/-}$*;Smcr8*$^{-/-}$ mice showed significant increased numbers of axonal swellings and autolysosome accumulations, as well as enlarged axonal terminals, compared with *Smcr8*$^{-/-}$ mice (Fig. 3.6-7). These results together suggest that C9orf72's function in motor neurons could be dominated by Smcr8, and C9orf72 deficiency promotes deficits in autophagy-lysosome degradation and axonal degeneration in the absence of Smcr8.

To understand the contribution of different hypothesized mechanisms to the disease progression and to model the reduced expression levels of C9orf72 in patient tissues, we crossed the *C9orf72*$^{-/-}$ mice with the *C9-BAC* mice and examined the consequences of "loss of function" in the background of "gain of toxicity" **(Chapter 4, Chapter 5)**. By comparing WT, *C9-BAC*, *C9orf72*$^{+/-}$*;C9-BAC* and *C9orf72*$^{-/-}$*;C9-BAC*

littermates, we found that C9orf72 deficiency promotes motor deficits of a C9ALS/FTD mouse model in a dose-dependent manner (Fig. 4.1, Fig. 5.1). Mechanistically, we found that C9orf72 and Smcr8 haploinsufficiency exacerbates the NMJ swellings of *C9-BAC* mice (Fig. 3.8, Fig. 5.2). To study dose-dependent roles of C9orf72 in FTD-like behaviors, we performed novel object recognition test and three-chambered sociability and social novelty test. We found that WT and *C9-Bac* mice are normal in the novel object recognition test, but *C9orf72*$^{+/-}$*;C9BAC* showed less preference for the novel object compared with WT (Fig. 5.1). Even though WT, *C9-BAC* and *C9orf72*$^{+/-}$*;C9-BAC* mice are normal in sociability, C9orf72 haploinsufficiency exacerbates the social novelty deficits of *C9-BAC* mice (Fig. 5.1). These results suggest that “loss of function” mechanisms and “gain of toxicity” mechanisms are not mutually exclusive, and they may both contribute to the disease progression.

We also addressed whether partial loss of function of C9orf72/Smcr8 promotes “gain of toxicity”. By comparing DPR abundance in *C9-BAC*, *C9orf72*$^{+/-}$*;C9-BAC* and *Smcr8*$^{+/-}$*;C9-BAC* mice in the motor cortex and spinal cord, we found that C9orf72 and Smcr8 haploinsufficiency exacerbates the DPR gain of toxicity of *C9-BAC* mice (Fig. 3.9, Fig. 5.5), indicating the interaction between the “loss of function” mechanisms and “gain of toxicity” mechanisms.

6.2.2 Remaining questions

The protein levels of Smcr8 is drastically decreased in the *C9orf72* deficient mice (Fig. 3.1; Ugolino et al., 2016; Amick et al., 2016; Lan et al., 2019). While *Smcr8* deficient mice show strong motor behavioral deficits (Fig. 3.2), *C9orf72* deficient mice show very mild to no motor behavioral deficits (Koppers et al., 2015; Jiang et al., 2016;

Anatasio et al, 2016). One possible explanation could be the residual little amount of Smcr8 is able to perform its function or even becomes more potent and is able to compensate for the loss of C9orf72's function. An alternative possibility might be in absence of C9orf72, Smcr8 is more likely to be degraded during in vitro cell lysis but not in vivo, considering that all four studies including ours examined Smcr8 protein levels using Western blot. Immunostaining approaches can be used to test this possibility with either high-quality antibody or an endogenous locus reporter for Smcr8.

Another intriguing question is about the cross talk between loss- and gain-of-function in the pathogenesis of C9ALS/FTD. Poly-GA and poly-GP aggregates are more abundant in *C9orf72*$^{+/-}$*;C9-BAC* and *Smcr8*$^{+/-}$*;C9-BAC* mice (Fig. 3.9, Fig. 5.5). Using C9ORF72 patient and *C9ORF72*$^{+/-}$ induced motor neurons, Shi et al. (2018) found dose-dependent decrease in the ability to clear DPR aggregates. The possible mechanisms might involve suboptimal autophagy (Boivin et al., 2020) or axonal transport (Abo-Rady et al., 2020) caused by the reduced C9ORF72 levels. It was surprising to observe that the DPR abundance was reduced in *C9orf72*$^{-/-}$*;C9-BAC* mice compared to *C9orf72*$^{+/-}$*;C9-BAC* mice. This could be due to enhanced autophagy flux caused by C9orf72 deficiency (Fig. 2.8; Ugolino et al. 2016) or increased microglia activation. Future research directions should examine how the normal functions of C9orf72 are affected in different cell types isolated from *C9orf72*$^{+/-}$*;C9-BAC* mice or derived from patient iPSCs and in co-cultures, to gain a more thorough perspective on the interactions between loss- and gain-of-function mechanisms.

Our *C9orf72*$^{+/-}$*;C9-BAC* mouse line has been proven potentially useful to model C9-ALS/FTD. These *C9orf72*$^{+/-}$*;C9-BAC* mice show exacerbated motor, social and

cognitive deficits compared with *C9-BAC* mice (Fig.4.1, Fig. 5.1). Using a different *C9-BAC* mouse line, Qiang et al. (2020) observed similar exacerbation of cognitive deficits due to reduced C9orf72 function. These results reinforce the normal function of C9orf72 in maintaining neuronal health and function. While recent major efforts for rescuing the C9ALS/FTD phenotypes focus on targeting RNA-mediated toxicity (Martier et al., 2019) and DPR proteins (Nguyen et al., 2019), it is also important to test whether restoring the normal expression levels of C9orf72 and Smcr8 in these mouse models can rescue the cellular, pathological and behavioral phenotypes. Future gene therapy approaches should consider combining antisense oligonucleotide which reduce gain-of-toxicity associated with the repeat expansion (Ly et al., 2018; Donnelly et al., 2013) with AAV gene deliveries that restore the normal protein levels of C9orf72 and Smcr8.

6.3 Conclusions

This work has identified important roles of C9orf72 and Smcr8 in maintaining neuron health, promoting motor and cognitive functions and alleviating toxicity caused by the expanded repeats. These studies have highlighted the synergic interactions between the loss- and gain-of-function mechanisms. While many questions still remain to be answered, these contributions will hopefully motivate further investigation in the cell-autonomous and non-cell-autonomous pathological mechanisms, and instruct future studies into restoring the normal levels and functions of C9orf72. Persistent research efforts and accumulated knowledge will hopefully lead to rapid translation into therapeutic strategies that could positively impact patients with these neurodegenerative diseases.

6.4 References

Eleftherios Karanasios, Eloise Stapleton, Maria Manifava, Takeshi Kaizuka, Noboru Mizushima, Simon A. Walker, Nicholas T. Ktistakis. Dynamic association of the ULK1 complex with omegasomes during autophagy induction. Journal of Cell Science 2013 126: 5224-5238; doi: 10.1242/jcs.132415

Christopher P Webster et al., The C9orf72 protein interacts with Rab1a and the ULK1 complex to regulate initiation of autophagy. The EMBO Journal (2016) 35: 1656–1676. https://doi.org/10.15252/embj.201694401

Jung et al. (2017) Multiplex image-based autophagy RNAi screening identifies SMCR8 as ULK1 kinase activity and gene expression regulator. eLife 2017;6:e23063 DOI: 10.7554/eLife.23063

Sullivan PM, Zhou X, Robins AM, Paushter DH, Kim D, Smolka MB, Hu F. 2016. The ALS/FTLD associated protein C9orf72 associates with SMCR8 and WDR41 to regulate the autophagy-lysosome pathway. Acta Neuropathol Commun 4: 51.

Balendra, R., Isaacs, A.M. C9orf72-mediated ALS and FTD: multiple pathways to disease. Nat Rev Neurol 14, 544–558 (2018). https://doi.org/10.1038/s41582-018-0047-2

Sellier C, Campanari ML, Julie Corbier C, Gaucherot A, Kolb-Cheynel I, Oulad-Abdelghani M, Ruffenach F, Page A, Ciura S, Kabashi E, et al. 2016. Loss of C9ORF72 impairs autophagy and synergizes with polyQ Ataxin-2 to induce motor neuron dysfunction and cell death. EMBO J 35: 1276–1297.

Amick J, Roczniak-Ferguson A, Ferguson SM. 2016. C9orf72 binds SMCR8, localizes to lysosomes, and regulates mTORC1 signaling. Mol Biol Cell 27: 3040–3051.

Qiang Shao, Mei Yang, Chen Liang, Li Ma, Wei Zhang, Zhiwen Jiang, Jun Luo, Jae-Kyung Lee, Chengyu Liang & Jian-Fu Chen (2019) C9orf72 and smcr8 mutant mice reveal MTORC1 activation due to impaired lysosomal degradation and exocytosis, Autophagy, DOI: 10.1080/15548627.2019.1703353

J. G. O'ROURKE et al. C9orf72 is required for proper macrophage and microglial function in mice. SCIENCE18 MAR 2016: 1324-1329

Lukasz Szpankowski, Sandra E. Encalada, Lawrence S. B. Goldstein. APP-dependent motor association on axonal vesicles. Proceedings of the National Academy of Sciences May 2012, 109 (22) 8582-8587; DOI: 10.1073/pnas.1120510109

Yungang Lan, Peter M. Sullivan & Fenghua Hu (2019) SMCR8 negatively regulates AKT and MTORC1 signaling to modulate lysosome biogenesis and tissue homeostasis, Autophagy, 15:5, 871-885, DOI: 10.1080/15548627.2019.1569914

Manon Boivin, Véronique Pfister, Angeline Gaucherot, Frank Ruffenach, Luc Negroni, Chantal Sellier, Nicolas Charlet-Berguerand. Reduced autophagy upon C9ORF72 loss synergizes with dipeptide repeat protein toxicity in G4C2 repeat expansion disorders. The EMBO Journal (2020) 39: e100574https://doi.org/10.15252/embj.2018100574

Shi, Y., Lin, S., Staats, K. et al. Haploinsufficiency leads to neurodegeneration in C9ORF72 ALS/FTD human induced motor neurons. Nat Med 24, 313–325 (2018). https://doi.org/10.1038/nm.4490

Zhu, Q., Jiang, J., Gendron, T.F. et al. Reduced C9ORF72 function exacerbates gain of toxicity from ALS/FTD-causing repeat expansion in C9orf72. Nat Neurosci 23, 615–624 (2020). https://doi.org/10.1038/s41593-020-0619-5

Martier R. et al. (2019) Targeting RNA-Mediated Toxicity in C9orf72 ALS and/or FTD by RNAi-Based Gene Therapy. Molecular Therapy Nucleic Acids. VOLUME 16, P26-37, JUNE 07, 2019

Donnelly C. J. et al. (2013) RNA Toxicity from the ALS/FTD C9ORF72 Expansion Is Mitigated by Antisense Intervention. Neuron. Volume 80, Issue 2, 16 October 2013, Pages 415-428

Nguyen L. et al. (2019) Antibody Therapy Targeting RAN Proteins Rescues C9 ALS/FTD Phenotypes in C9orf72 Mouse Model. Neuron. VOLUME 105, ISSUE 4, P645-662.E11, FEBRUARY 19, 2020.